



Available online at [www.sciencedirect.com](http://www.sciencedirect.com)



Progress in Materials Science 52 (2007) 1263–1334

[www.elsevier.com/locate/pmatsci](http://www.elsevier.com/locate/pmatsci)

---

Progress in  
Materials  
Science

---

# Nature's hierarchical materials

Peter Fratzl \*, Richard Weinkamer

*Max-Planck-Institute of Colloids and Interfaces, Department of Biomaterials, 14424 Potsdam, Germany*

---

## Abstract

Many biological tissues, such as wood and bone, are fiber composites with a hierarchical structure. Their exceptional mechanical properties are believed to be due to a functional adaptation of the structure at all levels of hierarchy. This article reviews the basic principles involved in designing hierarchical biological materials, such as cellular and composite architectures, adaptive growth and as well as remodeling. Some examples that are found to utilize these strategies include wood, bone, tendon, and glass sponges – all of which are discussed.

© 2007 Elsevier Ltd. All rights reserved.

---

## Contents

1. Introduction . . . . .	1264
2. Structural hierarchies in biological materials . . . . .	1267
2.1. Wood . . . . .	1267
2.2. Bone . . . . .	1270
2.3. Glass sponge skeletons . . . . .	1276
3. Anisotropic cellular structures . . . . .	1278
3.1. Natural cellular structures and Wolff's law . . . . .	1278
3.2. The cellular structure of wood . . . . .	1281
3.3. Trabecular bone . . . . .	1282
4. Building with fibers . . . . .	1287
4.1. Tendon: hierarchies of structure – hierarchies of deformation . . . . .	1287
4.2. The osteon in bone . . . . .	1290
4.3. The microfibril angle in wood . . . . .	1293

---

\* Corresponding author. Tel.: +49 331 567 9401; fax: +49 331 567 9402.

E-mail address: [fratzl@mpikg.mpg.de](mailto:fratzl@mpikg.mpg.de) (P. Fratzl).

5.	Nanocomposites . . . . .	1296
5.1.	Plastic deformation in reaction wood . . . . .	1296
5.2.	Nanoscale deformation in bone . . . . .	1299
5.3.	Stiff and tough composites by gluing – a simple model . . . . .	1302
6.	Adaptivity . . . . .	1306
6.1.	Mechanobiology and examples of functional adaptation . . . . .	1306
6.2.	Bone remodeling . . . . .	1309
6.2.1.	<i>In vivo</i> experiments . . . . .	1310
6.2.2.	<i>In vitro</i> experiments . . . . .	1312
6.2.3.	<i>In silico</i> experiments . . . . .	1313
6.3.	Bone healing . . . . .	1315
6.3.1.	Mechanobiological experiments of fracture healing . . . . .	1318
6.3.2.	Mechanobiological theories of fracture healing . . . . .	1318
7.	Outlook . . . . .	1321
	Acknowledgements . . . . .	1321
	References . . . . .	1322

---

## 1. Introduction

Biological materials are omnipresent in the world around us. They are the main constituents in plant and animal bodies and have a diversity of functions. A fundamental function is obviously mechanical providing protection and support for the body. But biological materials may also serve as ion reservoirs (bone is a typical example), as chemical barriers (like cell membranes), have catalytic function (such as enzymes), transfer chemical into kinetic energy (such as the muscle), etc. The present review article will focus on materials with a primarily (passive) mechanical function: cellulose tissues (such as wood), collagen tissues (such as tendon or cornea), mineralized tissues (such as bone, dentin and glass sponges). The main goal is to give an introduction to the current knowledge of the structure in these materials and how these structures relate to their (mostly mechanical) functions. Muscle, which has an active mechanical function, will not be discussed nor will the areas of fluid flow (blood circulation, for instance), friction and tribology (such as in articulations), or joining (attachment systems in insects, for instance), despite their obvious relation to mechanics. Hence, the view on Nature will be very much the one of a Materials Scientist interested in (bulk) structural materials.

Moreover, the article will not attempt to give an exhaustive review of structural details and mechanical properties of the materials covered. The emphasis will rather be on structural principles, on mechanisms for deformation and on functional adaptation. In particular, the aspect of functional adaptation is of interest for the Materials Scientist since Nature has developed a large number of ingenious solutions which still wait to be discovered and serve as a source of inspiration [1]. This subject was pioneered by Schwendener [2] and D'Arcy Wentworth Thomson in the classical book from 1917 (revised and reprinted in 1942) "On Growth and Form", which has been republished almost a century later [3]. This early text mostly relates the "form" (or shape) of biological objects to their function. A similar approach specifically focusing on trees has been pursued in the book by Mattheck and Kubler [4], with the specific aim to extract useful engineering principles from their observations. Adapting the *form* (of a whole part or organ, such as a branch or

a vertebra) is one aspect of functional adaptation. A second, which relates more directly to Materials Science, is the functional adaptation of the *microstructure* of the material itself (such as the wood in the branch or the bone in the vertebra). This dual optimization of the part's form and of the material's microstructure is well known for any engineering problem. However, in natural materials shape and microstructure are intimately related due to their common origin, which is the growth of the organ. This aspect has been discussed in detail by Jeronimidis in his introductory chapters to a book on “Structural Biological Materials” [5]. Growth implies that “form” and “microstructure” are created in the same process. The shape of a branch is created by the assembly of molecules to cells, and of cells to wood with a specific shape. Hence, at every size level, the branch is both form and material – the structure becomes hierarchical.

Textbooks on hierarchical biological materials include an overview by Currey [6] and the compilation of articles edited by Cowin [7] on structure and mechanical properties of bone. More general introductions to the behavior of biological materials can be found, e.g., in the books by Vincent [8] or Wainwright et al. [9]. Niklas gives an introduction to the relation between form and function in plants [10] (see also [11] and other articles of this special issue), and Mattheck specifically focuses on trees [12]. An interesting compilation of articles about the mechanical optimization in Nature can be found in [13]. Gibson and Ashby cover the aspect of cellular structure found in many natural materials (such as wood, cork, trabecular bone, etc.) in their textbook on cellular solids [14]. Main ideas about composite materials can be found in [15,16]. One of the main driving forces in studying biological materials from the viewpoint of Materials Science is to use the discovered natural structures and processes as inspiration for developing new materials. Large surveys have been carried out on this topic, for instance in the United States [17] or in France [18]. Terms such as “bionics” or “biomimetics” [19–23] are sometimes used for this new approach in Chemistry, Materials Science or Engineering. Textbooks, such as the ones on “Bionics” by Nachtigall [24], on “Design” by French [25] or on “Biominerization” by Mann [26] address these issues more or less directly.

It is not evident at all that the lessons learned from hierarchical biological materials will be applicable immediately to the design of new engineering materials. The reason arises from striking differences between the design strategies common in Engineering and those used by Nature (see Fig. 1). These differences are contributed by the different sets of elements used by Nature and the Engineer – with the Engineer having a greater choice of elements to choose from in the “toolbox”. Elements such as iron, chromium, nickel, etc. are very rare in biological tissues and are certainly not used in metallic form as, for example, in steels. Iron is found in red blood cells as an individual ion bound to the protein hemoglobin: its function is certainly not mechanical but rather chemical, to bind oxygen. Most of the structural materials used by Nature are polymers or composites of polymers and ceramic particles. Such materials would not be the first choice of an engineer who intends to build very stiff and long-lived mechanical structures. Nevertheless, Nature makes the best out of the limitations in the chemical environment, adverse temperatures and uses polymers and composites to build trees and skeletons [27–29]. Another major difference between materials from Nature and the Engineer is in the way they are made. While the Engineer *selects* a material to *fabricate* a part according to an exact design, Nature goes the opposite direction and *grows* both the material and the whole organism (a plant or an animal) using the principles of (biologically controlled) self-assembly. Moreover, biological structures are even able to remodel and adapt to changing environmental

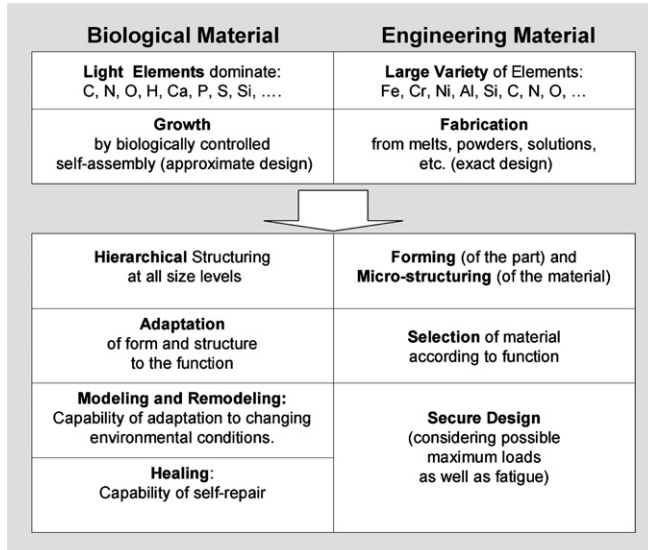


Fig. 1. Biological and engineering materials are governed by a very different choice of base elements and by a different mode of fabrication. From this are resulting different strategies for materials choice and development (under the arrow). See also [22].

conditions during their whole lifetime. This control over the structure at all levels of hierarchy is certainly the key to the successful use of polymers and composites as structural materials.

Different strategies in designing a material result from the two paradigms of “growth” and “fabrication” are shown in Fig. 1. In the case of engineering materials, a machine part is designed and the material is selected according to the functional prerequisites taking into account possible changes in those requirements during service (e.g. typical or maximum loads, etc.) and considering fatigue and other lifetime issues of the material. Here the strategy is a static one, where a design is made in the beginning and must satisfy all needs during the lifetime of the part. The fact that natural materials are growing rather than being fabricated leads to the possibility of a dynamic strategy. Taking a leaf as an example, it is not the exact design that is stored in the genes, but rather a recipe to build it. This means that the final result is obtained by an algorithm instead of copying an exact design. This approach allows for flexibility at all levels. Firstly, it permits adaptation to changing function during growth. A branch growing into the wind may grow differently than against the wind without requiring any change in the genetic code. Secondly, it allows the growth of hierarchical materials, where the microstructure at each position of the part is adapted to the local needs [5]. Functionally graded materials are examples of materials with hierarchical structure. Biological materials use this principle and the functional grading found in Nature may be extremely complex. Thirdly, the processes of growth and “remodeling” (this is a combination of growth and removal of old material) allow a constant renewal of the material, thus reducing problems of material fatigue. A change in environmental conditions can be (partially) compensated for by adapting the form and microstructure to new conditions. One may think about what happens to the growth direction of a tree

after a small land-slide occurs [4,30]. In addition to adaptation, growth and remodeling, processes occur which enable healing allowing for self-repair in biological materials.

These differences between the “growth” and “fabrication” paradigms will be a guiding idea throughout this paper. Hierarchical structure will be discussed in Section 2 with a number of examples. Bone and wood are chosen as prototypes of stiff materials for mechanical applications; one from the animal world and the other from the world of plants. Collagen in tendons is used to illustrate a hierarchical polymeric fiber composite. Sections 3 and 4 will focus on two wide-spread construction principles found in many natural hierarchical materials; the cellular structure (mostly in the micrometer to millimeter range) (see also [31]) and the composite structure (mostly in the nanometer to micrometer range). Section 5 will address the processes which enable the functional adaptation of biological materials.

## 2. Structural hierarchies in biological materials

Many biological materials are structured in a hierarchical way over many length scales. The following are three hierarchically structured biogenic tissues with entirely different chemical compositions: the wood cell wall, an almost pure polymeric composite, the skeleton of a glass sponge, which is composed of almost pure silica mineral, and bone, an organic–inorganic composite consisting of roughly half polymer and half mineral.

### 2.1. Wood

At the macroscopic level, spruce wood can be considered as a cellular solid, mainly composed of parallel hollow tubes, the wood cells. As an example, the hierarchical structure of spruce wood is shown in Fig. 2. The wood cells are clearly visible in Fig. 2a and they have a thicker cell wall in latewood (LW) than in earlywood (EW), within each annual ring. The cell wall is a fiber composite made of cellulose microfibrils embedded into a matrix of hemicelluloses and lignin [32].

The cellulose fibrils wind around the tube-like wood cells at an angle called the microfibril angle (MFA, see Figs. 2 and 3, often denoted by  $\mu$ ). The detailed distribution of fibril directions in the cell is shown in Fig. 3. These data are obtained by microdiffraction, scanning an X-ray beam of  $2\text{ }\mu\text{m}$  diameter over a cell cross-section (in steps of  $2\text{ }\mu\text{m}$ ) and measuring a diffraction pattern at every position on the specimen [34]. X-ray patterns turn out to be anisotropic and even asymmetric due to the non-standard diffraction geometry (Fig. 3, left). This asymmetry can be used to determine the orientation of the cellulose fibrils. An arrow corresponding to the projection of the unit vector following the fibril direction is shown in Fig. 3(right) at each point where a diffraction pattern is collected and the convention is that the vectors point out of the image plane. It is clearly visible that cellulose fibrils in each of the adjacent cells run according to a right-handed helix. The spatial resolution of this experiment is such that only the main cell-wall layer (called S2, Fig. 4) is imaged.

A more detailed three-dimensional sketch of the cell-wall structure of spruce, based on electron microscopy [32], X-ray diffraction [34] and AFM-results [35,36], is given in Fig. 4. Typically, the cell-wall consists of several layers ( $S_1, S_2, \dots$ ), where the  $S_2$  is by far the thickest. While the cellulose microfibrils in the  $S_1$ -layer run at almost  $90^\circ$  to the cell axis [32,37], the cellulose microfibrils in the  $S_2$  layer are more parallel to it (with microfibril

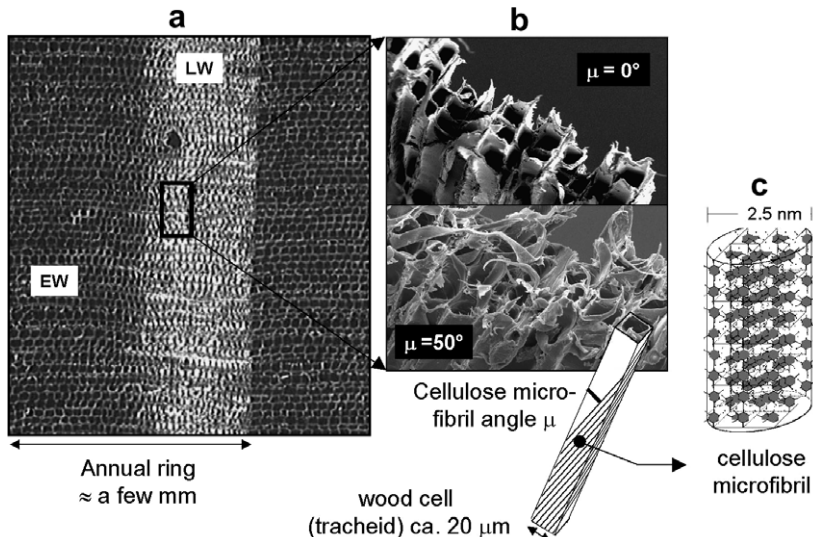


Fig. 2. Hierarchical structure of spruce wood. (a) Cross-section through the stem showing the succession of earlywood (EW) and latewood (LW) within an annual ring. Due to a reduction in cell diameter and an increased thickness of the cell walls, latewood is denser than earlywood. The width of the annual rings varies widely depending on climatic conditions during each particular year. (b) Scanning electron microscopic pictures of fracture surfaces of spruce wood with two different microfibril angles. One of the wood cells (tracheids) is drawn schematically showing the definition of the microfibril angle between the spiraling cellulose fibrils and the tracheid axis. (c) Sketch of the (crystalline part) of a cellulose microfibril (from [33] with permission).

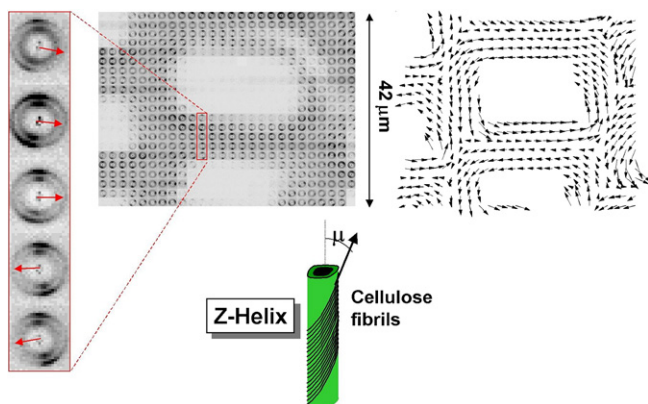


Fig. 3. X-ray microdiffraction experiment with a 2  $\mu\text{m}$  thick section of spruce wood embedded in resin (from [34]). Left: typical XRD-patterns from the crystalline part of the cellulose fibrils. Each pattern has been taken with a 2  $\mu\text{m}$  wide X-ray beam at the European Synchrotron Radiation Source, ESRF. In the middle, the diffraction patterns are drawn side by side as they were measured reproducing several wood cells in cross-section. The asymmetry of the patterns in the enlargement (far left) can be used to determine the local orientation of cellulose fibrils in the cell wall (denoted by arrows). The arrows are plotted in the right image with the convention that they represent the projection of a vector parallel to the fibrils onto the plane of the cross-section revealing a right-handed helix structure (from [33] with permission).

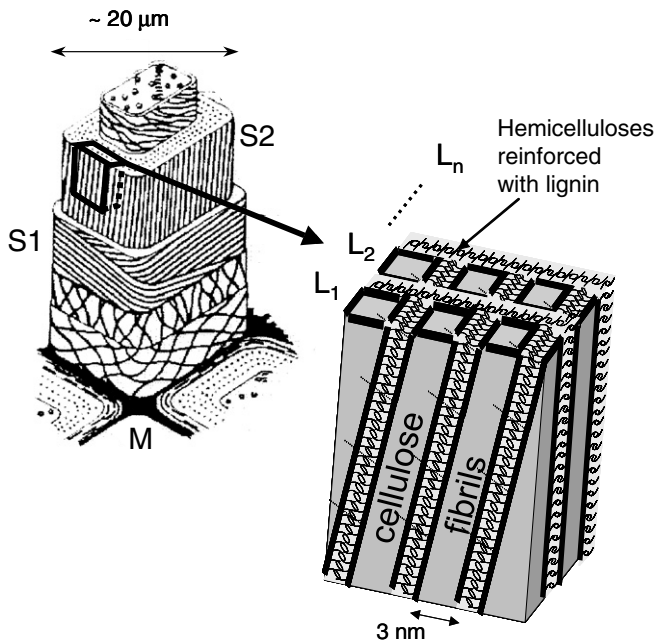


Fig. 4. Structure of the cell-wall of softwood tracheids based on recent investigations [32,34,35,37–39,42]. The sketch on the left is based on a classical drawing from the book by Fengel and Wegener [32], showing the main cell-wall layers S1 and S2, as well as the middle lamella (M) between cells. A structure consisting of a succession of concentric cellulose-rich and lignin-rich layers has been proposed for the S2-layer [35,43,44]. According to this model, hemicelluloses connect the cellulose and the lignin located between the fibrils (grey in the left part of the figure). Successive concentric cellulose-rich layers are indicated as  $L_1, L_2, \dots, L_n$ . It has been proposed that the matrix between the fibrils (containing both, lignin and hemicelluloses) permits relatively large shear deformation between neighboring fibrils [45].

angles ranging from  $0^\circ$  to about  $45^\circ$ ). The cellulose microfibrils have a thickness of about 2.5 nm in spruce [38] (and a somewhat larger diameter in other wood or cellulose-rich tissues [32,39]), and are embedded in a matrix of hemicelluloses and lignin. It is probable that the arrangement of cellulose fibrils constitutes sub-layers  $L_1, L_2, \dots, L_n$ , as sketched in Fig. 4 [35]. Other evidence points toward a more random arrangement of the cellulose fibrils in the cell-wall cross-section [40]. The lateral separation of neighboring cellulose microfibrils depends on the degree of hydration of the cell wall [41].

The typical variation of the cellulose tilt angle from one cell to the next is shown in Fig. 5. The nearly  $90^\circ$  orientation of the cellulose in the cell-wall layer S1 is clearly visible.

In summary, wood can be regarded as a *cellular material* at the scale of hundred micrometers to centimeters. Parameters which can be varied at this hierarchical level (and, therefore, used for adaptation to biological and mechanical needs) are the diameter and shape of the cell cross-section, as well as the thickness of the cell wall. In particular, the ratio of cell-wall thickness to cell diameter is directly related to the apparent density of wood which, in turn is an important determinant of the performance of light weight structures (see discussion in Sections 3.2 and 6.1). The stem is further organized in annual rings with *alternating layers* of thin- and thick-walled cells. This creates a fairly complex structure with layers of alternating density. At the lower hierarchical level, the complexity

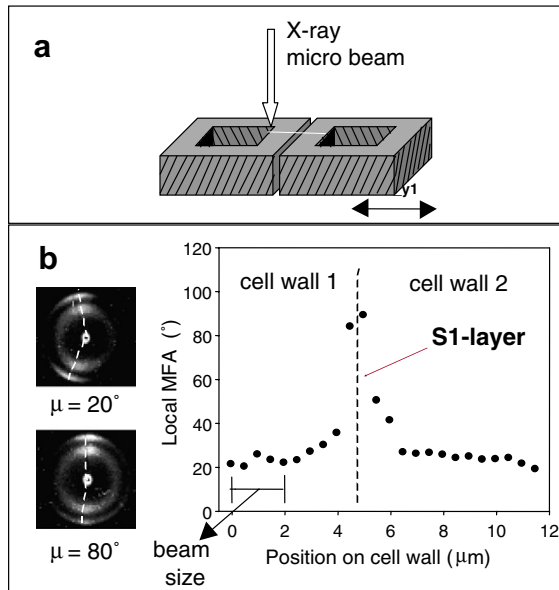


Fig. 5. Measurement of the tilt angle of cellulose fibrils in latewood of a spruce stem as measured with microfocus X-ray diffraction [37]. The trace of the X-ray microbeam is shown schematically in (a). Two X-ray diffraction diagrams corresponding to a cellulose tilt angle of 20° and 80° are shown in (b) on the left. The variation of the tilt angle (local MFA) is indicated in (b) on the right. The MFA is in the order of 20° in the majority of the cell wall (in the S2 layer) and reaches values close to 90° in the outermost layer S1 (compare also with the sketch in Fig. 4).

increases even further since the wall of individual cells is a *fiber composite*. As will be discussed in Section 4.3, the orientation of the cellulose fibril direction (microfibril angle, see Figs. 2–4) with respect to the cell axis has a major influence on the mechanical properties of the tissue as a whole, and – depending on the (biological or mechanical) needs – the microfibril angle can be adjusted locally.

## 2.2. Bone

The hierarchical structure of bone has been described in a number of reviews [46–48]. Starting from the macroscopic structural level, bones can have quite diverse shapes depending on their respective function. Several examples are shown in Fig. 6. Long bones, such as the femur or the tibia, are found in our extremities and provide stability against bending and buckling. In other cases, for instance for the vertebra or the head of the femur, the applied load is mainly compressive. In such cases, the bone shell can be filled with a “spongy” material called trabecular or cancellous bone (see Fig. 7). The walls of tube-like long bones and the walls surrounding trabecular bone regions are called cortical bone. The cortical bone shell (found at the outer surface of each bone) can reach a thickness between several tenths of a millimeter (in vertebra) to several millimeters or even centimeters (in the mid-shaft of long bones). The thickness of the struts in the “spongy” trabecular bone (Fig. 7, bottom) is fairly constant between one and three hundred micrometers.

Typical structures found at lower hierarchical levels in bone are shown in Fig. 8. Cortical bone is usually fairly dense with a porosity in the order of 6%, mainly due to

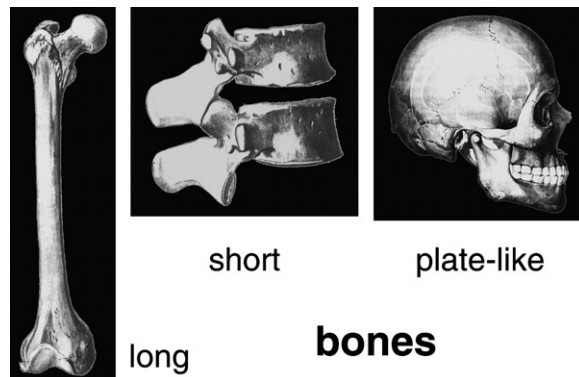


Fig. 6. Bones with different function differ strongly in shape. Long bones (such as the femur, left) provide stability against bending and buckling. Short bones (such as the vertebra, center) provide stability against compression (along the vertical axis, in the case of the vertebra). Plate-like bones (such as the skull, right) protect vital organs.

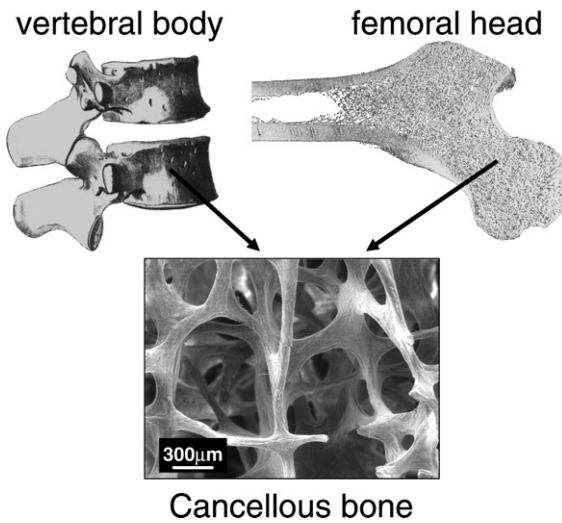


Fig. 7. Certain bones (or parts of bones), such as the vertebra or the femoral head, are filled with a spongy structure called trabecular bone. The struts (or trabeculae) have a thickness in the order of a few hundred micrometers.

the presence of blood vessels. They are surrounded by concentric layers of material, visible in Fig. 8b as a halo around each blood vessel. The blood vessel with its surrounding material is called an osteon and one such osteon is marked with "O" in Fig. 8b. The pictures of Fig. 8b and c are obtained by back-scattered electron imaging which yields grey-levels depending on the local calcium mineral content [49,50]. Lighter areas indicate more densely mineralized regions. Trabecular bone has a porosity in the order of 80% and can be considered as a foam-like network of bone trabeculae (Fig. 8c). The typical thickness of the trabeculae is about 200  $\mu\text{m}$  with an orientation that depends on the load distribution in the bone. Beside the larger holes corresponding to blood vessels, a large number of

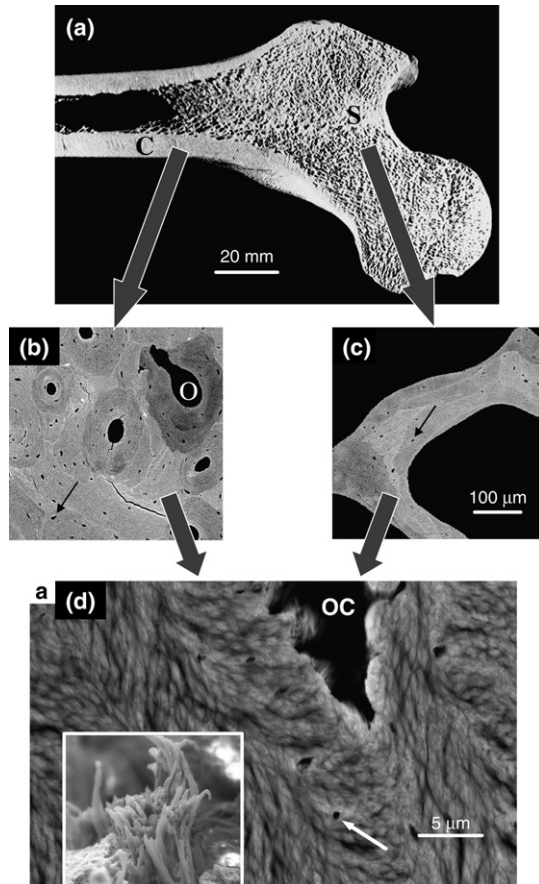


Fig. 8. Hierarchical structure of bone in the human femur. A section across the femur (a) reveals its tube-like structure with the walls made of cortical (or compact) bone, labeled “C” in the figure. The femoral head is filled with trabecular (or cancellous) bone, labeled “S”. Below, back-scattered electron images of both cortical (b) and cancellous bone (c) with the same scale in both images. The grey-level indicates the proportion of back-scattered electrons and is a measure for the local content of calcium phosphate mineral. In living bone the smaller holes (one of them marked in (b) and (c) by a black arrow) contain osteocytes. The scanning electron image in (d) reveals the lamellar arrangement and shows a hole formerly occupied by an osteocyte (“OC”). The white arrow indicates a canalculus connecting osteocytes. The inset shows a pack of mineralized collagen fibrils sticking out of a fracture surface, thus revealing the fibrous character of the material. Scanning electron micrographs used in this figure were kindly given to the authors by Paul Roschger (Ludwig Boltzmann Institute of Osteology, Vienna, Austria) (from [48] with permission).

smaller black spots can be observed in Fig. 8b and c (two marked by arrows). These are the remnants of bone cells called osteocytes, living completely encased in bone material and connected to each other and to the exterior by thin channels called canaliculi. A common hypothesis is that the osteocytes sense the mechanical deformation of bone and thus, play a crucial role in the permanent adaptation process of bone (see Section 6.2) The struts (or trabeculae) of trabecular bone (Fig. 8c) show some osteocyte lacunae (arrow), however, they generally do not contain osteons (which would normally be larger than the

thickness of individual trabeculae). The trabeculae are fully surrounded by bone marrow which contains blood and therefore, the nutrients needed by the osteocytes inside the bone material as well as by the bone cells sitting on the surface of trabeculae. Fig. 8d reveals a lamellar structure which is a very common motif in bone material. Indeed, bone is a composite of collagen fibers reinforced with calcium phosphate particles. Based on scanning and transmission electron microscopy, it has been proposed that the arrangement in lamellar bone corresponds to a rotated plywood structure, where the fibers are parallel within a thin sub-layer and where the fiber direction rotates around an axis perpendicular to the layers [51,52]. Examples for lamellar bone are osteons in cortical bone [53,54] (see Section 4.2). The origin of the rotated plywood structure could be a twisted-nematic (or cholesteric) liquid crystalline arrangement of collagen [55–57]. A twisted plywood structure has also been reported for teleost scales [58]. The arrangement of mineral particles in human trabecular bone, based on position-resolved pole-figure analysis [59] and scanning small-angle scattering [60–62] appears to be somewhat different compared to cortical lamellar bone. The particle arrangement does not reflect a rotated plywood structure (such as in cortical bone), but rather corresponds to a fiber texture, where all the mineral platelets are arranged parallel to a common direction (corresponding to the fiber direction of collagen). This common direction exhibits some distribution and is defined roughly within  $\pm 30^\circ$  [59].

At the lower levels of hierarchy, bone is a composite of collagen and mineral nanoparticles made of carbonated hydroxyapatite. Structure and properties have been reviewed recently [48]. The organic matrix of bone consists of collagen and a series of non-collagenous proteins and lipids. Some 85–90% of the total bone protein consists of collagen fibrils [63]. The mineralized collagen fibril of about 100 nm in diameter is the basic building block of the bone material (the inset in Fig. 8d clearly reveals the fibrillar nature of the tissue in a fracture surface). The fibrils consist of an assembly of 300 nm long and 1.5 nm thick collagen molecules, which are deposited by the osteoblasts (bone forming cells) into the extracellular space and then self-assemble into fibrils. Adjacent molecules with the fibrils are staggered along the axial direction by  $D \approx 67$  nm, generating a characteristic pattern of gap zones with 35 nm length and overlap zones with 32 nm length within the fibril [64] (Figs. 9 and 11). This banded structure of the fibril was demonstrated by TEM methods [65] and by neutron scattering [66]. Collagen fibrils are filled and coated

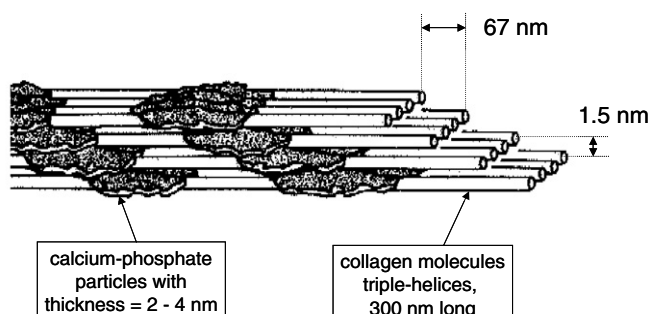


Fig. 9. The mineral crystals are arranged parallel to each other and parallel to the collagen fibrils in the bone composite, in a regularly repeating, staggered arrangement [65,67,83]. The staggering of the crystals is most likely due to the nucleation of mineral particles inside the gap zone of collagen fibrils (see Fig. 11).

by tiny mineral crystals. These crystals are mainly flat plates [67] and are mostly arranged parallel to each other and to the long axis of the collagen fibrils. Crystals occur at regular intervals along the fibrils, with an approximate repeat distance of 67 nm [68], which corresponds to the distance by which adjacent collagen molecules are staggered (Fig. 9). Crystal formation is triggered by collagen or – more likely – by other non-collageneous proteins acting as nucleation centers [69]. After nucleation, the crystals are elongated, typically plate-like [67,70,71], but extremely thin and they grow in thickness later [62,72]. In bone tissue from several different mammalian and non-mammalian species, bone mineral crystals have a thickness of 1.5–4.5 nm [48,72–77]. The size and shape of mineral particles in bone tissue are mainly analyzed by transmission electron microscopy [65,67,71,78] and small-angle X-ray scattering [60,72,77,79–81]. The basic hydroxyapatite mineral of bone –  $\text{Ca}_5(\text{PO}_4)_3\text{OH}$  – often contains other elements that replace either the calcium ions or the phosphate or hydroxyl groups, one of the most common occurrences being the replacement of the phosphate group by a carbonate group [46,48]. In addition to crystals embedded in fibrils, there is also extrafibrillar mineral [76], which probably coats the 50–200 nm thick collagen fibrils [82].

Neutron scattering experiments [84] also showed that the equatorial spacing between collagen molecules,  $d$ , is about 1.6 nm in non-mineralized wet fibrils, whereas in dried conditions the spacing of the molecules is reduced to 1.1 nm. In mineralized wet bone, an intermediate  $d$  value of 1.25 nm was found. Comparison of computer modeling and SAXS experiments confirmed the process of closer packing of the collageneous molecules when clusters of mineral crystals replace the water within the fibril [79]. Fig. 10 illustrates this scenario: When the packing density of molecules increases due to water loss from drying, the typical lateral spacing between molecules in the fibrils decreases from about 1.6 to 1.1 nm (Fig. 10a–c). If the water in Fig. 10a is replaced by mineral, the results may be a situation such as shown schematically in Fig. 10d. The growing mineral particles compress the molecule packets between them, effectively reducing the molecular spacing to the value

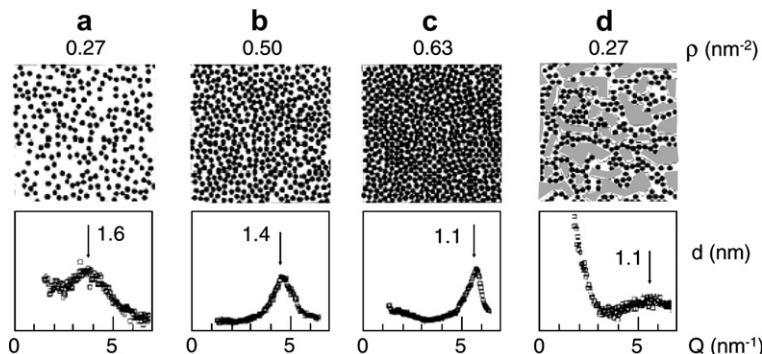


Fig. 10. Equatorial diffuse X-ray scattering peak showing the spacing of collagen molecules as a function of water content (decreasing from fully wet in (a) to fully dry in (b)). The black circles symbolize collagen molecules in the cross-section of a fibril.  $\rho$  is the number of collagen molecules per unit surface in the fibril cross-section. The mineral particles are elongated in the direction perpendicular to the page plane (which corresponds to the horizontal axis in Fig. 9) and are needle or plate shaped. Note that the number of molecules in (d) is about the same as in the fully wet case (a). The average spacing  $d$  between molecules as determined from the peak of the X-ray scattering data is about the same in mineralized and in dry fibrils [79].

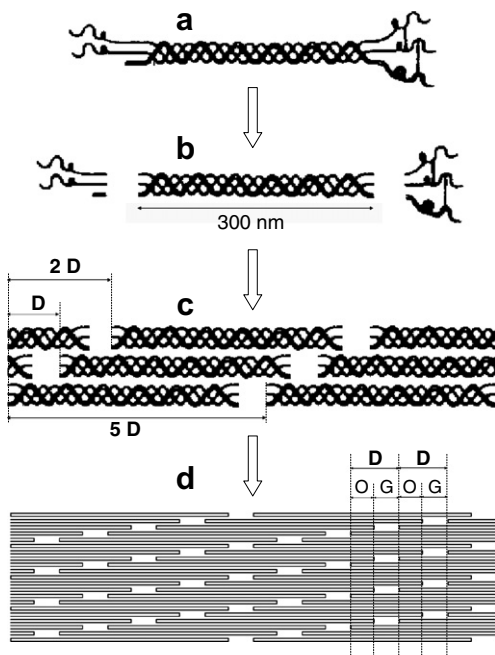


Fig. 11. Self-assembly of collagen fibrils (after [86]). (a) Procollagen molecule after excretion from the cell. (b) Collagen after cleavage of the propeptide ends. (c) Parallel self-assembly with a staggering period of  $D$ . (d) Periodic density variation along the fibril axis, resulting from the staggering. In the stripes labeled O, there is an overlap of all molecules. In the stripes labeled G (gap region), one molecule out of five is missing and the density is accordingly smaller.

in dry tendon. The peak at 1.1 nm is, however, much lower and broader in the fully mineralized fibril (Fig. 10d) than in a dry fibril (Fig. 4c), because the size of the islands with dense packing of collagen molecules is much smaller. Hence, the mineralized fibril has an average density of collagen molecules similar to the wet fibrils, but a typical molecular spacing similar to the dry fibril.

Collagen type I is a major constituent not only of bone but of many biological tissues, including tendon, ligaments, skin or cornea. As already mentioned, collagen molecules are triple helices with a length of about 300 nm. Collagen molecules assemble within the cell to form triple helices. After excretion, the globular ends are cleaved off by enzymes and the 300 nm long triple-helical (apart from short telopeptide ends) molecules remain [85,86]. These molecules then undergo a self-assembly process leading to a staggered arrangement of parallel molecules (Fig. 11), with a periodicity of  $D = 67$  nm. Gap regions appear as a consequence of this staggered arrangement of collagen molecules within fibrils [64,87,88] since the length of the molecules (300 nm) is not an integer multiple of the staggering period  $D$ . Hence, molecules have a length of a little less than  $5D$  periods ( $5 \times 67$  nm = 335 nm), leaving a gap of about 35 nm to the next molecule in axial direction (Fig. 11). Collagen molecules within fibrils are joined by just a few covalent cross-links, which mature with age [89].

Finally, the collagen I molecule is a large protein with a highly repetitive amino acid sequence based on –Gly–X–Y– (where Gly is glycine and X, Y are often proline and

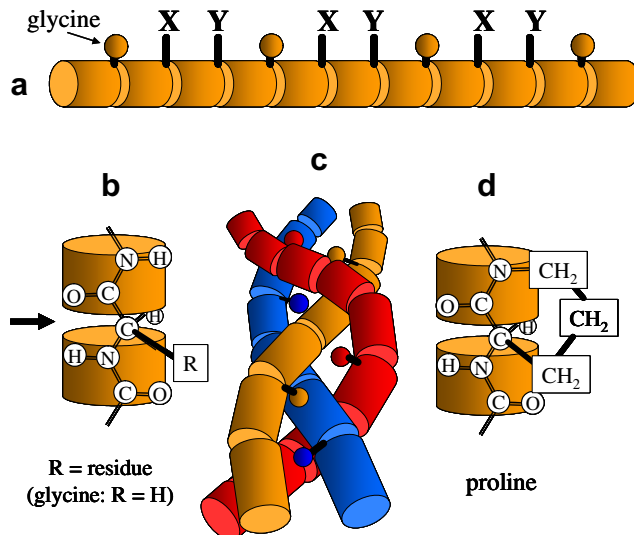


Fig. 12. Periodic repeat in the amino acid sequence of a pro-collagen molecule. (a) Every third residue is a glycine. The remaining residues, X and Y are frequently proline or hydroxyproline. (b) Glycine is the smallest amino acid where the residue is just a hydrogen atom. (c) The triple-helical arrangement requires the glycine residues to point towards the inside of the helix. The other residues are on the surface of the helix. (d) Proline and hydroxyproline have residues connecting back to the polypeptide chain, effectively stiffening the molecule.

hydroxyproline) [90–92]. This repetitive sequence allows three polypeptide chains (called  $\alpha$  chains; type I collagen is composed of two  $\alpha_1$  and one  $\alpha_2$  chains) to fold into a triple-helical structure. The two chains are similar but not identical. Proline and hydroxyproline are the only amino acids where the residue connects back to the nitrogen on the polypeptide chain (see Fig. 12d) thus hindering the rotation between adjacent residues in the chain.

### 2.3. Glass sponge skeletons

Glass is widely used as a building material in the biological world despite its fragility [93–101]. Organisms have evolved means to effectively reinforce this inherently brittle material. It has been shown that spicules in siliceous sponges exhibit exceptional flexibility and toughness compared with brittle synthetic glass rods of similar length scales [93,95]. The mechanical protection of diatom cells is suggested to arise from the increased strength of their silica frustules [94]. Structural and optical properties of individual spicules of the glass sponge *Euplectella*, a deep-sea, sediment-dwelling sponge from the Western Pacific are recently described [96–99]. Not only do these spicules have optical properties comparable to man-made optical fibers, but they are also structurally resistant. The individual spicules are, however, just one structural level in a highly sophisticated, nearly purely mineral skeleton of this siliceous sponge.

Fig. 13a is a photograph of the entire skeletal system obtained from *Euplectella* sp., showing the intricate, cylindrical cage-like structure (20–25 cm long, 2–4 cm in diameter) with lateral (so-called, oscular) openings (1–3 mm in diameter). The diameter of the cylinder and the size of the oscular openings gradually increase from the bottom to the top of the structure. The basal segment of *Euplectella* is anchored into the soft sediments of the

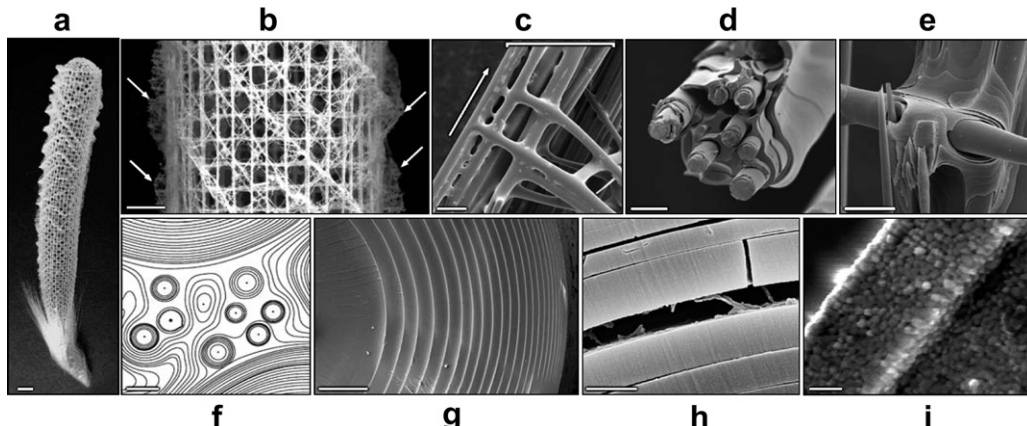


Fig. 13. Structural analysis of the mineralized skeletal system of *Euplectella* (from [97]): (a) Photograph of the entire skeleton, showing cylindrical glass cage. Scale bar (SB) 1 cm; (b) Fragment of the cage structure, showing the square grid lattice of vertical and horizontal struts with diagonal elements arranged in a “chess-board” manner. SB 5 mm; (c) Scanning electron micrograph (SEM) showing that each strut (enclosed by a bracket) is composed of bundled multiple spicules (the arrow indicates the long axis of the skeletal lattice). SB 100  $\mu\text{m}$ ; (d) SEM of a fractured and partially HF-etched single beam revealing its ceramic fiber-composite structure. SB 20  $\mu\text{m}$ ; (e) SEM of the HF-etched junction area showing that the lattice is cemented with laminated silica layers. SB 25  $\mu\text{m}$ ; (f) Contrast-enhanced SEM image of a cross-section through one of the spicular struts revealing that they are composed of a wide range of different-sized spicules surrounded by a laminated silica matrix. SB 10  $\mu\text{m}$ ; (g) SEM of a cross-section through a typical spicule in a strut showing its characteristic laminated architecture. SB 5  $\mu\text{m}$ ; (h) SEM of a fractured spicule, revealing an organic interlayer. SB 1  $\mu\text{m}$ ; (i) Bleaching of biosilica surface reveals its consolidated nanoparticulate nature. SB 500 nm.

sea floor and is loosely connected to the rigid cage structure, which is exposed to ocean currents and supports the living portion of the sponge responsible for filtering and metabolite trapping [100]. The characteristic sizes and construction mechanisms of the *Euplectella* sp. skeletal system are expected to be fine-tuned for these functions.

At the macroscale, the cylindrical structure is reinforced by external ridges that extend perpendicular to the surface of the cylinder and spiral the cage at an angle of 45° (shown by arrows in Fig. 13b). The pitch of the external ridges decreases from the basal to the top portion of the cage. The surface of the cylinder consists of a regular square lattice composed of a series of cemented vertical and horizontal struts (Fig. 13b), each consisting of bundled spicules aligned parallel to one another (Fig. 13c), with diagonal elements positioned in every second square cell. Cross-sectional analyses of these beams at the micrometer scale reveal that they are composed of collections of silica spicules (5–50  $\mu\text{m}$  in diameter) embedded in a layered silica matrix (Fig. 13d–f). Higher solubility of the cement when treated with hydrofluoric acid (HF), compared to the underlying spicules, suggests that the cement is composed of more hydrated silica (Fig. 13d and e). The constituent spicules have a concentric lamellar structure with the layer thickness decreasing from ca. 1.5  $\mu\text{m}$  at the center of the spicule to ca. 0.2  $\mu\text{m}$  at the spicule periphery (Fig. 13g). These layers are arranged in a cylindrical fashion around a central proteinaceous filament and are separated from one another by organic interlayers (Fig. 13h). Etching of spicule layers and the surrounding cement showed that at the nanoscale the fundamental construction unit consists of consolidated hydrated silica nanoparticles (50–200 nm in diameter) (Fig. 13i).

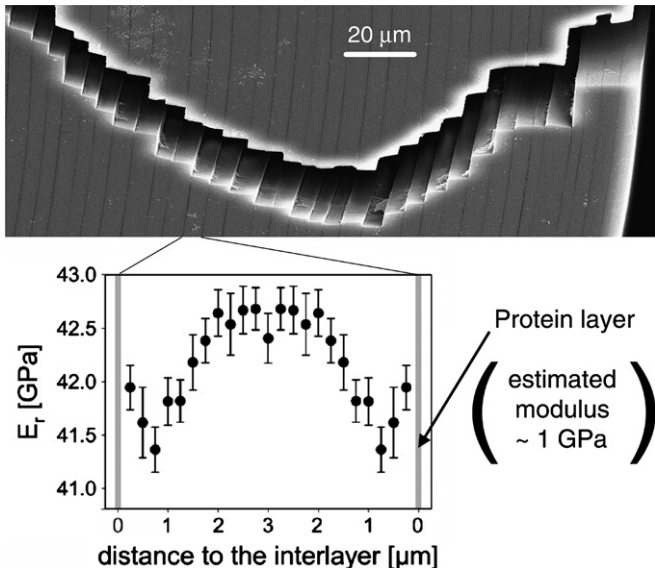


Fig. 14. Spatial variation of the nanoindentation modulus in glass layers of a spicule of *M. chuni* (from [96]).

Another example of biogenic glass with outstanding mechanical properties is the spicule of *M. chuni* which can be several meters long [96]. This spicule is also made of concentric, a few micrometer thick glass layers separated by much thinner protein layers (Fig. 14). The glass itself is colloidal and is half as stiff (see Fig. 14) as technical quartz glass, with a Young's modulus in the range of 80 GPa [96]. The layered structure of the glass deviates cracks (Fig. 14) and, therefore contributes to the extraordinary fracture resistance of those spicules.

### 3. Anisotropic cellular structures

#### 3.1. Natural cellular structures and Wolff's law

The use of cellular structures allows a material to have good mechanical properties at low weight [14]. Nature adopts this advantageous strategy on numerous occasions in biological systems like wood, bone, cork, plant stems, glass sponges, and bird beaks. In situations where there is a preferred loading direction, like the vertical direction of gravity in a tree trunk or along the spine in human vertebral bone, the cellular structure is arranged in a specific way to make a more efficient use of its material. Although, for example, the structure of trabecular bone inside a human vertebra visually resembles food foams like meringues, they enclose in their structures mechanical ideas that humans use in the construction of gothic cathedrals or truss structures like the Eiffel tower, i.e., placing the material at positions where it is mechanically needed. In its most sophisticated form, natural cellular structures are even able to adapt their architectures to changing mechanical environments (see Section 6 for a detailed discussion).

The influencing factors for the mechanical performance of a cellular structure are apparent density, the architecture and the underlying material properties [14] (in case of

“dynamic” cellular structures like trabecular bone also remodeling parameters have to be considered [102]). Although not the case in natural cellular structures, in model calculations the material properties are typically assumed to be as simple as possible, i.e., a linear elastic and isotropic material. The apparent density is defined as the ratio between the density of the cellular solid and the density of the material,  $\rho^*/\rho_s$  (with the star (\*) referring to properties of the overall cellular solid, and the subscript s to the material), which is equivalent to the volume fraction the material occupies. The main influencing factors referring to the structure can be characterized as “how much material is there” (density) and “how this material is arranged” (architecture). Studying regular cellular structures and assuming a prevalent mode of deformation and failure, respectively, Gibson and Ashby [14,31] obtained simple power-law relations between the density of the cellular solid and its mechanical properties, i.e. elastic modulus  $E^*$  and strength  $\sigma^*$ ,

$$\frac{E^*}{E_s} = C_E \left( \frac{\rho^*}{\rho_s} \right)^{v_E} \quad \text{and} \quad \frac{\sigma^*}{\sigma_s} = C_\sigma \left( \frac{\rho^*}{\rho_s} \right)^{v_\sigma}. \quad (1)$$

For a three-dimensional cellular structure they predict that the exponent for the elastic modulus is equal to 3 when bending is the prevalent mode of deformation. For strength, the predicted exponent should equal 2 when assuming failure by elastic buckling, while failure by the formation of plastic hinges or by brittle crushing results in an exponent  $v_\sigma = 3/2$ . Differences in the architecture should only enter in the prefactors  $C_E$  and  $C_\sigma$ , respectively. The influence of architecture is explored using rapid prototyping techniques to produce cellular polymer structures all with the same density, but different regular architecture [103] (Fig. 15). Compression testing of the samples reveal a variation in stiffness and strength by a factor of three, while the ratio between them was nearly constant in agreement with the above considerations,  $\frac{\sigma^*}{E^*} = \frac{C_\sigma}{C_E} = \text{const}$ .

Beside completely regular cellular structures, random cellular structures and their structure–property relationships are also of interest, in particular due to their high technological importance (see e.g. [104] for aluminum foams and [105] for cellular ceramics).

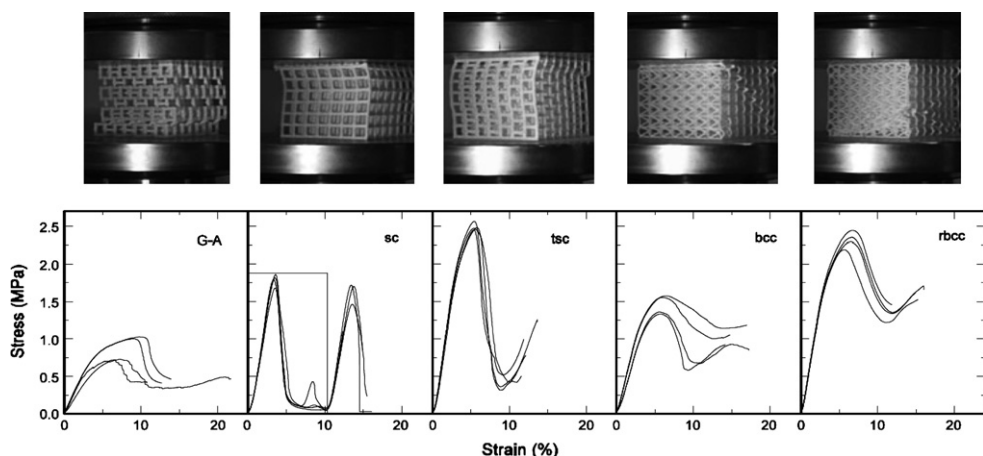


Fig. 15. Pictures of the deformed structures in a compression test and corresponding stress strain curve. The structures made of polyamide had a side length of 5 cm; G-A Gibson–Ashby structure [14], sc simple cubic, tsc translated simple cubic, bcc body centered cubic, rbcc reinforced bcc (from [103] with permission).

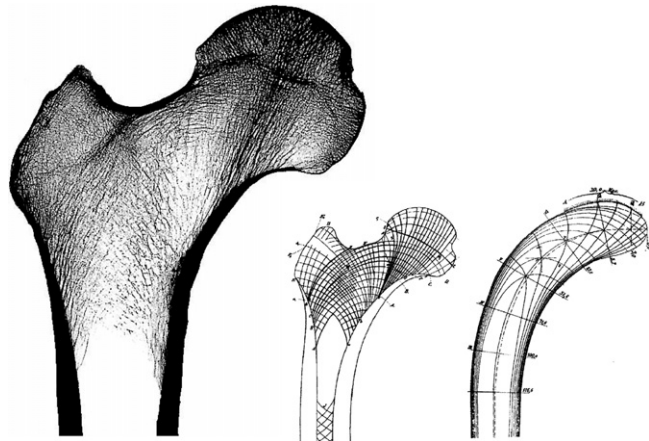


Fig. 16. Trabecular architecture in the mid-frontal section of the proximal femur (left). To the right comparison between a sketch of the trabeculae by the anatomist Meyer and the trajectories of principal stresses in a crane model analyzed by Culmann in the second half of the 19th century (adapted from [107]).

Classical theoretical models to produce random cellular solids use Voronoi tessellations or level-cut Gaussian random fields [16,106]. Tests of open-cell random cellular solids of low density using the finite-element method also resulted in a power law of elastic modulus as a function of density Eq. (1), but exponents vary in a wide range between 1.3 and 3 [106].

The architecture of many natural cellular solids is neither completely regular nor random. The arrangement of the bone material inside a human femur is a beautiful example of an anisotropic cellular architecture (Fig. 16). The comparison of an anatomist's sketch of the course of the trabeculae with an engineer's calculation of the stress trajectories in a similarly shaped crane under comparable loading (Fig. 16) demonstrate striking similarities. It is "obvious" that the specific trabecular orientation fulfills a mechanical function, but after more than 100 years a stringent formulation of the mechanical principle to explain the trabecular architecture is still missing. The original formulation of the so-called Wolff's law which states that the trabeculae embody the stress trajectories does not make sense [108]. This formulation is based on a comparison of two conceptually different objects, the real cellular bone structure and a continuous elastic object of the same shape, both loaded in the same way. The appearance of a good agreement (Fig. 16) stems to a large part from selecting the "right" stress trajectories from the infinite number of stress trajectories [108]. A lot of research focused on finding an optimization principle that bone follows, or in a more elegant formulation it was asked: "If bone is the answer, then what is the question?" [107]. A major problem in all these studies is that bones are subjected to varying loads in daily life, and details of these loads are still unknown. Since bone is a living material which is constantly remodeled, the trabecular architecture can adapt itself to changes in external loading. Instead of searching for global optimization principles, a more appropriate approach seems to look for local regulation principles, which are based on mechanical principles (see Section 6.2). From this point of view, the correspondence of trabecular architecture and stress trajectories is only a by-product of a mechanically regulated renewing process [107].

Recent technological progress allows new methods of investigating the structure–property relations of natural cellular solids. Microcomputed tomography ( $\mu$ -CT), in particular using synchrotron radiation, can be used to image the three-dimensional structure of trabecular bone non-destructively with a spatial resolution of a few micrometers. The combination of these new imaging techniques with simultaneous mechanical testing seems particularly promising [109]. The  $\mu$ -CT data can be used as input for a fabrication of a (up-scaled) plastic model using rapid prototyping techniques or a computational finite-element model. Using microfinite-element analyses and parallel supercomputers, the trabecular load distribution inside a whole vertebra could be analyzed [110]. Both model approaches, rapid prototyping and finite-element models share similar disadvantages and advantages. They both neglect the complex material properties the cellular structure is made of. This can be even seen as an advantage since it allows the separation of the influence of material and architecture. While a mechanical test leading to fracture can be performed, for example, on a real bone sample only once, mechanical testing on many identical rapid prototyping models and *in silico* models enable a much more precise characterization of the mechanical properties as a function of architecture.

### 3.2. The cellular structure of wood

In Section 2.1 spruce wood is introduced as a cellular solid consisting of long prismatic cells, the tracheids (Fig. 2). The common orientation of the cells introduces a strong geometric anisotropy which is also reflected in its mechanical properties. The stiffness and strength of wood is much higher along the long axis of the cells than perpendicular to this direction [111]. From simple regular arrays of honeycomb-shaped cells, one obtains for the power-law relation Eq. (1) between elastic modulus and density an estimated exponent of 1 for on-axis loading, and 3 for perpendicular loading [14]. This different mechanical behavior is well supported by mechanical test of wood of different apparent densities [14]. A further result of the alignment of the tracheids is that wood has a lower compressive than tensile strength. This strength asymmetry can be important, for example, in wood in the stem loaded under compression. To compensate for this natural weakness, the wood cells are under some natural tensile pre-stress [4], much like in the man-made pre-stressed (but here compressive) reinforced concrete.

To motivate the cellular design of wood, a line of argumentation is used that will reappear in more detail in Section 4.3. The function of the stem of a tree is to help the leaves be exposed to sunlight. Therefore, the stem should be as high as possible, but with the lowest amount of mass possible to minimize energetic costs [112,113]. These two requirements come into conflict since the mechanical stability of the stem has to be guaranteed. For a cylindrical stem of diameter  $D$ , height  $H$  and mass  $m$ , (see Fig. 30) and considering buckling under the gravitational load of its own weight as a failure criterion, the classical Euler criterion reads [114],

$$H < 2.8 \sqrt{\frac{E^* I}{mg}}, \quad (2)$$

where the moment of inertia for a circular cross-section is  $I = \pi D^4/64$  and the mass expressed as a function of density  $\rho^*$  and volume,  $m = \pi D^2 H \rho^*/4$ . Eliminating the diameter  $D$ , the stability criterion becomes,

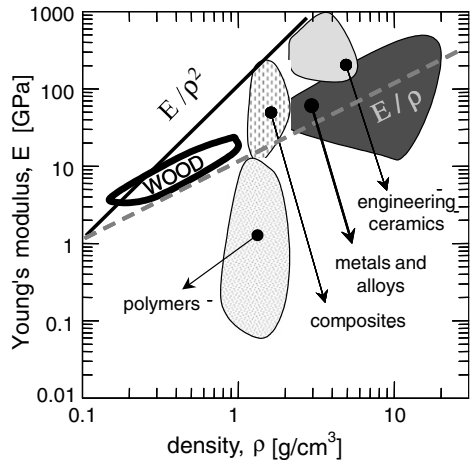


Fig. 17. So-called Ashby map [117] of the elastic modulus versus the density for different materials. The data of similar materials is summarized by regions in the plot. “Wood” refers to the properties of wood along the fiber direction.

$$H^4 < 0.6 \frac{m}{g} \frac{E^*}{(\rho^*)^2}.$$

For a fixed given mass, the largest height (or equivalently, a given height with the lowest value of the mass) of the cylindrical stem can be achieved with a material having a maximum value for the performance index  $E^*/(\rho^*)^2$  [111,115,116].

In Fig. 17, a schematic materials selection chart [117] is shown which relates the elastic modulus,  $E$ , and the density,  $\rho$ , for some of the main classes of materials. Since both scales are logarithmic, points with constant values of  $E/\rho^2$  fall on straight lines with slope 2. Wood corresponds to the best possible choice for the purpose of building high columns which do not buckle. Even though wood is itself a polymeric material, its mechanical performance for this task is better than typical polymeric materials used in engineering. This advantage in the performance index  $E/\rho^2$  results mainly from its low density (Fig. 17). Using the above mentioned power law for the apparent elastic modulus  $E^*$  with an exponent  $v_E = 1$ , the stability criterion reads,

$$H^4 < 0.6 \frac{m}{g} C_E \frac{E_s}{\rho_s} \frac{1}{\rho^*}.$$

Due to the last term on the right, a tree as “cellular as possible”, i.e., with the least amount of wood material in a given volume would be best in bringing up the leaves to large heights. Further optimization criteria for trees are discussed in Section 4.3.

### 3.3. Trabecular bone

Trabecular bone is the spongy type of bone, which is found in humans, for example, in vertebral bodies and near the end of long bones (see Fig. 8). The porous space left free by the bone material is filled with marrow and living cells. A typical dimension of the micro-structure is defined by the thickness of one of the strut-like elements, a trabecula, which is

about 200 µm. Although the material of a bone lamella is similar to cortical bone, its organization is not in cylindrical sheets forming “overlapping osteons” (see Section 4.2), but rather in a simply layered structure forming “overlapping” bone packets as a result of ongoing remodeling (see Section 6.2). The bone in a newly deposited packet is unmineralized, with time it increases its mineral content, thereby changing the mechanical properties from tough to stiff. On the hierarchical level of the tissue material trabecular bone therefore can be described as a patchwork of bone packets of different mineral content. This material heterogeneity defined by a frequency distribution of the mineral content, however, remains almost unchanged in healthy humans [50]. On the level of the nanocomposite between collagen fibrils and mineral particles it is shown that the main orientation of both collagen fibrils and mineral particles follows quite closely the orientation of trabeculae [59,60,62].

A better understanding of the mechanical properties of trabecular bone is of particular importance regarding an assessment of bone fracture risk. Fractures, specifically in connection with bone disorders like osteoporosis, occur frequently in regions of trabecular bone, like spontaneous collapses of vertebrae or fracture of the femoral neck. In the following, stiffness, strength and damage properties of trabecular bone are reviewed.

During daily activities, the strains in bone are usually below 0.3%. In this strain range, trabecular bone can be described approximately [118] as a linear elastic material. Viscoelastic contributions have their origin in the viscous flow of the marrow in the pore space and in the viscoelastic properties of the bone material itself. For physiological strain rates, viscoelastic effects are small [119].

To define elastic properties on the level of a whole bone specimen, i.e., the apparent level, trabecular bone is described as a continuum material, where the properties are defined as the average over a representative volume. For trabecular bone the linear dimension of this representative volume should cover at least the lengths of five trabecular spacings, i.e., roughly 3–5 mm [121]. The number of independent components of the stiffness tensor, which relates the stress and strain tensor in a generalized Hooke's law, depends on the underlying symmetry of the material. Trabecular bone can be well described as an orthotropic material, i.e., with only nine independent parameters [122]. In humans, the on-axis apparent elastic modulus can vary over at least four orders of magnitude, i.e., about 0.3–3000 MPa. Most of these strong variations can be understood on the basis of different volume fraction of bone material. Even the overall morphology can change being more plate-like at high volume fractions and more rod-like at low volume fractions (see Fig. 18). Investigating trabecular bone from different sites in the human skeleton, the data could be fitted by a power law (see Eq. (1)) with a common exponent slightly smaller than 2, but the prefactors differed significantly between different anatomical sites. At a given apparent density, specimens from the proximal tibia and trochanter had higher moduli than those from the vertebral body [123]. A preferred orientation of the trabeculae can be characterized by a fabric tensor. The fabric tensor is defined as a symmetric second rank tensor and can therefore be visualized by an ellipsoid (Fig. 19). The ratio between the eigen-values of the fabric tensor, i.e., between the principal radii of the ellipsoid, is a useful quantity to describe the anisotropy in the bone structure. A standard way to define the fabric is to calculate the mean intercept length when the bone structure is superimposed with “grills” of different orientation (Fig. 19), but also alternative volume-based definitions have been proposed [124,125]. Independent of its specific definition, the fabric and mechanical principal directions are closely related [126]. Assuming orthotropic elasticity,

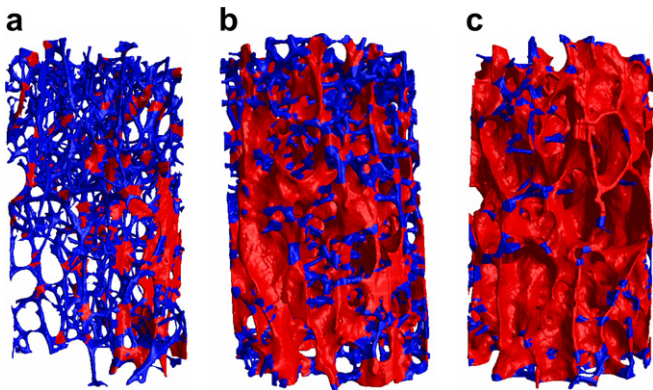


Fig. 18. Different architectures of trabecular bone for varying bone volume fractions: (a) rod-like, (b) rod-plate-like and (c) plate-like. For better visibility rods are colored in blue, plates in red (from [120] with permission).

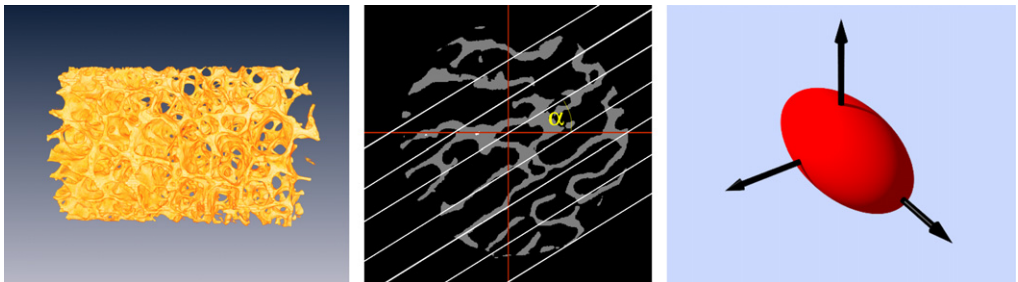


Fig. 19. Three-dimensional architecture of trabecular bone of a proximal tibia determined by microcomputed tomography (left) (by courtesy of P. Saparin, ESA project MAP AO-99-030). The architecture is superimposed with a linear grid (white lines) with different orientation (here only shown for a two-dimensional cross-section, grid rotated by an angle  $\alpha$ ). From the length of the intercepts between grid and bone structure the mean intercept length is calculated. A plot of the mean intercept length as a function of the grid orientation can be well fitted by an ellipsoid, which represents a second-rank fabric tensor.

a relationship between the stiffness tensor and the fabric tensor can be formulated, which include a number of parameters which have to be determined from experiments [127,128].

Still unclear is the role of connectivity on the stiffness of trabecular bone. Studies using microstructural finite-element modeling have found no relationship between stiffness and connectivity [129,130]. Cellular solid theory, however predicts that connectivity plays an important role in the switch from bending dominated architectures, which are soft to much stiffer stretching dominated architectures. For three-dimensional cellular structures, the node connectivity should be at least 12 to ensure tensile/compressive deformation in all the struts [131]. In trabecular bone such high connectivities, for example, obtained by trabeculae connecting diagonally nodes in the structure, are not observed. Beside biological reasons, the observations can be seen as a result of Wolff's law. The trabeculae are oriented in such a way to be loaded in either compressive or stretching modes.

The failure of trabecular bone is characterized by its strength. Due to a strong linear correlation between elastic modulus and strength [132], the knowledge of the elastic

properties can also be used to predict strength. In the following we restrict the discussion to strength under uniaxial loading, for multiaxial loading criteria see e.g. [133]. Strength is again an anisotropic property. Interestingly, the ratio between longitudinal and transverse compressive strengths in human vertebral bone increases with the loss of bone mass associated with ageing [134]. Concerning the strength-density relation for trabecular bone, a good fit of the experimental data at different skeletal sites is obtained by a power law with an exponent close to 2, although at a specific site, a linear fit seems similarly appropriate [133,135]. According to cellular solid theory [14], an exponent of 2 indicates failure by elastic buckling of struts. Using time-lapsed microcomputed tomographic imaging, such buckling failure of individual trabeculae could be observed [136]. In contrast to the elastic properties, the strength is asymmetric under compressive/tensile loading conditions with a higher strength in compression than tension [137]. Since a similar behavior is known to occur in cortical bone, the reason for this asymmetry in trabecular bone is assumed to come from the material level. The failure behavior of trabecular bone becomes surprisingly simple, when characterized by measures of strain instead of stress [138]. Already the above mentioned strong correlation between strength and elastic modulus indicates a relatively constant failure strain. The yield strain under tensile loading is independent of density around 0.8%, it is slightly higher in compression with a weak tendency to increase with density [137] (Fig. 20). It was concluded that this uniformity of yield strains in trabecular bone is again a manifestation of Wolff's law, i.e., a highly oriented architecture that minimizes bending [139].

An important question in connection with osteoporotic bone fractures is how, for a given trabecular architecture, strength is reduced through loss of bone mass. Two different mechanisms of bone loss can be assumed: a uniform thinning of all the trabeculae or a complete removal of individual struts. Different computational studies on idealized model structures demonstrate that a random removal of struts is more detrimental to bone strength than thinning of the struts [140–142]. It is also important to note the consequences of this for treatments, in that a subsequent increase of bone mass to the original

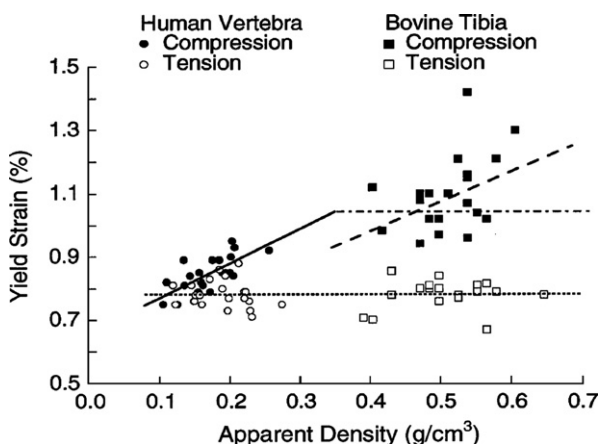


Fig. 20. Comparison between the yield strain of trabecular bone of a human vertebra and a bovine tibia as a function of apparent density. While the tensile yield strain is independent of density and anatomic site, the compressive yield strain increases slightly with density. Note the small range of yield strains on the y-axis (from [137] with permission).

value by thickening the remaining struts (corresponding to a current successful drug therapy) does not restore the mechanical properties [129,142]. This indicates that a preservation of the trabecular connectivity should be a major aim of future drug therapies.

When trabecular bone is loaded past its yield point, it shows a residual strain upon unloading to zero stress. On reloading only for very small deformations is the initial modulus regained, but then develops a reduced value for both the elastic modulus and strength. This degradation of mechanical properties can be interpreted as a measure of damage in the specimen. A rather simple concept, also used in classical modeling approaches, is that damage causes a loss of continuity in the material [143,144]. The reduction of the load-carrying area in the material leads to the observed degradation of modulus and strength. Damage can result from high strains, called creep damage, which has to be distinguished from fatigue damage resulting from an accumulation of damage at low strain amplitudes. The clinical relevance of damage stems from the fact that isolated overloads and fatigue, although not resulting in an immediate fracture, can lead as a later consequence to unexpected fractures in daily life activities. Different types of damage can be distinguished even under the optical microscope: cracks of different orientation, shear bands and complete trabecular fractures [145]. More advanced microscopic and spectroscopic techniques allow a direct observation of crack initiation and propagation, see [146,147] for recent reviews. However, the problem of a clear quantification of microdamage still remains open. The fatigue behavior of human trabecular bone under compressive loading was investigated as a function of applied stress amplitude and architecture. The number of cycles to failure can be related to the applied stress normalized by the pre-fatigue elastic modulus by a power law (Fig. 21) [148,149]. Taking into consideration architecture in the form of eigen-values of the fabric tensor, a high correlation of a power-law relationship could be obtained [150]. The observation that such different trabecular bone types like elderly human vertebral and young bovine tibial show very similar fatigue behavior, lead the authors to the conclusion that the dominant failure mechanism in trabecular bone for cyclic loading occurs at the ultrastructural level [148].

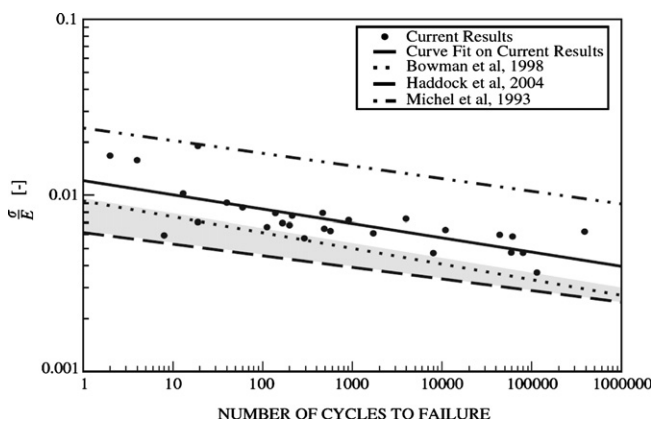


Fig. 21. Relationship between the applied fatigue stresses normalized by the initial elastic modulus and the number of cycles to failure for different studies. Current results refer to [150]. In all studies the samples were kept in wet conditions, but sample geometry, stress frequency (around 2 Hz) and stress protocol (sine-shaped or triangular shaped) were different (from [150] with permission).

#### 4. Building with fibers

Fibers are the most frequent motives in the design of natural materials. They can be based on very different chemical substances, such as sugars, for example. Indeed, the polysaccharides cellulose and chitin are the most abundant polymers on earth. The first reinforces most plant cell walls and the second is found for example, in the carapaces of insects [31]. Other types of strong fibers are based on proteins, such as collagen, keratin or silk. The first is found, for example, in skin, tendons, ligaments and bone, the second in hair or horn. Spider silk is among the toughest polymer filaments known to date [151,152]. Clearly, constructing with fibers requires a special design, as fibers are usually strong in tension, but rather weak in compression (as they have a tendency to buckle). Such design principles are well known in the engineering of fiber composites [15] and it is quite interesting to see how Nature uses some of these principles to construct stiff and tough materials. Some examples are given below.

##### 4.1. Tendon: hierarchies of structure – hierarchies of deformation

The hierarchical structure of tendon is summarized in Fig. 22. Tendon is based on the same type of collagen fibrils as bone, with the difference that tendon is not normally mineralized (with some notable exceptions, like the mineralized turkey leg tendon [153–156]). Collagen fibrils in tendons have a diameter of typically a few hundred nanometers and are

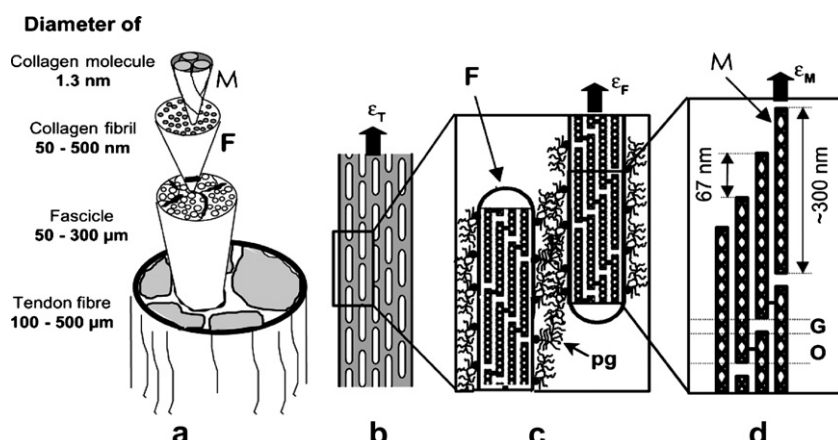


Fig. 22. (a) Simplified tendon structure: tendon is made of a number of parallel fascicles containing collagen fibrils (marked F), which are assemblies of parallel molecules (marked M). (b) The tendon fascicle can be viewed as a composite of collagen fibrils (having a thickness of several hundred nanometers and a length in the order of 10  $\mu\text{m}$ ) in a proteoglycan-rich matrix, subjected to a strain  $\varepsilon_T$ . (c) Some of the strain will be taken up by a deformation of the proteoglycan (pg) matrix. The remaining strain,  $\varepsilon_F$ , is transmitted to the fibrils (F). (d) Triple-helical collagen molecules (M) are packed within fibrils in a staggered way with an axial spacing of  $D = 67 \text{ nm}$ , when there is no load on the tendon. Since the length of the molecules (300 nm) is not an integer multiple of the staggering period, there is a succession of gap (G) and overlap (O) zones. The lateral spacing of the molecules is around 1.5 nm. The full three-dimensional arrangement is not yet fully clarified, but seems to contain both regions of crystalline order and disorder [56,157,158]. The strain in the molecules,  $\varepsilon_M$ , may be different from the strain in the fibril,  $\varepsilon_F$  (from [33] with permission).

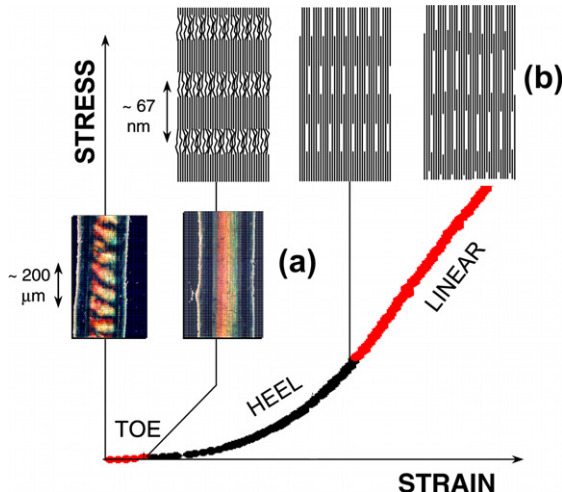


Fig. 23. Schematic behavior of the normal collagen fibril structure from rat tail tendon during tensile deformation (from [166]). The experiment was performed at a strain-rate where the actual strain of the fibril ( $\varepsilon_F$ ) was about 40% of the total strain of the tendon ( $\varepsilon_T$ ) in the linear region. Plotted on the horizontal axis is the total strain of the tendon ( $\varepsilon_T$ ). For an explanation of the three distinct regions (toe, heel and linear) and the underlying deformation at different structural levels see text.

decorated with proteoglycans, which form a matrix between fibrils (Fig. 22b and c). Fibrils are assembled into fascicles and, finally, into a tendon (Fig. 22a).

The outstanding mechanical properties of tendons are due to the optimization of their structure (see Fig. 22) on many levels of hierarchy [159–161]. One of the challenges is to work out the respective influence of these different levels. A sketch of the stress–strain curve of tendon is shown in Fig. 23. Most remarkably, the stiffness increases with strain up to an elastic modulus in the order of 1–2 GPa. The strength of tendons is typically around 100 MPa. Moreover, tendons are viscoelastic and their deformation behavior depends on the strain rate as well as on the strain itself. The maximum strain reaches values in the order of 8–10% for slow stretching. *In vivo*, it is very likely that tendons are always somewhat pre-strained (even if the muscles are at rest). Hence, they are normally working in the intermediate (“heel”, see Fig. 23) and high modulus regions [8]. In this context, it is also interesting to compare the maximum stress generated in muscle (in the order of 300 kPa) to the strength of tendon which is about 300 times larger. This explains why tendons and ligaments can be much thinner than muscle.

The stress/strain curve of tendons usually shows three distinct regions [8], which can be correlated to deformations at different structural levels (Fig. 23). In the “toe” region, at small strains, a very small stress is sufficient to elongate the tendon. This corresponds to the removal of a macroscopic crimp of the fibrils [162] visible in polarized light (Fig. 23, left). In the second region, at higher strains (Fig. 23, center), the stiffness of the tendon increases considerably with extension. An entropic mechanism, where disordered molecular kinks in the gap region of collagen fibrils are straightened out, has been proposed to explain the increasing stiffness with increasing strain [163]. When all the kinks are straightened however, another mechanism of deformation must come into play in order to explain the linear dependence of stress and strain in this region of the force-elongation curve

(Fig. 23, right). The most likely processes are thought to be the stretching of the collagen triple-helices and the cross-links between the helices, implying a side-by-side gliding of neighboring molecules, leading to structural changes at the level of the collagen fibrils. This has previously been investigated by use of synchrotron radiation diffraction experiments [164–170]. By monitoring the structure factors of the second and third order maxima, it can be shown that the length ratio of the gap to the overlap region may increase during stretching by as much as  $\sim 10\%$ , implying a considerable gliding of neighboring molecules [165,166]. In addition, the triple-helical molecules can be slightly stretched as well, leading to a change of the helix pitch [167,169].

The main results of these investigations, in which simultaneous tensile testing and synchrotron X-ray diffraction characterization are employed, can be summarized as follows:

- The extension of collagen fibrils inside the tendon is always considerably less than the total extension of the tendon [166]. Typically, the strain of the fibrils,  $\varepsilon_F$ , is less than half that in the whole tendon,  $\varepsilon_T$ . This indicates that considerable deformation must occur outside the collagen fibrils, presumably in the proteoglycan-rich matrix [172], which mediates deformation by shearing between fibrils (Fig. 22c).
- In normal collagen, the ratio between the extension of the fibrils and of the tendon increases with the strain rate [171] (Fig. 24). This indicates that most of the viscous deformation is due to the viscosity of the proteoglycan matrix. The (mature) collagen fibrils can be considered as mostly elastic at sufficiently large strains.
- In cross-linked deficient collagen, the ratio between the extension of the fibrils and of the tendon decreases with the strain rate [171] (Fig. 24). The appearance of a plateau in the load/extension curve indicates pronounced creep behavior. Therefore, additional slippage of molecules or sub-fibril-structures may result from the absence of covalent cross-linking between molecules in the fibrils. This indicates that collagen cross-links are crucial in determining the stiffness of the fibrils, remaining in agreement with earlier studies [173–177]. The mechanical behavior of cross-link deficient collagen is in this respect somewhat similar to immature collagen, where lower fracture stress and enhanced creep behavior are also observed [178].

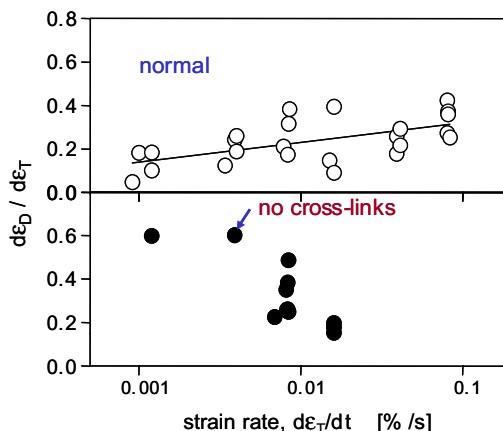


Fig. 24. Strain-rate dependence of the ratio of fibril elongation  $d\varepsilon_D$  to tendon elongation  $d\varepsilon_T$  [171].

Recent modeling work suggests that the design of collagen fibrils in a staggered array of ultralong tropocollagen molecules provides large strength and energy dissipation during deformation. The mechanics of the fibril can be understood quantitatively in terms of two length scales, which characterize when, firstly, deformation changes from homogeneous intermolecular shear to propagation of slip pulses, and when, secondly, covalent bonds within the tropocollagen molecules start to fracture [179]. Single molecule experiments on (type I) collagen molecules employing atomic force microscopy [180,181] or optical tweezers [182] and fitting the data with a worm-like chain model [183], resulted in a persistence length of about 15 nm [182], a value close to the predictions of atomistic simulation of (type XI) collagen molecules [184]. These results confirm that collagen molecules are flexible rather than rigid, rod-like molecules [182].

#### 4.2. The osteon in bone

Mineralized fibrils in cortical bone self-assemble into fibril arrays (sometimes called fibers) on the scale of 1–10  $\mu\text{m}$ . While a diversity of structural motifs exist between bone tissues [46], the most common in bone is the lamellar unit [52,57]. A lamella refers to a planar layer of bone tissue, around 5  $\mu\text{m}$  thick, which is found in a repetitive stacked arrangement in both trabecular (cancellous) and osteonal (compact) bone. In what follows, we consider lamellae belonging to the cylindrical secondary osteon (see also [185]). The secondary osteon is the basic building block of compact bone, and is essentially a hollow cylindrical laminate composite ( $\sim 200 \mu\text{m}$  in diameter) surrounding a blood vessel traversing the outer shaft of long bones (Fig. 25).

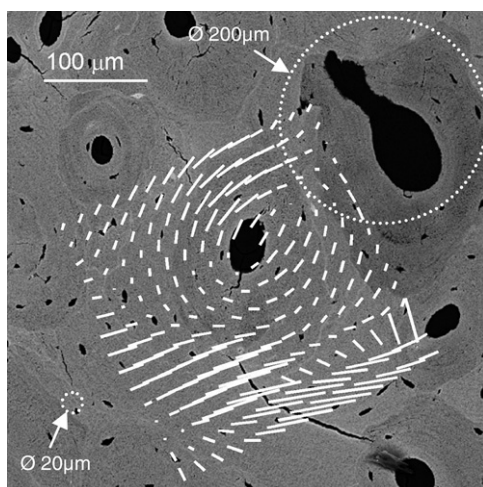


Fig. 25. Orientation of mineral particle around an osteon in human compact bone (from [81]). The black ellipse in the center is the trace of a blood vessel and there are concentric layers of bone lamellae around it, forming the osteon. Several osteons are visible on the back-scattered electron image (BEI). The bars are results from scanning-SAXS, obtained at the synchrotron and superimposed on the BEI. The direction of the bars indicates the orientation of mineral platelets, their length the degree of alignment. The specimen thickness and the diameter of the X-ray beam were 20  $\mu\text{m}$  in this case. For comparison, a circle with the radius of 200  $\mu\text{m}$  is shown (dotted line).

While the existence of the lamellar unit in bone has been known for over a century [186], the internal structure of this basic building block and its correlation to mechanical function have remained unclear for a long time. Light microscopic imaging led Ascenzi and co-workers [187–189] to classify lamellae as either (a) orthogonal plywood with alternate layers showing a fibril orientation parallel and perpendicular to the cylindrical axis of the osteon, or (b) unidirectional plywood, with the fibril orientation predominantly parallel or perpendicular to the osteon axis. Electron microscopic analysis by Marie Giraud-Guille and co-workers suggest the existence of a “twisted plywood” structure [57], with fibril orientation ranging continuously over a period of 90° across the width of the lamella. Weiner and co-workers refine this to a “rotated plywood” configuration [52], where the fibrils not only rotate with respect to the osteon axis, but also around their own axis across the width of the lamella. An alternate model suggests that alternate dense and loosely packed fibrils give the impression of lamellar units in bone tissue [190].

Detailed quantitative information on the osteon structure has been obtained with a novel method combining synchrotron X-ray texture measurements with a 1 μm wide beam and scanning of a thin (3–5 μm thick) section of a secondary osteon in steps of 1 μm [185,191,192]. The results are summarized in Fig. 26, which shows the variation of the fibril orientation across and within bone lamellae, with 1 μm spatial resolution. The fiber axis orientation varies periodically with a period of 5 μm corresponding approximately to the width of a single lamella. This implies that each lamella consists of a series of fibril layers oriented at different angles to the osteon axis. What is more surprising is that the angles are always positive, implying that on average each lamellae has a non-zero spiral fibril angle with respect to the long axis of the osteon, with a right-handed helicity.

These results thus show that osteonal lamellae are built as three-dimensional helicoids around the central blood vessel. Such helicoidal structures have been found in other

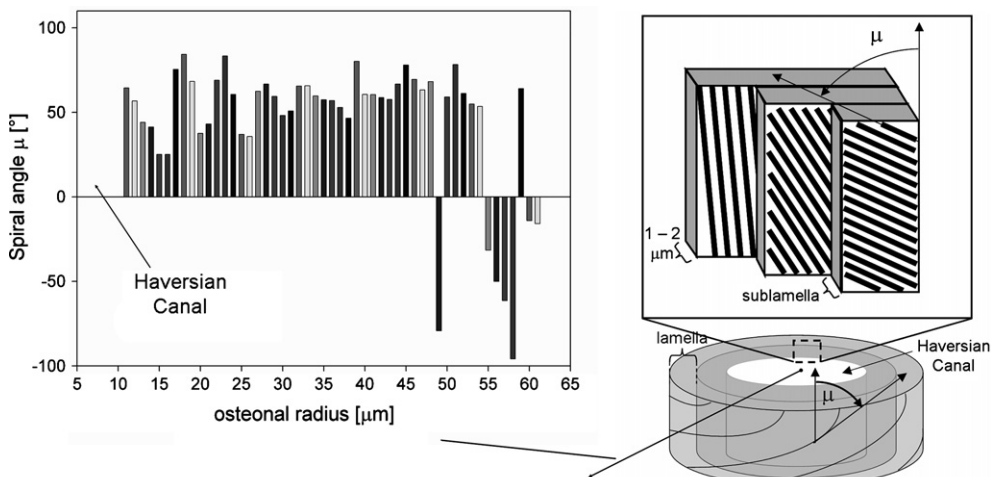


Fig. 26. A model of the fiber orientation inside the lamellae of an osteon (a). The fibers are arranged at different angles inside single lamellae (b). On average they have a positive spiral angle  $\mu$ , implying that on average, the fibers form a right-handed spiral around the osteon axis like a spring. In addition, there is a periodic variation of the spiral angle  $\mu$  across the osteon diameter (c), with a period close to the lamellar width ( $\sim 5 \mu\text{m}$ ). The spiral angle is always positive, except for radii larger than 40 μm when a cross-over to interstitial bone surrounding the osteon occurs (from [185]).

connective tissues, for example in the secondary wood cell wall [34,193] and in insect cuticle [193]. Remarkably, the sense of the helicity (right-handedness) is the same for both the bone osteon and the wood cell wall. Both structures fulfill a similar biomechanical support and protection function – the osteon for the inner blood vessels, and the wood cell wall for the water/nutrient transport within the cambium – indicating that they represent an example of an optimal mechanical design used in two different phyla. Indeed, the helicoidal principle of fiber composite design in biomaterials has been proposed as a major unifying concept across different species [193]. Such a helicoidal structure has biomechanical advantages as well. From a biophysical standpoint, the non-zero average spiral angle means that the osteon is extensible (and compressible) like a spring along its long axis. The elastic extensibility thus imparted would be useful in absorbing energy during *in vivo* mechanical loading, and may help in protecting the sensitive inner blood vessels from being disrupted structurally by microcracks propagating from the highly calcified interstitial tissue through the osteon to the central Haversian canal [194].

Complementary nanomechanical investigations of the local stiffness and hardness of the osteon reveal a modulation of micromechanical properties at the lamellar level [195]. Specifically, the compressive modulus of the sub-lamellae within a single lamella, as measured by nanoindentation, varies from about 17 to 23 GPa, with thin layers of lower stiffness alternating with wider layers of higher stiffness (Fig. 27). Quantitative back-scattered electron imaging (qBEI) is used to determine the local mineral content at the same positions as those measured by nanoindentation. The lower axial stiffness is partly due to the lower stiffness of a fiber normal to its long axis relative to the stiffness along its long axis. However, the results also show that the regions of lower stiffness have a lower mineral content. This implies that the mechanical difference is not merely due to anisotropy but is also linked to a variation in composition. Hence, the differently oriented sub-lamellae have also a different mineral content, with the fibers at a large spiral angle being less calcified. Mechanically, such a modulated structure can serve as a natural example of a crack stopping mechanism. It is known that microcracks are more frequent in the surrounding interstitial bone than in the osteon itself [196]. It can be therefore speculated that the modulated

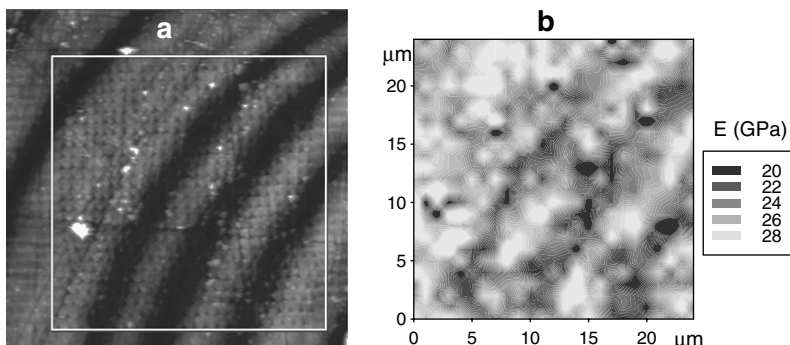


Fig. 27. Two dimensional scanning nanoindentation measurements of local stiffness variations inside bone osteons reveal that the lamellar structure results in a periodic mechanical modulation. (a) Scanning force microscopy (topography) image of a sector of osteon from a polished cross-section through a human femur, with the two-dimensional grid of indents visible (inside the white square). (b) The corresponding two-dimensional plot of indentation modulus  $E$  (stiffness) [195] (from [185]).

structure at the lamellar level acts to trap microcracks from propagating from the interstitial bone to the inner blood vessel. Modulations in yield strength and stiffness have been shown to be effective crack stopping mechanisms in artificial multilayered composites [197–199].

#### 4.3. The microfibril angle in wood

The cellulose microfibril angle (MFA),  $\mu$ , in the wood cell wall (see Section 2.1. and Fig. 28) determines to a large extent the elastic modulus and the fracture strain of wood. When the stiff cellulose fibrils are essentially parallel to the cell axis ( $\mu = 0$ ), the stiffness is largest and the extensibility is rather small and mostly determined by the extensibility of cellulose. Increasing the microfibril angle up to  $\mu = 40^\circ$ , decreases the stiffness by about one order of magnitude and increases the extensibility by about the same factor (Fig. 28) [200,201]. The wood cell behaves like an elastic spring because the stiff cellulose fibrils are wound helically. The steeper the winding angle, the stiffer the wood. This property can be used by the tree to vary considerably the local mechanical properties by growing cells with different microfibril angle. The MFA reflects some seasonal variations in plant growth [38,202]. With the possibilities given by the hierarchical structure, a growing tree can include graded properties into the stem or the branch, according to functional requirements which may change during its lifetime (see examples below and in Section 6.1).

The distribution of microfibril angles is used by the plant to introduce property gradients into the material and to tune the mechanical properties according to needs. A striking example is the distribution of  $\mu$  in the stem. For softwood species (such as spruce or pine) and to some extent also for hardwoods (such as oak), the MFA decreases in older trees from a large value in the pith (about  $40^\circ$ ) to very small values closer to the bark [116,203] (Fig. 29). Similar results are also obtained for a number of other tree species, including eucalyptus [204–206] or birch [207]. Since the stem thickens by apposition of

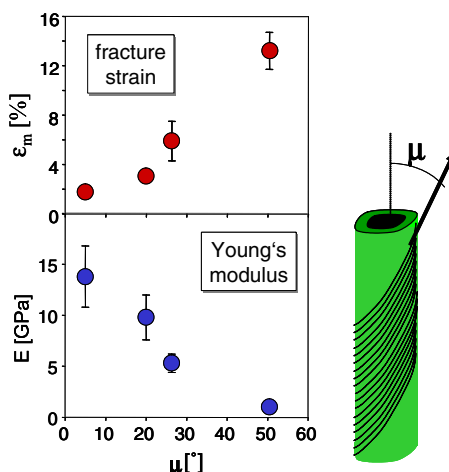


Fig. 28. Fracture strain and tensile Young's modulus of spruce wood as a function of the microfibril angle  $\mu$  (from [201]).

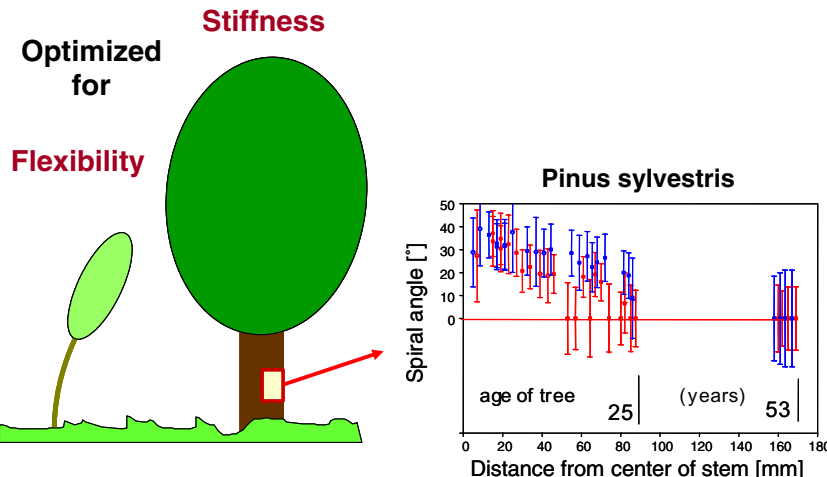


Fig. 29. Microfibril (spiral) angle in the stem of pine, as a function of the distance from the pith (from [116]). Since the annual rings reflect the age of the tree, the data show that young trees have a flexible stem (with a large microfibril angle), while the stem in older trees becomes more rigid with age (with low MFA in the outer annual rings).

annual rings at the exterior, the history of a tree is recorded in the succession of annual rings. Hence, the observation that the MFA decreases from pith to bark indicates that younger trees are optimized for flexibility, while the stem becomes more and more optimized for bending stiffness when the tree gets older (Fig. 29).

A possible explanation for this change in strategy can be a compromise between resistance against buckling (which needs stiffness) and flexibility in bending to resist fracture [116,208].

Three possible loading cases are considered in Fig. 30 approximating the stem as a cylinder of height  $H$  and diameter  $D$  [116]. The first case (left) corresponds to a force  $F_L$  applied laterally to the crown (e.g., by side winds). Under those circumstances, the cylinder (which is firmly attached to the ground) will not fail as long as the height is smaller than the expression given in the figure, which is proportional to the strength  $\sigma_0$  of the material. As a consequence, the possible height of the tree is limited by the strength of the material. What is more, at any given height, failure will not occur as long as the forces remain below the limit of  $2I\sigma_0/DH = 2\pi D^3\sigma_0/32H$ . In order to withstand (rarely occurring) exceptionally high forces, the structure has to be considerably over designed. This is particularly difficult for young trees which still have a small diameter  $D$ , since the limiting force depends on the third power of  $D$ . A second loading case is shown in the center of Fig. 30. Trees with a large crown will experience a vertical load as shown. For such loads, the height of the tree is limited by Euler buckling and, therefore, by Young's modulus  $E$  of the material. This means that a tree carrying a large crown needs above all a stiff material (that is, a small MFA) in the stem to reduce the risk of buckling. This is most probably the explanation why older and, therefore, large trees maximize the stiffness of the tissue, in particular in the outer layers of the stem which are most critical for bending stiffness. Young trees with small stem diameters are again handicapped due to the fact that the critical buckling force scales as  $D^2$ . However, the vertical forces

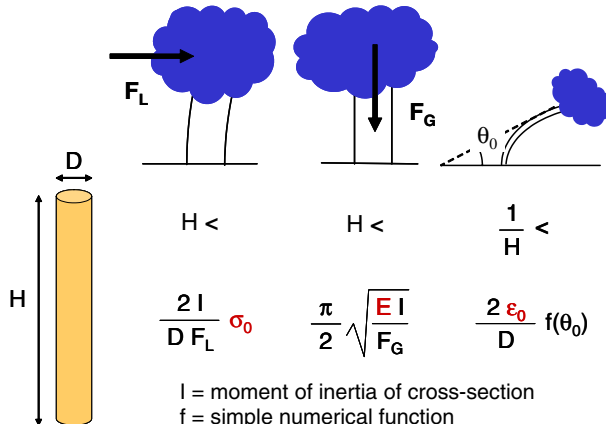


Fig. 30. Model calculations for the failure of a cylinder under lateral (left) or vertical (center) load [116]. To prevent failure for a given load, the height of the cylinder must be smaller than the expression indicated.  $\sigma_0$  and  $E$  are the strength and Young's modulus of the material, respectively. To prevent failure in bending up to a given angle  $\theta_0$  (which could be close to  $0^\circ$ , for example), the height must be larger than the expression indicated ( $\epsilon_0$  is the fracture strain of the material). The moment of inertia  $I$  for a cylinder is given by  $I = \pi D^4/64$ .

(unlike the lateral ones due to wind) are fairly predictable as they depend mainly on the weight of the plant. It seems that young trees are not optimized for this load case, as the large microfibril angle in young trees reduces the modulus  $E$  by more than an order of magnitude (for the importance of the cellular structure of wood for this loading case see Section 3.2). The last case in Fig. 30 (right) assumes that the plant is bending up to a critical angle  $\theta_0$  (of, say,  $0^\circ$ ) in order to escape lateral forces rather than to withstand them. The interesting result is that in order to resist such loading, a minimum (rather than a maximum) height for the stem is required. Indeed, large aspect ratios  $H/D$  are favorable for bending. The limiting material property is now the fracture strain  $\epsilon_0$  (also denoted  $\epsilon_m$  in Fig. 28). Interestingly, the large values of the MFA increase the fracture strain by about an order of magnitude (Fig. 28). This leads us to the conclusion that the change in microfibril angle from young to older tissue (as shown in Fig. 29) might reflect a change in strategy. Young trees (with a small diameter) would then be optimized to escape lateral loads by bending all the way to the ground if needed. When the weight of the crown increases, buckling becomes a more serious issue and the strategy is changed to increase the stiffness of the material in the stem. With this change in strategy, greater heights  $H$  can then be reached without buckling.

This example shows how an extremely simple microstructural parameter, such as the microfibril angle  $\mu$ , can be used by the plant to tune the material properties in a wide range according to the required function. The MFA and the detailed structure of the cell wall not only influence the mechanical properties but also the shrinkage during drying [41,209–212]. This is not surprising since drying introduces internal stresses, and the response to those stresses is governed by the (very anisotropic) mechanical properties of the wood cells. For the technical use of wood, an understanding of the drying behavior is of great importance.

A tight control of cellulose fiber orientation is required at the cellular level to allow the deposition of the cell walls with the right microstructure. Research on cellulose

biosynthesis is very active and progress has been reviewed from different perspectives, e.g., in [213–215]. One of the key features is that plasma membrane bound protein complexes (rosettes) are operational in catalyzing the chain elongation. The chain initiation can occur in a distinct process by means of a specific primer molecule [216]. The so-formed glucan chains are then assembled into cellulose fibrils. The cellulose structure in most plant cell walls is of the well-known type I, but there is generally some variety of possible cellulose structures, which still need clarification. Investigations with high-resolution revealed new structural details in crystals of cellulose I $\beta$  and I $\alpha$  using XRD [217] and AFM [218], respectively. Furthermore, a new type of cellulose aggregation with nematic liquid-crystal like ordering was proposed as a precursor in cellulose assembly [219].

The assembly processes at higher levels of hierarchy, the cell morphogenesis and cell elongation, are still a matter of debate [220]. Current models, which have been reviewed in [221], assume that microtubules are directing the orientation of cellulose microfibrils (and therefore the microfibril angle  $\mu$ ) in the cell wall. Additional evidence for this view has been produced in experiments on the development of cell-wall modifications, such as pits or perforations [222]. Recently, it is shown that the role of the microtubules is better described as a system which provides guidance for the movement of the cellulose synthase complexes [223]. Taking into account geometrical constraints, a self-assembly process resembling the formation of cholesteric liquid crystals has been proposed [224]. Such a spontaneous ordering has the advantage that little biological control is needed for the formation of aligned microfibrils.

## 5. Nanocomposites

Virtually all stiff biological materials are composites with components mostly in the size-range of nanometers. In some cases (plants or insect cuticles, for example), a polymeric matrix is reinforced by stiff polymer fibers, such as cellulose or chitin [8]. Even stiffer structures are obtained when a (fibrous) polymeric matrix is reinforced by hard particles, such as carbonated hydroxyapatite in the case of bone or dentin. The general mechanical performance of these composites is quite remarkable. In particular, they combine two properties which are usually quite contradictory, but essential for the function of these materials. Bones, for example, need to be stiff to prevent bending and buckling, but they must also be tough since they should not break catastrophically even when the load exceeds the normal range. How well these two conditions are fulfilled, becomes obvious in the (schematic) Ashby-map [27–29] in Fig. 31. Proteins (collagen in the case of bone and dentin) are tough but not very stiff. Mineral, on the contrary, is stiff but not very tough. It is obvious from Fig. 31 that bone and dentin combine the good properties of both.

Recent work using *in situ* deformation studies has unveiled some of the mechanisms by which Nature is able to create both stiff and tough composites. This is reviewed in the following sub-sections.

### 5.1. Plastic deformation in reaction wood

A large effort has been undertaken to model the mechanical properties taking into account the composite character of the cell wall of wood [43,44,210–212,225]. The

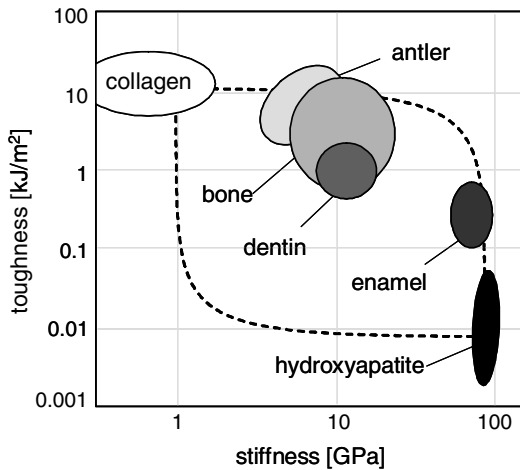


Fig. 31. Typical values of stiffness (Young's modulus) and toughness (fracture energy) for tissues mineralized with hydroxyapatite following the ideas of Ashby and co-workers [27–29]. The dotted lines represent the extreme cases of linear and inverse rules of mixture for both parameters (from [185]).

deformation behavior of plant cells is quite intricate, particularly at large deformations [226–228]. A typical feature of the stress–strain curve is a fairly stiff behavior at low strains followed by a much “softer” behavior at large strains (corresponding to a steep increase followed by a smaller slope of the stress–strain curve, Fig. 32c). The mechanisms underlying this deformation behavior have been studied recently by the diffraction of synchrotron radiation during deformation [45]. Some results of this investigation are shown in Fig. 32. First, the microfibril angle  $\mu$  (see Fig. 28 for a definition of  $\mu$ ) was found to decrease continuously with the applied strain. This relation between microfibril angle and strain turned out to be independent of the stress at any given strain. This is shown by stress relaxation experiments (visible as spikes in Fig. 32c), where both strain and microfibril angle stay constant, while the stress varies.

In the simplest possible picture, the decrease of the microfibril angle is related to a deformation of each wood cell in a way similar to a spring: The spiral angle of the cellulose microfibrils is reduced from  $\mu$  to some smaller value  $\mu'$  and the matrix in-between the fibrils is sheared (Fig. 32b and f). In fact, if it is assumed that the elongation of the cellulose microfibrils is negligible, then the elongation of the cell depends solely on the reduction of the microfibril angle as

$$\text{micro-strain} = d(\cos \mu) / \cos \mu = -\tan \mu d\mu. \quad (3)$$

This expression is plotted in Fig. 32e as a function of the measured macroscopic elongation ( $\varepsilon_{\text{macroscopic}}$ ) of the wood tissue. The graph shows that the wood cells actually extend like an elastic spring, and the fact that the cellulose fibrils are not totally inextensible accounts for the slight deviation between the measured data and the straight line in Fig. 32e.

There is, however, one major difference between the behavior of the wood cell and an elastic spring: indeed – beyond the change in slope in Fig. 32c – the deformation becomes partially irreversible, but without serious damage to the material [45,227]. The model

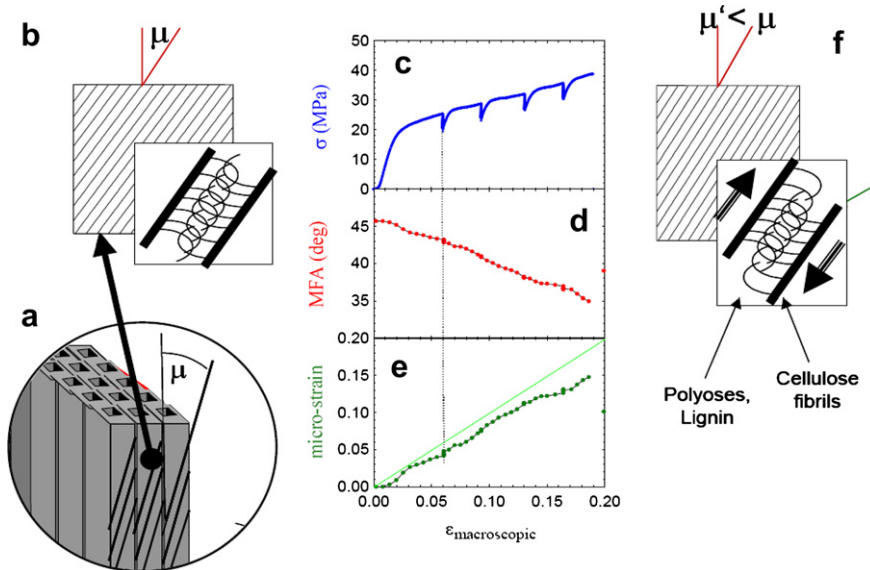


Fig. 32. In situ X-ray diffraction investigation [45] of the deformation of the wood cell wall inside an intact wood section (compression wood of spruce), shown schematically in (a). The dominant cell-wall layer (b) contains cellulose microfibrils tilted with the microfibril angle  $\mu$ . (c) Stress–strain curve during the deformation experiment. The spikes in the graph correspond to stress relaxation experiments, where the elongation was kept constant. (d) Change in microfibril angle during the elongation of the specimen. A microstrain (e) is calculated under the assumption that the cellulose fibrils are rigid and all the deformation is just a tilting of the fibrils and shearing of the matrix in-between (f). The nearly one-to-one correspondence (e) of micro- and macro-strain shows that this is, indeed, the principal mechanism of elongation and that the cellulose fibrils themselves stretch only very little (from [229]).

which can be inferred from the synchrotron diffraction data in Fig. 32 is as follows: When the cell elongates, the microfibril angle decreases and the matrix between the cellulose fibrils is sheared. This corresponds to the initial stiff behavior of the wood cells (initial slope in Fig. 32c). Beyond a certain critical strain, the matrix is sheared to an extent, where bonds are broken and the shearing becomes irreversible. Since some of the bonds are broken, the response is now “softer”. After releasing the stress, the unspecific bonds in the matrix reform immediately (a bit like in a Velcro connection) and the cell is arrested in the elongated position. In such a model, the matrix is not irreversibly damaged even though the cell is irreversibly elongated [45].

An interesting consequence of this deformation behavior is that the (stiff) cellulose fibrils carry most of the load practically without deformation, while almost all of the deformation takes place by shearing of the (deformable) hemicellulose/lignin matrix [230]. This combination confers both stiffness and deformability (and, therefore, toughness) to the cell wall. A strong binding of the matrix to the fibrils is, however, an important condition for this type of deformation mechanism. Most probably, this strong binding is enabled by the chemical similarity of fibrils and hemicelluloses which are both polyoses. The data of Köhler and Spatz [227] and Keckes et al. [45] indicate that it is most likely that the hemicelluloses act as a glue between cellulose fibrils and allow deformation by shear [231]. This is schematically shown in Fig. 33.

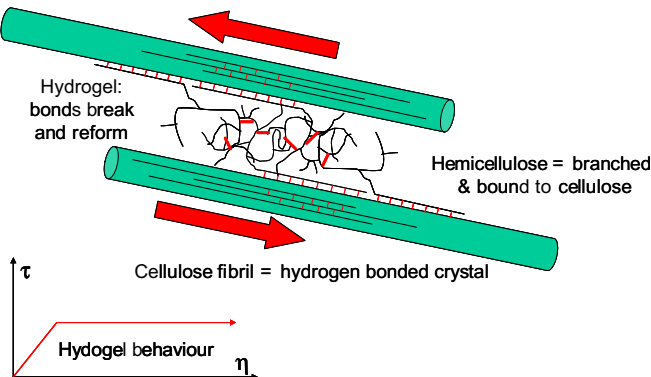


Fig. 33. Model for the deformation of hemicelluloses in the plant cell wall. Hemicelluloses are attached with one end (to the crystalline parts of) cellulose fibrils (cylinders in the sketch). The other ends form a hydrogel-like matrix, probably via hydrogen bonds. According to Fig. 32, tensile (or compressive) deformation of the cell wall along its axis is transformed into a shearing of the hemicellulose matrix (arrows in the sketch). This matrix is assumed to exhibit a mechanical response as shown in the schematic plot, shear stress,  $\tau$ , versus shear strain,  $\eta$ , at the bottom left: Beyond a critical shear stress, the matrix starts to flow, probably by opening and reforming of hydrogen bonds [45,231].

### 5.2. Nanoscale deformation in bone

The high toughness of bone results from the ability of its microstructure to dissipate deformation energy without propagation of the crack [232,233]. Different toughening mechanisms have been identified in bone [234]: the formation of non-connected micro-cracks ahead of the crack tip [235,236], crack deflection and crack blunting at interlamellar interfaces and cement lines [237], and crack bridging in the wake zone of the crack [238–240], which was attributed a dominant role [238]. Striking is the strong anisotropy of the fracture properties of bone. The crack extension energy differed almost two orders of magnitudes between a crack which propagated in close alignment with the collagen fibrils and a crack which proceeded in a zigzag manner perpendicular to the collagen orientation [234] (see Fig. 34). The important influence of the organic matrix, which may vary with genetic background and age of the individual, on the fracture resistance of bone is investigated in [48,241–246]. The following discussion concentrates on the relation between the outstanding mechanical properties of bone and its structure on the microscopic level.

In biomineralized tissues such as bone, the recurring structural motif at the supramolecular level is an anisotropic stiff inorganic component reinforcing the soft organic matrix [241,247]. Important contributions to the high toughness and defect tolerance of natural biomineralized composites are believed to arise from these nanometer scale structural motifs. In recent work [248], it is shown that both mineral nanoparticles and the mineralized fibrils deform at first elastically, but to different degrees. Using *in situ* tensile testing combined with high brilliance synchrotron X-ray diffraction and scattering, it is found that tissue, fibrils, and mineral particles take up successively lower levels of strain, in a ratio of 12:5:2. The maximum strain seen in mineral nanoparticles (0.15–0.20%) can reach up to twice the fracture strain calculated for bulk apatite. The results are consistent with a staggered model of load transfer in the bone matrix, exemplifying the hierarchical nature of bone deformation (see Fig. 35).

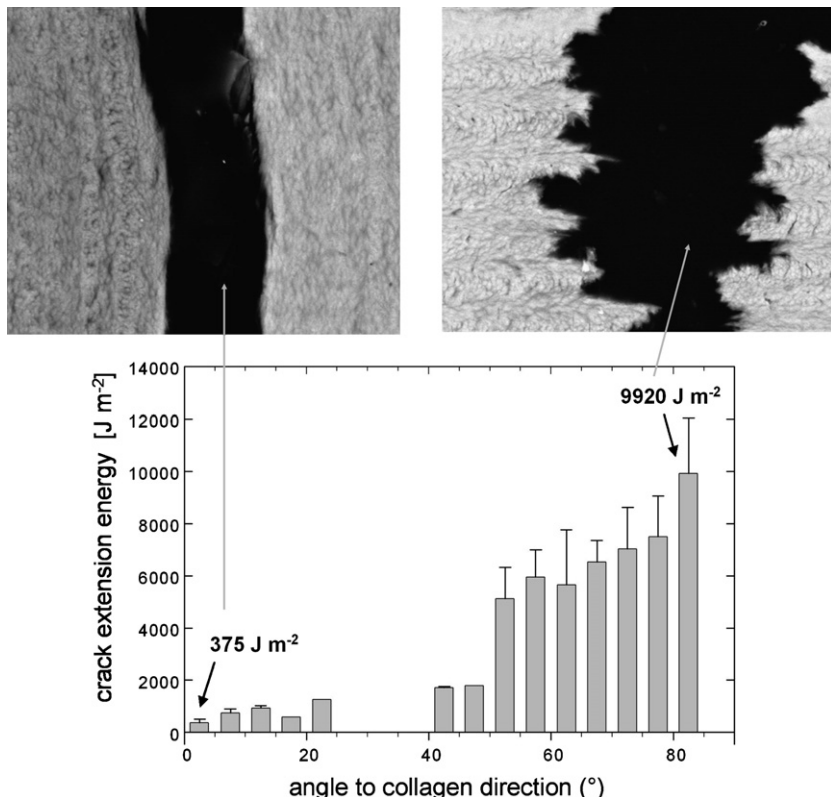


Fig. 34. Bottom: crack extension energy as a function of the angle between the crack propagation and the collagen direction defined by the lamellae. Top: comparison between the corresponding crack shapes using scanning electron microscopy (from [185,234]).

The long ( $>5\text{--}10\ \mu\text{m}$  length) [82,249,250] and thin (100–200 nm diameter) mineralized fibrils lie parallel to each other and are separated by a thin layer (1–2 nm thick) of extrafibrillar matrix. When external tensile load is applied to the tissue, it is resolved into a tensile deformation of the mineralized fibrils and a shearing deformation in the extrafibrillar matrix [251]. While no precise data on its mechanical behavior or its composition is available, it is likely that it is comprised of non-collageneous proteins like osteopontin and proteoglycans like decorin. Single molecule spectroscopy of fractured bone surfaces showed that the extrafibrillar matrix has properties similar to a glue-layer between the fibrils – specifically, it is relatively weak but ductile and deforms by the successive breaking of a series of “sacrificial bonds” [82,252]. The matrix may also be partially calcified [253], which would increase its shear stiffness and reduce its deformability.

These results point towards a deformation mechanism where the matrix/fibril interface is disrupted beyond the yield point, and the matrix moves past the fibrils, forming and reforming the bonds with the fibrils while moving (see Fig. 36). An alternative explanation would be the disruption of bonds between the matrix and hydroxyapatite particles and a modification of the frictional stress between fibril structures [254].

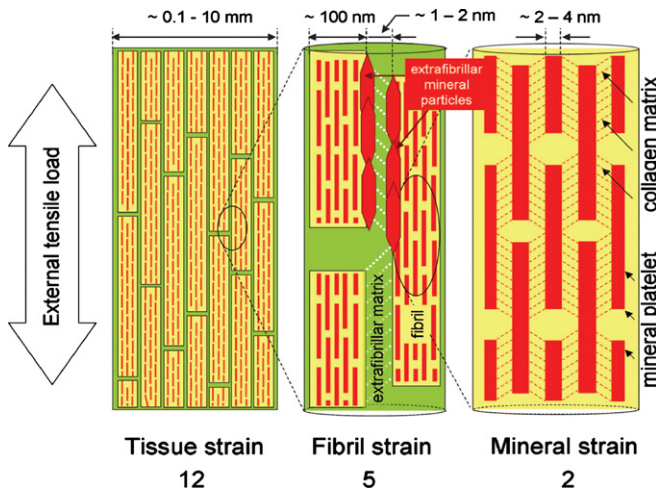


Fig. 35. Schematic model for bone deformation in response to external tensile load at three levels in the structural hierarchy (from [248]): at the tissue level (left), fibril array level (center), and mineralized collagen fibrils (right). The stiff mineralized fibrils deform in tension and transfer the stress between adjacent fibrils by shearing in the thin layers of extrafibrillar matrix (white dotted lines in the center plot show direction of shear in the extrafibrillar matrix). The fibrils are covered with extrafibrillar mineral particles, shown only over a selected part of the fibrils (red hexagons) so as not to obscure the internal structure of the mineralized fibril. Right: within each mineralized fibril, the stiff mineral platelets deform in tension and transfer the stress between adjacent platelets through shear in the interparticle collagen matrix (red dashed lines indicate shearing qualitatively and do not imply homogeneous deformation).

Furthermore, mechanical tests established a high sensitivity of the macroscopic plastic deformation of bone to the strain rate and temperature. These results suggest that the elementary process controlling bone plasticity at the molecular level is localized to within  $1 \text{ nm}^3$ , and has an activation energy in the order of 1 eV [255]. Most likely, this process is localized in a small fraction of the bone tissue – the extrafibrillar matrix – and corresponds to the disruption of calcium-mediated ionic bonds between the long and irregular chains of molecules constituting this matrix. The picture which emerges is that plastic deformation is controlled by an elementary process where segments of molecules in the interfibrillar layer are connected by charge interactions (Fig. 36). This is in excellent agreement with previous work showing that the deformation in bone might be associated with (calcium-dependent) sacrificial bonds [82,252,256] and with the observation that plastic deformation occurs in a thin ‘glue’ layer between fibrils [248,251].

Finally, deformation in the mineralized matrix does not only occur at the hierarchical level of the mineralized fibril/extrafibrillar matrix alone, but can also occur at the next higher level of the fibril arrays. We considered the case of partially mineralized collagen from mineralized turkey leg tendons [156]. At this level, the fibrils aggregate into  $1-4 \mu\text{m}$  diameter fiber bundles. Back-scattered electron imaging of the local mineral content at the level of the individual bundles showed that the fibrils are inhomogeneously mineralized – a mixture of mineralized fibrils coexists with unmineralized fiber bundles [155]. When stretched to failure, we observed a novel two-step fracture process at the micron length scale. For low strains below 1–2%, all the fibrils stretch homogeneously. For larger strains, the stiff mineralized fibers break or detach from the neighboring ductile

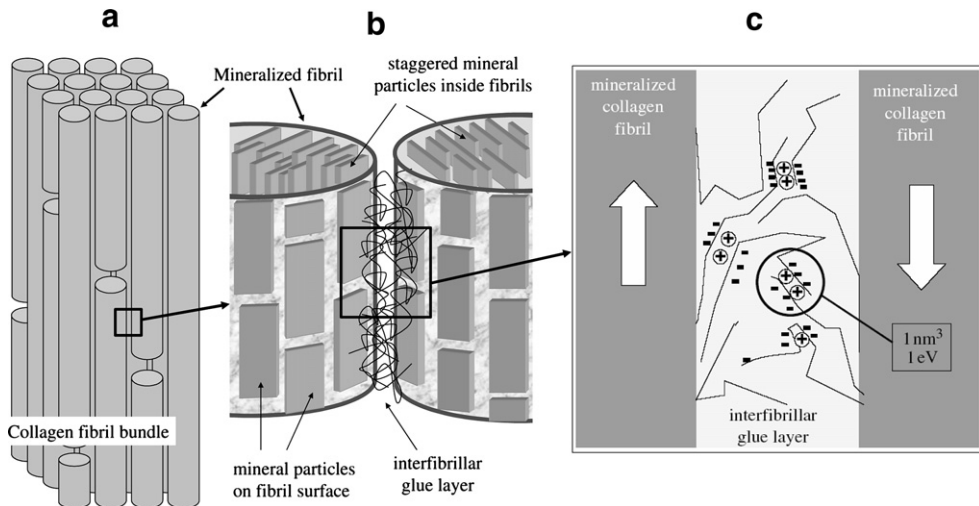


Fig. 36. Sketch of the putative function of the thin glue layer between collagen fibrils in bone (according to [251,255]): (a) Fibril bundle. (b) Fibrils with intra- and interfibrillar mineral joined by a thin glue layer. (The thickness of this layer is very likely just a few nanometers and appears highly exaggerated in the figure). (c) Putative structure of the glue layer formed by chains of molecules (possibly negatively charged polyelectrolytes, like osteopontin [69], fetuin A [257] or proteoglycans [258], or combinations of those), interacting by charges, probably with the help of multivalent cations, such as calcium (circles). A number of charges located on a given molecular segment have to be broken simultaneously (as also observed in other polyelectrolyte systems [259]), giving rise to the experimentally observed [255] activation enthalpy of approximately 1 eV within a typical volume of  $1 \text{ nm}^3$ . The arrows indicate the movement of the collagen fibrils giving rise to shear in the glue layer. Mineral particles are not explicitly drawn, but are present in the fibrils as well as in the interfibrillar space.

unmineralized fibers, but the tissue as a whole remains intact [156]. The macroscopic cohesion comes about because the unmineralized fibers bear the remaining load, stretching by as much as 8–10%. The breakage of the stiff component is correlated with the reduction of the slope of the stress-strain curve (reduction in effective stiffness). By this mechanism, we believe the tendon achieves both a high stiffness in the normal physiological regime of low working strains (<0.2% [260]) as well as a structural protection against sudden, traumatic loads.

### 5.3. Stiff and tough composites by gluing – a simple model

It is very interesting to remark that biological composites as different as tendon (Section 4.1), bone (Section 5.2) and the wood cell wall (Section 5.1) show a common feature of fibers joined by a thin glue layer which is loaded under shear. Plastic deformation is mediated in these systems mostly by plastic flow of the glue layer. In this way, the biological composites seem to acquire both stiffness (from the fibers) and toughness (from the plastic deformation of the glue). This plastic deformation of the glue matrix is most likely due to recoverable molecular bonds [45,248,261–263]. However, plastic deformation of the glue layers is only one of the conditions enabling for a tough composite. The second condition is that the matrix must adhere very strongly to the fibers to avoid failure at the interface. Most interestingly, Nature seems to have evolved special types of amphiphilic molecules for this type of function [231]. Proteoglycans and hemicelluloses seem to be designed to

bind strongly to collagen fibrils in tendon and cellulose fibrils in the wood cell wall, respectively. In the case of hemicelluloses, the chemical similarity to cellulose is the important factor, while proteoglycans have a protein linker probably designed for the binding to collagen. Second, both hemicelluloses and proteoglycans are extremely hydrophilic and able to form gel-like, hydrated networks. According to the experiments reviewed here, both proteoglycans and hemicelluloses seem to be able to flow beyond a certain critical shear stress and, thus, fulfill both conditions mentioned above.

In addition to the increase in toughness of the composite by the plastic deformation of the matrix, gluing of fibers is a construction principle which is extremely flexible and allows a tuning of the mechanical properties of the composite. In order to explore the possibilities of combining stiffness and toughness in composites, a very simple generic model is discussed in the following, which has been originally introduced to describe the mechanical behavior of mineralized collagen fibrils [264] and generalized later to describe a variety of biological composites [248,265].

We use a two-dimensional model, as shown in Fig. 37, where stripe-like stiff objects of length  $L$  and thickness  $D$  are glued together by a matrix. Such a model can easily be generalized to a three-dimensional situation of glued multilayers or fibers. The advantage of the two-dimensional model is that very simple expressions can be obtained analytically, even without the use of finite-element modeling. It should be mentioned, however, that the (approximate) expressions derived here, have been verified by finite-element calculations [265].

The essence of the model is that stiff fibers or platelets are arranged in a staggered fashion. This provides the best load transfer between the stiff elements when the composite is loaded under tension as indicated in Fig. 37.

We use the following notations:

$\varepsilon^M$ ,  $\varepsilon^P$ ,  $\varepsilon^C$  mean tensile strain in the matrix, the particles and the composite, respectively  
 $\sigma^M$ ,  $\sigma^P$ ,  $\sigma^C$  tensile stress in the matrix, the particles and the composite, respectively

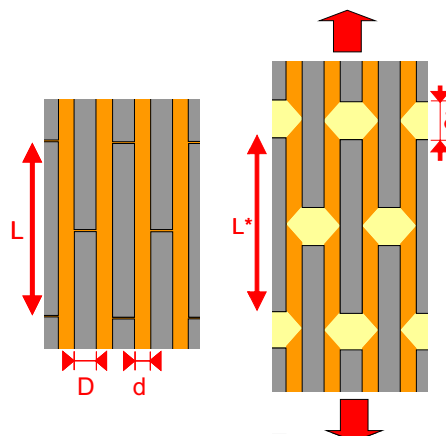


Fig. 37. Sketch of the two-dimensional model for a composite with stiff staggered elements (length  $L$ , thickness  $D$ , lateral spacing  $d$ ) and glued together by a matrix. The interface between matrix and particles is supposed to be so strong that it will not fail before fracture of the components.

$E^M, E^P, E^C$  Young's modulus of the matrix, the particles and the composite, respectively  
 $\tau^M, \eta^M, G^M$  shear stress, shear strain and shear modulus in the matrix

$L, D, d$  length, thickness and spacing of the particles (see Fig. 37)

$\Phi$   $D/(D + d)$  = volume fraction of particles

$\rho$   $L/D$  = aspect ratio of particles

$\delta$  increase of the particle spacing in loading direction

$L^*$  length of loaded particles

For the calculation, we introduce an intermediate quantity which is the force  $F$  acting on a single particle. The stress in the composite splits between contributions of the matrix and the particles, which implies  $\sigma^C = (1 - \Phi)\sigma^M + F/(2D + 2d)$ , due to the fact that the particles are in parallel with stripes of matrix. Note the factor 2 in the second term, which comes from the fact that there is a load-carrying particle only every  $2(D + d)$ . The next step is the calculation of the (average) strain in the particle. The problem is that the strain (and the stress) are not constant along the particle, due to the loading condition when the matrix transmits load by shear as sketched in Fig. 38. The simplest assumption is a linear approximation of the stress (Fig. 38). Then the stress is obviously zero at the ends and equal to  $F/D$  in the center.

The average stress in the particle,  $\sigma^P$ , is just  $\sigma^P = F/(2D)$ , where another factor of two appears due to averaging the stress along the particle (Fig. 38). Moreover, one gets  $\delta = L(\varepsilon^C - \varepsilon^P) = 2d\eta^M$ , and  $\tau^M = (F/2)/(L/2)$ , since half the force  $F$  has to be provided to the particle from each side. Combining all these expressions results in

$$\begin{cases} \sigma^C = (1 - \Phi)\sigma^M + \Phi\sigma^P \\ \varepsilon^C = \frac{2}{\rho} \frac{1-\Phi}{\Phi} \eta^M + \varepsilon^P \\ \tau^M = \frac{2}{\rho} \sigma^P \\ \varepsilon^M = \varepsilon^C \end{cases} \quad (4)$$

These are purely geometrical relations following the construction of the composite as shown in Fig. 37. In the simplest case (that is, for small deformations), where all the

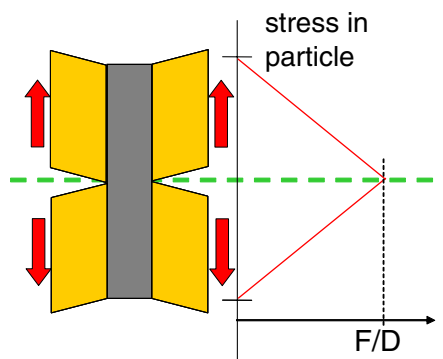


Fig. 38. Approximate stress distribution in a particle where load (arrows) is transmitted through the matrix by shear.

materials can be described by Hooke's law ( $\sigma^C = E^C \varepsilon^C$ ,  $\sigma^P = E^P \varepsilon^P$ ,  $\sigma^M = E^M \varepsilon^M$ ,  $\tau^M = G^M \eta^M$ ), the modulus of the composite can be calculated to be [248,265,266]:

$$E^C = (1 - \Phi)E^M + \Phi E^P/k, \quad \text{and} \quad \varepsilon^C = k \varepsilon^P, \quad \text{where } k = 1 + \frac{4}{\rho^2} \frac{1 - \Phi}{\Phi} \frac{E^P}{G^M} \quad (5)$$

Normally, we expect the shear modulus of the glue layer to be much smaller than the Young's modulus of the particles. As a consequence,  $k$  would become large and the stiffness of the composite would be dominated by the (low) stiffness of the matrix. This can, however, be easily compensated by a large aspect ratio of the particles. For example, if the aspect ratio is  $\rho = 30$ , this would already compensate for a ratio of 900 between the two moduli  $E^P$  and  $G^M$ . This means that, just by geometrical arrangement, the stiffness of the composite can be made of the same order of magnitude as the stiff particles, even when the volume fraction of the glue is not vanishingly small. For example, taking values estimated for mineral particle in collagen tissue [266]  $E^P \approx 100$  GPa,  $E^M \approx G^M \approx 1$  GPa,  $\rho \approx 30$ ,  $\Phi \approx 0.5$ , we obtain  $k \approx 5.4$  and  $E^C \approx 10$  GPa, which is not far from the actual stiffness of compact bone [6]. The downside of this is, however, that by virtue of the same equation, the overall strain of the composite will be hardly larger than the strain in the particles. This means that when the particles are brittle, for example made of mineral, then the composite will also be brittle.

Here it must be remembered that all material laws are taken to be linear elastic. This is not what is found in biological materials, such as tendon, wood or bone. In fact, the matrix is found to start plastic deformation beyond a certain critical shear stress, which we might denote  $\tau^*$ . Hence, the shear stress in the matrix is expected to stay below this value, that is  $\tau^M < \tau^*$ . This is, where the third relation of Eq. (4) above becomes crucial. If one can make sure that  $\rho \tau^*$  is smaller than the strength of the particles, then the matrix will flow before the peak stress in the particles ( $2\sigma^P$ , see Fig. 38) reaches its critical value. Clearly, the composite will be able to strain much more than the particles. Such a composite is going to be both stiff and tough.

This effect is illustrated in a numerical example in Fig. 39. The mechanical behavior of the particles is supposed to be linear elastic up to their fracture. Two different assumptions are made for the matrix (red and green in Fig. 39). The area under the stress strain curves is the same, as well as the initial slope. Estimating the toughness as the area under the stress-strain curve, both assumptions correspond to a matrix with the same stiffness and toughness. This is visible in Fig. 39, right where toughness and stiffness are indicated in an Ashby plot [117]. At a volume fraction  $\Phi = 0.5$ , if both particles and matrix are linear elastic (red), the stiffness is reduced by about an order of magnitude compared to the particles and the toughness by two orders of magnitude compared to the matrix. With the matrix which is allowed to flow beyond a critical shear stress (green), the toughness of the composite is almost as large as the one of the matrix alone. For comparison, we have also indicated the values for a stripe-like geometry parallel or perpendicular to the applied stress. In the first case, the toughness and the stiffness correspond roughly to the particles (within a factor of 2) and in the second to the matrix.

The size of the particles may also play a role. As is evident in the discussion above, the strength of the particles limits the performance of the composite, if the geometrical design is optimal. This may be improved by using (brittle) particles small enough that their inherent strength is not limited by defects anymore. As has been shown by numerical calculations [265], glued composites (as described in Fig. 37) become flaw-tolerant if the particles

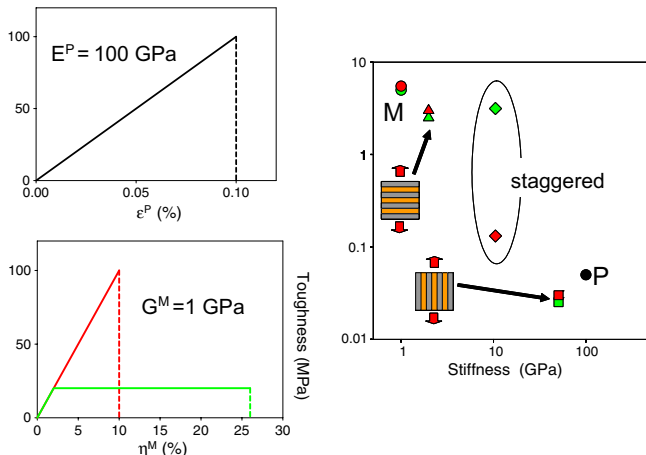


Fig. 39. Stiffness and toughness of a composite structured as in Fig. 37 and referred to as “staggered” (plot at the right). In comparison values obtained for geometrical arrangements in stripes (Reuss and Voigt model) are also indicated. The material laws assumed for the particles and the matrix are indicated by stress–strain curves (left). Two cases are considered for the matrix (red and green). The right graph indicates stiffness and toughness (estimated by the area under the stress–strain curve). M corresponds to the matrix, and P to the particles.

become smaller than a critical length  $h^* \approx \pi\gamma E^P/\sigma_{th}^2$ , where  $\gamma$  is the surface energy of the particle material and  $\sigma_{th}$  its theoretical strength. The reason is that the strength of a particle with a flaw decreases with the square-root of the flaw size (Griffith's law). Particles with a size smaller than  $h^*$  cannot have flaws large enough to affect the strength in a significant way [265]. As a consequence, nanocomposites become flaw-tolerant, if the particle size is smaller than  $h^*$ . An estimate for mineral particles gives  $h^* \approx 30 \text{ nm}$  [265].

Finally, Gao has shown recently [267] that the flaw-tolerance can even be improved by a hierarchical arrangement of composites, where the stiff fiber (or platelet) at each hierarchical level is in fact a composite of much smaller particles glued together. Such a composite of a composite of a composite may become insensitive to flaws at all length scales [267].

## 6. Adaptivity

### 6.1. Mechanobiology and examples of functional adaptation

Biological structures and materials must not be thought as statically determined by the genetic blueprint, but rather as systems actively responding to the biophysical stimuli of their environment. During growth, they are able to adapt their architecture to improve their functionality according to external constraints. Later on, after growth, biological systems can adapt to changes in the environment and re-establish the “agreement” with the outside world. Even without external changes, repair mechanisms can be active to reduce the damage present in the system, thereby improving performance.

The adaptive strategies are manifold since they depend on such basic inputs like whether the system is locally fixed or can move. Concerning the optimization of mechanical performance, typical strategies are to add new material, possibly with specific mechanical properties, or to maintain the existing material using repair mechanisms. The research

field that deals with the development, maintenance and adaptation of load-bearing tissues as a response to external loading, is called mechanobiology. The difference between classical biomechanics can be best explained in the relation between form and function of the biological system. In biomechanics, the form is assumed to be fixed, and questions focus on how well this form fulfills its mechanical function. Mechanobiology, in contrast, builds on the idea of “form follows function”, the response of the form to fulfill its function. In the following, the meaning of mechanobiology is illustrated with four examples, three connected to bone, one to wood.

Fig. 40 shows the trabecular structure inside the vertebral body of an 85 year old man with trabeculae running mainly in vertical and horizontal directions. Due to the bony projection on the upper left, termed a bone spur or osteophyte, the vertebra was not loaded *in vivo* via the vertebral disks as usual, but directly from one vertebra to the next via the osteophyte. The lower left of the vertebral body is pervaded by diagonal trabeculae, which are unknown in healthy patients without osteophytes. The change in loading due to the osteophyte caused an adaptive response of the trabecular architecture by the formation of diagonal stress-bridges [268].

The second example refers to early phases in the development of long bones, which develop by the formation of cartilage models and their subsequent replacement by bone and bone marrow. To answer the questions how much bone development is predetermined genetically and how much is a mechanobiological response, Chalmers and Ray performed a classic experiment [269]. The cartilage model of a femur from a fetal mouse was transplanted into the spleen, which is thought to be free of mechanical loading. Even outside its normal biological environment, the cartilage model developed into a recognizable femur, demonstrating that cartilage is endowed with a potential for growing into a specific bone shape. The refinements of the bone structure associated with its normal function, however, were largely missing, e.g., the exact shaping of the femoral head close to the hip joint and the internal trabecular structure [269,270].

The top row of Fig. 41 shows the evolution of the trabecular architecture inside a vertebra from the embryonal state to adulthood. The pattern of the trabeculae changes from

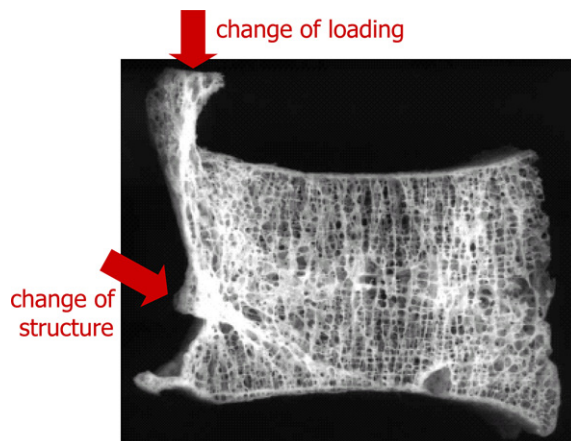


Fig. 40. The trabecular architecture responded with a change of structure to a change of loading. Vertebral body from an 85 year old man with an osteophyte on the upper left and a diagonal stress-bridge (adapted from [268]).

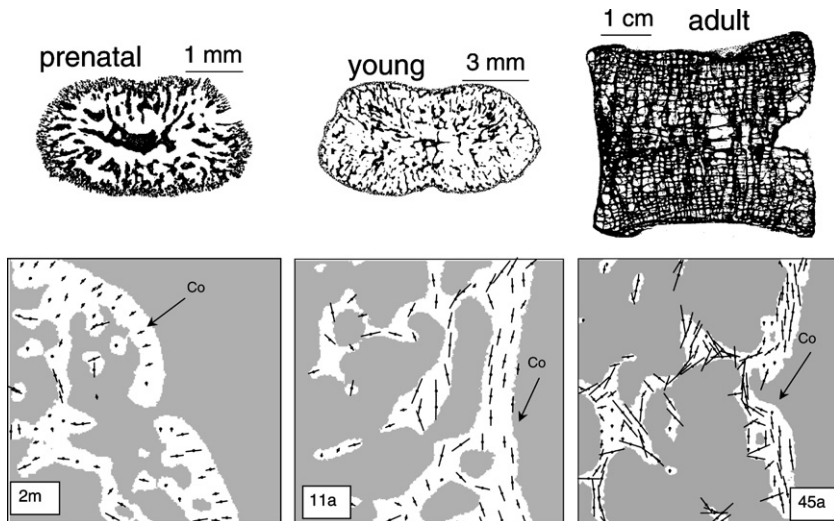


Fig. 41. Evolution of the trabecular architecture (top row) and the orientation of the collagen-mineral composite (bottom row) in human vertebra from the prenatal to the adult state [62]. Only a small fraction of the outer part of the vertebra is shown in the bottom row, where the rim labeled Co marks the outer cortical shell; white areas correspond to bone, grey ones to marrow space. The age of the individuals was 2 months, 11 and 45 years. The direction of the bars indicates the predominant orientation of the elongated (plate-like) mineral nanoparticles. The length of the bars indicates the degree of alignment.

a preferred radial orientation of the mineralized cartilage before birth to a pattern in which the trabeculae are oriented predominantly along vertical and horizontal directions in bone [62]. While the radially oriented structure of the embryonal vertebra is probably due to the early isotropic growth process (or a more isotropic loading), the reorientation of the trabecular network starts with the vertical loading in compression along the spine after birth. These changes on the architectural level of the trabeculae are also accompanied by changes taking place at the nanostructural level. Investigations using scanning-SAXS reveal that in the inside of the vertebral body the orientation of the mineral particles follow the direction of the trabeculae. In the outer cortical shell of adults, the particles are also oriented parallel to the surface. Remarkably, this is different in the embryonic vertebra, where the mineral particles prefer an orientation perpendicular to the outer surface (Fig. 41) [62]. The degree of alignment is generally much less pronounced in the growth cartilage than in the developing vertebra.

The last example for an adaptive response to mechanical loading is taken from the plant world. During its growth, a branch has to adapt to increasing gravitational loads that bend the branch downwards. Since more material is added at the lower side of the branch, a cross-section of the branch show annual rings with a pronounced radial eccentricity. The branch has to be both stiff and flexible in order to prevent the loss of its function, i.e., to expose the leaves or needles to the sun and to bend until heavy loads like snow will slide off. The material which is added during the growth process has properties which depend crucially on the position on the branch and therefore, how it is mechanically loaded. On the lower side, especially close to the stem, the wood cells have to withstand large compressive forces, while the upper side of the branch is loaded under tension. The light

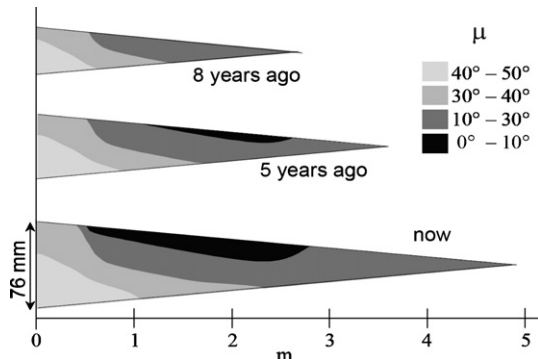


Fig. 42. Distribution of microfibril angles measured in a branch of spruce [271]. The age-evolution was deduced from the pattern of annual rings (from [33] with permission).

microscope reveals the adaptation at the microscopic level. The wood on the lower side called compression or reaction wood displays rounded cells in contrast to the square-like cell shapes on the upper side termed opposite wood. A study with scanning-SAXS on a branch of Norway spruce [271] demonstrate the adaptation of wood on the nanoscale via the tilt angle of the cellulose fibrils (microfibril angle, MFA, see Fig. 28). Once the MFA is measured at different positions in the branch, a plot of the MFA distribution for different ages of the branch (Fig. 42) is straightforward since the history of growth is stored in the succession of annual rings. The young branch (8 years before it was cut) is composed predominantly of flexible wood (i.e., with large microfibril angle). The MFA in compression wood is found to decrease continuously from about 45° near the trunk to about 20° at the tip of the branch. On the upper side, however, the course of the MFA with position changes with the age of the branch. With increasing length of the branch and hence increasing gravitational forces, a stiff region displaying a MFA close to zero emerges in opposite wood [271]. The asymmetry in the loading pattern is consequently reflected in an asymmetry of the cell microstructure. What is more, this asymmetry develops during growth as an adaptive response to a change in the loading. Since wood is twice as strong in tension as in compression, it may be speculated that the stiffening on the upper side of the branch serves to reduce the stresses in compression wood and therefore avoiding compressive failure. In cases of an asymmetric loading of the whole tree, e.g., due to strong winds blowing preferential from one side, such effects including the formation of compression wood can also occur in the stem [4].

## 6.2. Bone remodeling

The ability of bone to adapt to a changing mechanical environment is based on a permanent remodeling of the material. Historically the two processes of bone modeling and remodeling are distinguished, where bone modeling specifically refers to the adaptation to new mechanical requirements including adaptations during growth. The term bone remodeling is then reserved for the continuous renewal and the maintenance of bone. Since this distinction is rather vague and, above all, recent investigations suggest that a singular regulation mechanism is enough to explain both processes [272], we prefer to use bone remodeling to describe all processes involving resorption and deposition of bone [273].

The renewal of bone occurs through an interplay between different bone cells. In trabecular bone, osteoclasts resorb a bone packet and leave behind a cavity with a depth of about 60 µm [274]. This hole is then filled with new bone matrix by the osteoblasts. The newly deposited matrix, initially unmineralized, increases its mechanical stiffness by increasing the mineral content. While the resorption phase takes 1–3 weeks, the time for the formation of new material is about several months. The mineralization process starts with an initial surge to reach a level of more than half of its final mineralization after about 10 days, but then slows down and continues to slowly increase over a time scale of years [48,275]. In cortical bone, the outer surface accessible to the osteoclasts is strongly reduced compared to trabecular bone. Cortical bone is, therefore, remodeled by forming new osteons. Osteoclasts resorb a tunnel with a speed of about 20–40 µm/day [274]. Osteoblasts then fill the tunnel again, leaving in the middle a channel for a blood vessel. As a consequence of the different remodeling geometry, only about 5% of cortical bone is renewed each year compared to 25% of trabecular bone, but these percentages are site dependent with a reduced remodeling rate in the peripheral skeleton [276]. In general, bone remodeling occurs at about 1–2 million microscopic sites in the adult skeleton.

The study of the trabecular structure in the femoral head, dates back to the end of the 19th century and led to the conclusion that bone remodeling is not a random exchange of old bone matrix with new one, but a mechanically controlled process. The so-called Wolff-Roux law states that bone is deposited wherever mechanically needed and is resorbed wherever there is no mechanical need. This idea was further developed by Frost who proposed that a mechanically controlled feedback loop is active in bone and regulating bone mass and architecture. The term mechanostat was coined to describe this process, in analogy with a thermostat, which switches a heater on or off according to its set-points [277,278]. Once there is a local mechanical overloading, e.g., due to a new intensive sport activity or due to a locally reduced bone mass caused by osteoclast resorption, the mechanostat gives the signal for bone deposition. New bone will be added as long as normal strains in this local region are regained. The same principle, but with opposite effect occurs in the case of mechanical disuse, e.g., due to prolonged bed rest. The mechanostat makes sure that the mechanically dispensable bone is removed. Estimates for the thresholds for local strains are about 0.15–0.3% for bone deposition and 0.01–0.03% for bone resorption, respectively [277]. Some principal results on the mechanobiological aspects of bone remodeling [279,280] as investigated using *in vivo*, *in vitro* and *in silico* models are reviewed in the following sections.

### *6.2.1. In vivo experiments*

The idea of mechanobiological experiments to investigate bone remodeling is to change the mechanical loading on bone and study the resulting change in bone mass and structure. This could either be an increase in the mechanical load by e.g., increased exercise or specific loading devices, or a reduction of the loading, for example by casting, bed rest or microgravity conditions in space. The challenge in these experiments is to apply a modified load to the system in a manner that is well defined, and yet minimizes irritations to the biological system as much as possible [281]. A natural mechanobiological effect can be observed in racing greyhounds whose leg bones are asymmetrically loaded since they sprint around the track always in the same counter-clockwise direction. The more strongly loaded outer bones show denser bone and thicker trabeculae, an effect that recedes with “retirement” [282]. In the search for exercises which have the strongest osteogenic effect

in humans, it is found that activities like swimming and cycling have no positive influence on bone mass. Sport activities that involve unusual and sudden loading of the skeleton like tennis and squash are found to be preferable with respect to bone formation (but probably not for the joints!) [283]. An extreme example of impact loading occurs during triple jumping where the bones are loaded for a short time beyond 20-times the body weight. A study on the tibiae of professional triple jumpers reveals a strong influence on bone mass and size deviating in some parameters from controls by more than 50% [284].

A classic approach in animal experiments is to remove surgically a bone in a limb segment, where more than one is present, and study the effect on the remaining supporting bone. Important information is gained from strain gauges, which are directly attached to the bone surface. The removal of the ulna in pigs results in an increase of the principal compressive strain by a factor of more than two in the remaining radius. A rapid and substantial adaptive response in the radius leads to a compensation of the lost ulnar bone area by new formed bone within three months [285]. Another well-studied invasive animal model is the avian ulna model in which the bone retains its normal muscular and vascular attachments. Otherwise, the ulna is completely isolated from any loading input but the one originating from an external loading apparatus [286]. Important findings are that only a dynamic and not a static mechanical stimulus of the same strain magnitude elicits a bone forming response [287], and that higher strain rates provide a greater osteogenic stimulus in the rat ulna model (Fig. 43) [288]. Surprisingly, as few as four loading cycles per day are found to be sufficient to maintain the bone mass [286]. The bone loss is also inhibited by very low, sub-physiological mechanical stimuli of high frequency (30 Hz) [289]. Important medical implications include the observation that older rats have a reduced sensitivity to mechanical stimulation [290]. A recently presented non-invasive animal model, i.e., one that avoids surgery and associated effects on cell metabolism, allows the study of the effect of loading on both cortical and trabecular bone. A mouse tibia is fixed between two padded cups and controlled axial loads are applied. The produced strains have to exceed 3-times the physiological strains during walking and jumping in order to significantly modify the extent of new bone formation [291].

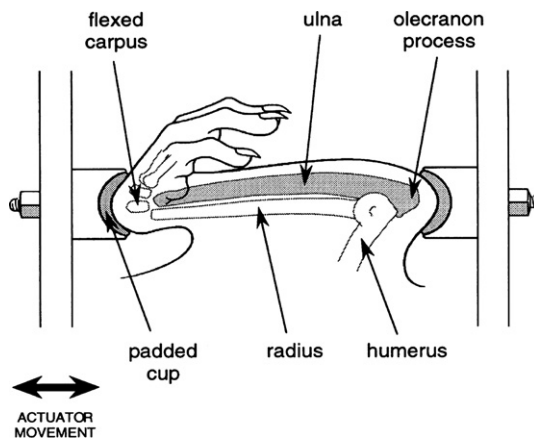


Fig. 43. Schematic drawing of a non-invasive loading system for the ulna of a rat. The forearm is held between padded cups and cyclic loading is applied (from [288] with permission).

A reduced mechanical loading on the skeleton results in bone loss. This effect is most relevant for the human endeavor of living and working in space. The condition of microgravity causes an uneven bone loss throughout the skeleton with the lower limbs being most affected. Although non-linear and different in cortical and trabecular bone, the bone loss can be roughly quantified by 0.4% per month [292]. The ground-based version of mechanical disuse investigations are bed rest studies in which subjects have to lay in bed for months. Mechanical disuse not only causes loss of bone, but also muscle volume. Since the largest forces on the bones are provoked by muscle pull and not simply by gravitational forces, it is argued that bone loss is the consequence of a reduction in muscle force [293]. Striking in all these investigations under reduced loading are the strong inter-individual variations including subjects more or less “insensitive” to the change in the mechanical environment.

### 6.2.2. *In vitro* experiments

The aim of bone cell culture experiments is to find the cell biological basis of the Wolff-Roux law [294]. The local mechanical condition must be sensed by cells and translated into a cellular signal, which is then possibly transmitted to the effector cells at the bone surface: osteoclasts and osteoblasts. A key role in this mechanotransduction process is typically assigned to osteocytes (see their location in bone in Fig. 8). An osteoblast, which is left behind during the remodeling process and therefore completely surrounded by bone matrix, differentiates to become an osteocyte. The supply with nutrients is ensured through small channels called canaliculi which are only about 0.2 μm in diameter. The osteocytes use these canaliculi to reach out their fine cell processes, which can be as many as 80, to make contact with neighboring osteocytes via gap junctions [295]. *In vitro* studies show that bone cells have to be strained on the order of 1–10% to obtain a cellular response, which is almost an order of magnitude larger than physiological strains. In search for an amplification system, it is proposed that loading of the bones causes interstitial liquid to be squeezed through the canicular pores. Due to the ionic composition of the interstitial liquid, the osteocytes are stimulated not only mechanically from the fluid shear stress, but also electromagnetically by the strain-generated potentials. The canicular fluid flow theory [296] is supported from cell culture experiments, which show that the osteocytes are more mechanosensitive than osteoblasts and fibroblasts, and they react stronger to fluid flow than to intermittent hydrostatic compression [297]. Comparing the influence of different modes of fluid flow, it was found that oscillating flow was less potent in stimulating cell reaction than either steady or pulsing flow [298]. Cell response is classically measured by the production of prostaglandin and nitric oxide, both important messenger molecules for bone cells [294,296]. Significant progress has been made in our understanding of how a mechanical stimulus is processed within the cell, revealing a tremendously complex system of multiple signaling pathways that control gene expression [299]. The three-dimensional network of osteocytes, including resting osteoblasts that cover the bone surface, the so-called lining cells, is hypothesized to act as the mechanosensitive control system, which collects information about the local mechanical loading necessary to fulfill the function of the mechanostat [295]. An alternative hypothesis uses microdamage as the crucial element that triggers bone remodeling [300]. From the observed strong spatial correlation between microdamage, controlled osteocyte death and subsequent remodeling events [301] it is concluded that microscopic cracks disrupt the network of osteocytes resulting in cell death. Before dying, the osteocytes signal the bone surface to attract osteoclasts

for removal of damaged bone. This hypothesis is appealing due to the close connection between a clear mechanical reason for remodeling – removal of microdamage to avoid fatigue – and the microcracks themselves as stimulus for remodeling.

### 6.2.3. *In silico* experiments

In the last 30 years, computational modeling has contributed to our understanding of bone remodeling and has helped to test our understanding. The obvious advantages of computer simulations, in particular compared to animal experiments, are that they are cheap, fast in their realization and usually free from complications [302]. Furthermore, in a model all the defined parameters are known at every time step without errors of measurement. Although naturally aimed at improving our understanding of reality, a crucial advantage of models is that they are not from the outset restricted by the “laws of Nature”. Such models can be used to investigate the consequences of design principals that are either not found or unattainable in Nature. This can help to understand not only “how” biological systems work, but even “why” they are realized this way. The results of model approaches, however, have to be assessed while keeping in mind the massive simplifications which are required to restrain Nature’s complexity into a manageable mathematical formulation. The hopeless effort to formulate realistic models of biological systems should be substituted by the search for useful models. Although *in silico* experiments cannot completely substitute *in vivo* experiments, they can improve the design of animal experiments by increasing the significance of the experimental results [302]. An example of successful applications of computer models is the improved long-term stability of bone implants [303].

Models of bone remodeling can be classified concerning their accuracy in biological description, spatial resolution and temporal course: (i) Is the model of the control mechanism acting in bone aiming at a description including the specific cell actions or do they settle for a phenomenological description? (ii) Is the effect of remodeling (specifically in trabecular bone) described as an action exclusively restricted to the bone surface and therefore resulting in a movement of the bone surface (surface remodeling), or does the length scale of the model description already include “internally” several trabeculae and therefore describe remodeling as an increase/decrease of a bone density variable (internal remodeling) [302,304]? (iii) Does the model only aim to predict a final state of the bone structure in the sense of an optimization problem, or is the evolution with time, meant to reproduce the adaptation process in bone [305]?

Most of the models used include an iterative procedure implemented in a computer program. Although an analytical treatment is limited to simple remodeling problems, a short presentation of the concept of adaptive elasticity proposed by Hegedus and Cowin [306] is instructive showing the two main model constituents in the form of two equations. The first equation relates the stress,  $\sigma$ , and strain,  $\varepsilon$ , with the structure, which is in this continuous model a function of the density  $\rho$  only,

$$\sigma = D(\rho)\varepsilon. \quad (6)$$

For a given external loading, Eq. (6) can be used to calculate the strain  $\varepsilon$ , which acts as the mechanical stimulus. A second equation, the remodeling rate equation, relates the temporal change in the density parameter  $\rho$  with a function that depends on two parameters, the difference of  $\rho$  from a reference value  $\rho_0$ , and the mechanical stimulus  $\varepsilon$ ,

$$\frac{\partial \rho}{\partial t} = f(\rho - \rho_0, \varepsilon). \quad (7)$$

A simplified remodeling rate equation is obtained by performing a Taylor expansion and use of a truncated expression of  $f$ . The resulting equation is non-linear since the mixed term between the density and the mechanical stimulus has to be retained to reproduce the acting feedback loop [302]. We focus our discussion on model structure and recent developments in simulation of trabecular bone remodeling. For a more general review on bone adaptation models, see [307].

An iterative computer model, which describes the mechanical feedback loop acting in bone [308], has as its main constituents the analogues of the two equations above. The first task is for a given loading to perform a mechanical assessment. This “mechanical” part of the algorithm calculates the mechanical stimulus in each part of the bone structure. The second part, where biology enters, is to connect the mechanical stimulus with cell action, and therefore, with changes in the structure. Fig. 44 shows a schematic outline of the different steps required to simulate the process of bone remodeling. At a certain point in time, the bone structure and the bone material properties are defined. In a lattice model, the structure is defined by a set of full voxels corresponding to bone, while empty voxels define the marrow space [309]. The material properties are generally assumed to be as simple as possible, i.e., isotropic elastic. An alternative presentation of the structure is through a continuous density  $\rho$ . The elastic modulus of an element with density  $\rho$  is then obtained employing a power-law relation for cellular structures, which connects density and elastic modulus at the apparent level (see Eq. (1) in Section 3.1) [272,310]. Since the loading and loading history [311] on the simulated bone is not completely known, a simplified loading pattern is assumed. For simplicity sake, the time dependence of the load is omitted and a static load instead of a dynamic load is applied in the simulation, since the mechanics behind both problems are equivalent [107]. The standard technique used to calculate the stresses and strains in the trabecular structure for a given loading is the finite-element method. Much faster, but also less accurate methods, include mechanical assessments

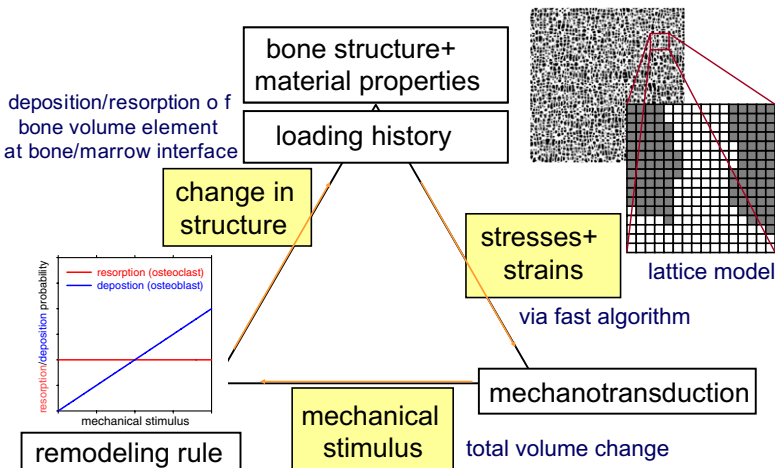


Fig. 44. Model structure of a lattice model for bone remodeling [309]. In the first step a mechanical assessment gives the mechanical loading in each lattice element. Biology enters in the phenomenological remodeling rules, which connect stimulus with resorption/deposition probabilities. The structure is changed by removal or adding a bone packet in form of a voxel element at the bone surface.

using efficient algorithms [309]. The mechanical information must then be condensed into a local mechanical stimulus, which requires assumptions about the following question: What is the mechanical stimulus, i.e., the biologically relevant quantity of the mechanical loading? Currey distinguished between the “proximate” stimuli the bone cells are reacting to, and the “ultimate” stimuli as the significant features of the strain environment that are being reacted to [312] and which is here referred to as mechanical stimulus. Since the mechanosensitive system does not respond instantaneously, another question is how the loading signal is integrated over time. Generally the nine tensor components of stresses and strains are reduced to a scalar quantity like invariants of the strain or stress tensor (e.g., trace of the strain tensor corresponding to volume change or maximal principal strain), von Mises stress or strain energy density [313]. Alternatively, damage parameters have been considered as mechanical stimulus [314]. Selecting a point at the bone surface, another question arises: how is mechanical information from the bone volume beneath the selected point processed to result in the remodeling stimulus for bone deposition and resorption? Not only does the contributing volume have to be specified, but also how the contributions “add up”. Typical assumptions used to solve this include the introduction of a “spatial influence function” which decays with distance from the surface point and serves as a weighting function for an otherwise simple summation of the local contributions [315]. The bone structure will change according to the remodeling stimulus at the bone surface. In lattice models, the remodeling rule for osteoclasts and osteoblasts define the probability for bone resorption and deposition. Analogous to the exchange of bone packets in real bone, a bone voxel is added to or removed from the bone surface [309]. In simulation models where the structure is defined by a continuous density, a differential equation analogous to Eq. (7) is used to perform a local change of the density [310]. Once the structure is changed, a new iteration in the simulation starts with the mechanical reassessment of the structure.

Computer simulations modeling vertebral trabecular bone show that starting with a homogeneous configuration lead to the emergence of a trabecular network of vertical and horizontal trabeculae. This structure coarsens with time by a reduction in the number of trabeculae and a concurrent thickening of the remaining ones. This natural “aging” of the bone structures can be contrasted to “disease” scenarios, which correspond to the effects of changes in the mechanical feedback loop (Fig. 45).

A single feedback regulation is sufficient to explain both, the maintenance of the trabecular architecture, and its adaptation to changed external loads, processes normally distinguished as remodeling and modeling, respectively [272]. Fig. 46 shows the adaptive realignment of the trabecular architecture after the loading direction is rotated by 20° [310]. The use of different mechanical stimuli, like strain-energy-density, principal strain, volumetric strain and their gradients, respectively, results in similar trabecular architectures [313]. Although first results have been obtained [309,313,316–318] the connection between the details of the regulation loop and the temporal evolution and the spatial arrangement of the trabeculae is still unclear.

### 6.3. Bone healing

The aim of materials science to design and produce self-healing materials has stimulated increasing interest into how Nature realizes and controls healing responses. Perhaps the most striking example is the complete regrowth of lost limbs in salamanders [319].

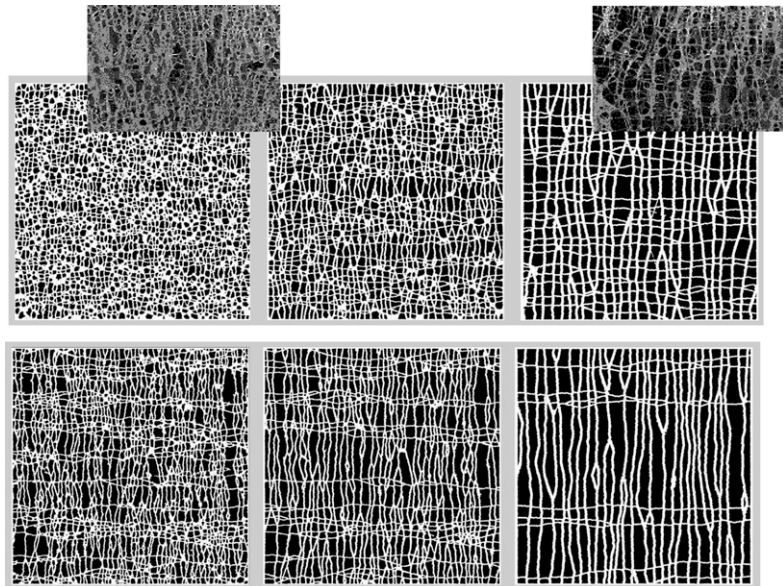


Fig. 45. Time evolution of the trabecular architecture in two different model scenarios, normal mechanosensitivity of the bone cells (top row) [309] and reduced sensitivity (bottom row). The structure “ages” by a reduction of the trabeculae and a thickening of the remaining ones. Insets on the top show the comparison with real bone of young and old age. Reduced mechanosensitivity reduces the bone mass, and the architecture is characterized by a low number of horizontal trabeculae. Simulated bone specimen has a side length of approximately 3 cm.

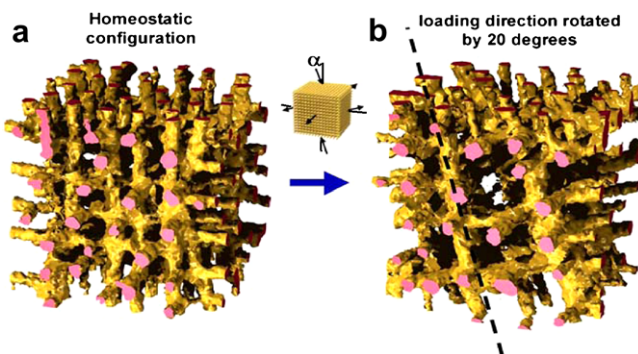


Fig. 46. Changing the external loading (rotation by 20°), results in an adaptive response of the structure by a reorientation of the trabeculae along the new loading direction (from [310] with permission).

Although such limb regeneration does not occur in humans, bone healing is an example of how even after significant damage, the human biological system can not only return to full functionality, but completely restore the initial structure. In contrast to other tissues, which are repaired by producing scar tissue, bone has the capability to regenerate itself, thereby returning basically to the pre-fracture state. Since the underlying biology and gene expression resembles strikingly what happens during the bone development in the embryonic phase, it is hypothesized that in bone regeneration basic steps of skeletal development

are recapitulated [320]. In addition to biological factors [321], such as the importance of restoring the vascularization to avoid cell death due to lack of oxygen and the overwhelming presence of signaling molecules, the mechanical loading within the fracture site plays a crucial role for the healing [322,323].

Already the fundamental distinction between primary and secondary fracture healing is based on how the fracture is stabilized. Primary (or direct) fracture healing occurs when the fracture fragments are immobilized and ideally compressed against each other. The remaining gap is bridged by bone remodeling with the creation of new osteons that connect the two bone fragments. Although such a direct healing would seem to be the ideal healing response, it has the disadvantage besides surgical problems, that the broken bone remains unstable for months and even years until healing is complete [270]. In this time reloading must be avoided.

For the situation in which small movements of the fracture fragments is allowed, healing proceeds via a stabilization of the bone fragments through the formation of an external callus [324]. The different stages of secondary bone healing in a long bone like a femur or a tibia can be summarized as follows: The starting point of a bone fracture is typically an incident in which the bone is loaded beyond its maximal strength. Beside the disruption of the bone material, the blood supply, most importantly in the periosteum or outer “skin” layer of the bone, is interrupted and cells die. The incipient inflammation has three tasks: to clean the fracture region from dead material, to initiate processes to restore the blood supply, and to congregate mesenchymal stem cells (Fig. 47). A key process, which is thought to be mechanically regulated, is the differentiation of these precursor cells into cells that can produce different tissues: cartilage, fibro-cartilage, fibrous tissue and bone. Interestingly, in secondary healing not only the direct formation of bone in a process called intramembranous ossification occurs (Fig. 47), but also an ossification process which involves a “detour” via the formation of cartilage (endochondral ossification)

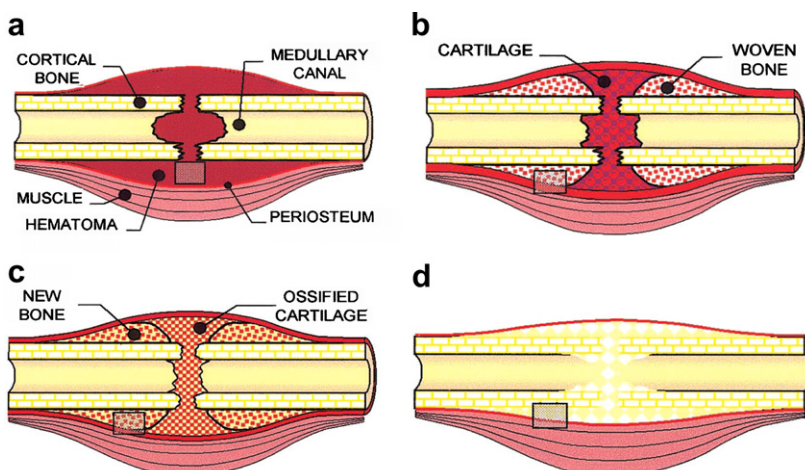


Fig. 47. Different phases in secondary fracture healing: the formation of a hematoma in the inflammatory phase (a); new bone formation at the outside of the bone fragments by intramembranous ossification (b); the cartilage within the fracture gap mineralizes (c) and a bone bridge is formed at the outside of the fracture fragments (d) leading to a union of the bone fragments; shaded boxes refer to areas of investigation and should be neglected (adapted from [325] with permission).

(Fig. 47). This detour in the “material selection” is accompanied by a geometrical detour by not immediately constructing an osseous bridge between the fracture ends. Instead a hard bone shell is formed around the fracture site, while the fracture gap itself is filled with soft tissue (cartilage), which then mineralizes and is finally substituted by bone. In the final phase bone remodeling and resorption take over leading to a removal of the, at this point dispensable, bone around the original fracture and therefore completing the restoration of the broken bone [322,323]. The essence of secondary fracture healing is consequently a fast reaction which aims at stabilizing the fracture gap by the formation of a transient over-dimensional biological splint. The fracture ends themselves are joined together in a “tentative” process which essentially follows the course known from bone development. This intricate, though indirect, method of bone healing, nevertheless allows a fast return to pre-fracture values of bone strength and stiffness.

#### *6.3.1. Mechanobiological experiments of fracture healing*

Over the last four decades, controlled animal experiments have been the key for a better understanding of the influence of mechanics on bone healing. A classical model is the sheep, which has a mass comparable to humans but due to having four legs the effect of gravity is reduced by a factor two. A transverse diaphyseal osteotomy of a long bone like the tibia is performed, i.e., the bone is cut into two at its mid-shaft. Parameters which are controlled are the gap size between the two bone ends [326] and the mechanical loading and the strain within the gap [327–329], respectively, using sophisticated fixation devices. The loading within the fracture gap during healing can be estimated by performing a gait analysis on the animals [330,331] and by direct mechanical characterization of the fixation devices outside of the animal. The importance of mechanical factors becomes obvious from the results of the two extreme cases of fixation; with either high or low rigidity. If the fixation is too rigid, the system does not form a stabilizing callus and the gap is consequently not bridged successfully by new bone. For fixations that are insufficiently rigid, again non-union occurs, this time through the formation of a false joint with cartilage caps at the ends of the fracture fragments [327]. The aim is now to find within these two extremes the mechanical environment which optimally fosters the healing process. It is demonstrated that cyclic interfragmentary micromotion applied only for short periods early in the healing period result in a significant improvement in healing [332].

#### *6.3.2. Mechanobiological theories of fracture healing*

The first clues that cell differentiation during fracture healing is mechanically controlled date back to the late 19th century and were again formulated by Roux [333]. The Interfragmentary Strain Theory proposed by Perren and Cordey states that the fracture gap can be filled only with a tissue which can withstand the strain in the fracture gap without rupture [334]. This implicates that the fracture gap is initially occupied by a tough, but generally soft tissue. Healing proceeds by successive steps of tissue formation of increasing stiffness (or decreasing strain tolerance). The soft, tough tissue which forms initially, lowers the interfragmentary strain sufficiently to allow the next tissue (stiffer and less tough) to fill the gap, therefore further reducing the interfragmentary strain. This progressive increase in the elastic modulus of the regenerating tissue leads finally to a sufficient reduction of the strain within the gap so that the least strain tolerant tissue, bone, can fill the gap, bringing back the strain levels to normal values. A gross simplification of the theory is that it does not consider the complex heterogeneous loading pattern present in the

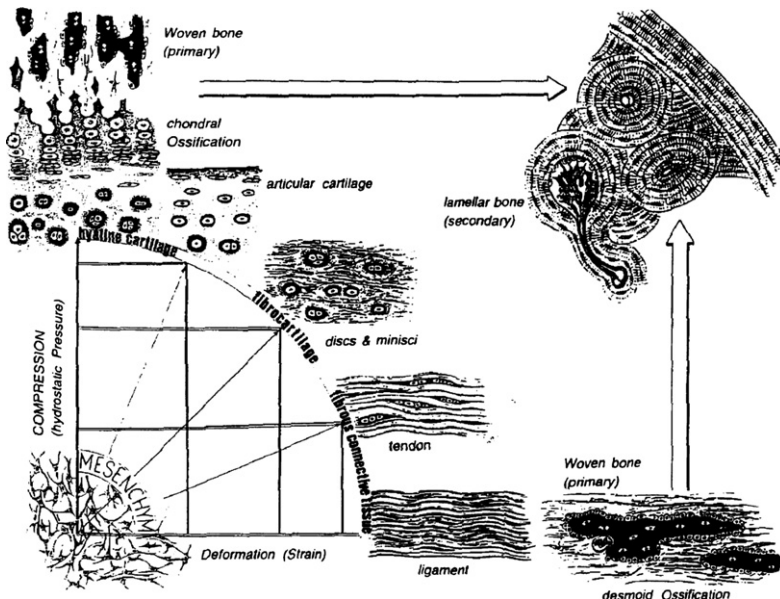


Fig. 48. Schematic presentation of Pauwels' idea of how the mechanical stimulus influences tissue differentiation. Predominant deviatoric stress (or here strain) causes connective tissue formation, while hydrostatic pressure leads to the formation of cartilage (from [336] with permission).

callus. Based on the division of the stress into a dilatational (hydrostatic, and therefore causing only volume change) and deviatoric components (causing only shape change), Pauwels proposed that tissue differentiation is routed by which of the two stress components dominates. While hydrostatic compression stimulates cell differentiation towards cartilage, deviatoric stress is responsible for the formation of connective tissue [335] (Fig. 48). This idea can be condensed in a kind of “phase diagram”, where the parameter space defined by the mechanical stimuli (here, the hydrostatic and the deviatoric stress) is subdivided into regions of different tissue differentiation.

The phase diagram of tissue differentiation is further refined to include the possibility of direct bone formation at low stress levels. Furthermore, the possibility of tensile hydrostatic stresses is also taken into account [337]. Since biological responses seem to be linked to changes in cell shape and deformations of the surrounding matrix, it is further argued that the appropriate mechanical quantities for the formulation of the phase diagram should be strain measures rather than stress measures [338]. A big unknown in all mechanobiological theories is how to deal with the complex loading history. Here, an analysis in number of loading cycles with given amplitude and frequency is proposed [337]. Carter et al. include also non-mechanical factors in their model arguing that poor vascularity can divert tissue differentiation from a bone pathway towards cartilage [337]. A formulation in quantitative terms hypothesizes that intramembranous ossification is only possible in the low strain regime smaller than 5% and below a hydrostatic pressures of  $-0.15 \text{ MPa}$ . For larger pressures, endochondral ossification occurs as long as the strains do not exceed 15% [339]. A different approach views the tissues not only as elastic materials but as material composed of a solid and liquid phase [340]. The loading of the tissue not only causes a deformation, but also a fluid flow which can stimulate the cells. Cell

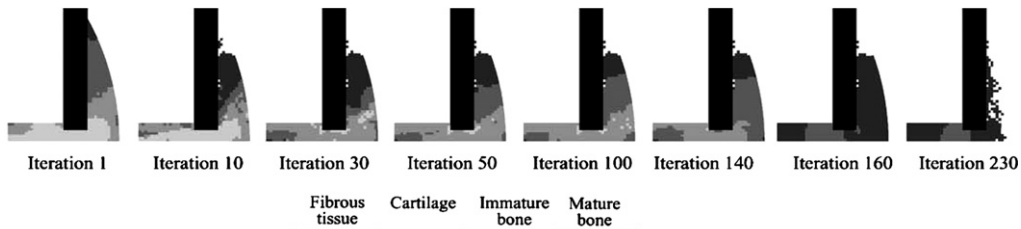


Fig. 49. Fracture healing patterns predicted from computer simulations based on a poroelastic finite-element model. The different stages from cartilage formation in the fracture gap, development of an osseous bridge at the outside and finally bone resorption after a direct bone bridge was formed between the fracture ends (from [342] with permission).

differentiation is then described within a phase diagram with shear strain and fluid flow defining the axis [341]. In general, a phase diagram provides only the path of tissue differentiation, but not how fast the differentiation proceeds. To go beyond a static survey towards a dynamical description of healing, the rates of tissue differentiation have to be defined in form of regulation rules. Using a biphasic poroelastic finite-element model, Prendergast and co-workers simulated the time-course of tissue differentiation during fracture healing. Their results of the effect of gap size and loading magnitude are in reasonable agreement with experimental observations (Fig. 49) [342]. Considering a finite diffusion constant with which the precursor cells spread over the callus, the origin of the precursor cells – surrounding muscle, bone marrow or periosteum – have a massive effect on the healing pattern [343]. Having different mechanobiological theories of fracture healing at hand, a natural question which arises is: “which one is the best?” A comparative study shows that all proposed theories predict satisfactorily the spatial and temporal tissue differentiation patterns in normal fracture healing. Surprisingly, a healing model considering only tissue deformation as mechanical stimulus also accurately predicted the course of normal healing [344]. The simulations models differ in their predictions for healing under torsion loading. None of them successfully predict the course of healing as observed in animal experiments, however, the model based on deviatoric strain and fluid velocity give results that are closest to experiments [345].

The focus on the mechanobiological aspect of bone fracture healing in the selection of research presented above, should not mislead the reader in underestimating the importance of biological stimuli during the healing. Cytokines, like bone morphogenetic proteins to name only one important family, demonstrate a high potency to induce bone *in vitro* in animal models [346]. Interestingly, this potency could not be successfully repeated in human patients [347]. Initial attempts to include biological stimuli in computational models have been performed [348,349], but it remains unclear how to deal with the complexity of the regulatory cytokine network and also the probable coupling between mechanical and biological stimuli. An optimistic assessment of future computational models of fracture healing is based on animal experiments with a well-defined geometry and loading, and with histological and mechanical data of the fracture callus for multiple time points during healing. Reliable data will significantly help to separate successful from less successful model approaches. With a set of regulation rules for tissue differentiation which allow a realistic reproduction of the healing process, simulations can then be used to gain insight into the significance and the robustness of these rules. This will in turn improving

the understanding of the regulatory mechanism which may inspire the construction of man-made self-healing materials. With the progress in our understanding of genetic signalling pathways, the long-time goal has to be to go beyond the phenomenological regulation rules used in the models nowadays and to include our knowledge about mechanotransduction in cells [350]. It will be an exciting moment when bottom-up approaches, nowadays typically referred to as systems biology [351], make contact with the top-down mechano-biological models of fracture healing.

## 7. Outlook

Biological materials have evolved to their intriguing structures in a very long evolutionary process. Nevertheless, it is not evident at all that the lessons learned from biological materials will be directly applicable to the design of new engineering materials. Indeed, bio-inspiration is not just a consequence of an observation of naturally occurring structures. The reason is that Nature has to live with boundary conditions which might not be relevant in the engineering problem, but which might be important for the development of the structure observed [352]. While it is true that the structures we observe are probably good solutions found by a long adaptation process during evolution, we do not exactly know which problems have been solved in this way. The reason for a given structure found in Nature may just be to provide a strong material but also to meet some quite different biological constraints. This implies that we might be fooled, if we just take solutions found by Nature as optimal for a certain requirement which we hardly know. As a consequence, we have to study carefully the biological system and understand the structure–function relation of the biological material in the context of its physical and biological constraints. We hope that the present review may provide the materials scientist with some basic information on the relation between structure, properties and biological function, at least in a few prominent examples of biological materials. We believe that biomimetic materials science has a great potential for finding new solutions of engineering problems, provided the biological materials are studied within their natural biological context.

## Acknowledgements

The authors are grateful to all the collaborators with whom they had the pleasure to interact over the years. We report the work of many gifted PhD- and diploma students whose publications are cited in this review, Helga Lichtenegger, Alex Reiterer, Susanne Rinnerthaler, Sabine Schreiber, Klaus Misof, Barbara Misof, Hannes Jakob, Ivo Zizak, Wolfgang Wagermaier, Alex Wöß, Davide Ruffoni, Markus Hartmann, Barbara Aichmayer, Angelika Valenta, Walter Tesch, Markus Weber, Jong Seto, Jörg Färber, Ulla Stachewicz, René Puxkandl, Daniel Jaschouz. P.F. thanks in particular Nadja Fratzl-Zelman and Klaus Klaushofer (Ludwig Boltzmann Institute of Osteology, Vienna) with who joint research work on bone was started more than 15 years ago. Concerning the most recent work, we warmly thank Paul Roschger (Ludwig Boltzmann Institute of Osteology, Vienna), Himadri Gupta (Max Planck Institute of Colloids and Interfaces, Potsdam) and Herwig Peterlik (University of Vienna) for longstanding joint work on bone structure and function, Ingo Burgert (Max Planck Institute of Colloids and Interfaces, Potsdam) and Stefanie Stanzl-Tschegg (University of Natural Resources and Applied Life Sciences, Vienna) for continued collaboration in the investigation of the plant cell-wall structure,

and Joanna Aizenberg (Bell Labs), Dan Morse and James Weaver (UCSB), for their collaboration on glass sponges. Oskar Paris (Max Planck Institute of Colloids and Interfaces, Potsdam) is acknowledged for his continued contributions to all these subjects. Finally, we are most grateful to John Dunlop and Jong Seto for a critical reading of this manuscript.

## References

- [1] Aksay IA, Weiner S. Biomaterials – is this really a field of research? *Curr Opin Solid State Mater Sci* 1998;3:219–20.
- [2] Schwendener S. Das mechanische Prinzip im anatomischen Bau der Monocotylen mit vergleichenden Ausblicken auf die übrigen Pflanzenklassen. Engelmann Verlag: Leipzig; 1874.
- [3] Thompson AW. On growth and form – the complete revised edition (unaltered republication of Cambridge Univ. Press, 1942) ed.. Dover Publications; 1992.
- [4] Mattheck C, Kubler H. The internal optimization of trees. Berlin: Springer Verlag; 1995.
- [5] Jeronimidis G. In: Elices M, editor. Structural biological materials, design and structure–property relationships. Amsterdam: Pergamon; 2000. p. 3–29 [chapters 1 and 2].
- [6] Currey JD. Bones – structure and mechanics. Princeton: Princeton University Press; 2002. p. 436.
- [7] Cowin SC. Bone mechanics handbook. Boca Raton: CRC Press; 2001.
- [8] Vincent JFV. Structural biomaterials. revised ed. Princeton: Princeton University Press; 1990.
- [9] Wainwright SA, Biggs WD, Currey JD, Gosline JM. Mechanical design in organisms. Princeton University Press; 1982. p. 423.
- [10] Niklas KJ. Plant biomechanics: an engineering approach to plant form and function. Chicago: University of Chicago Press; 1992. p. 607.
- [11] Niklas KJ, Spatz HC, Vincent J. Plant biomechanics: an overview and prospectus. *Am J Bot* 2006;93:1369–78.
- [12] Mattheck C. Design in nature: learning from trees. Berlin, New York: Springer-Verlag; 1998. p. xiv, 276 p.
- [13] Collins MW, Hunt GD, Atherton MAe. Optimisation mechanics in Nature. Southampton, Boston: Wit Press; 2004.
- [14] Gibson LJ, Ashby MF. Cellular solids, structure and properties. 2nd ed. Cambridge: Cambridge University Press; 1999. p. 510.
- [15] Hull D, Clyne TW. An introduction to composite materials. 2nd ed. Cambridge, UK: Cambridge University Press; 1996.
- [16] Torquato S. Random heterogeneous materials: microstructure and macroscopic properties. New York: Springer; 2002. p. xxi, 701 p.
- [17] Tirrell DA. Hierarchical structures in biology as a guide for new materials technology. Washington: National Academy Press; 1994. p. 130.
- [18] Sanchez C. Biomimétisme et Matériaux. Paris: OFTA; 2001.
- [19] Sarikaya M. Biomimetics: materials fabrication through biology. *Proc Natl Acad Sci USA* 1999;96:14183–5.
- [20] Vincent JFV, Bogatyrev OA, Bogatyrev NR, Bowyer A, Pahl A-K. Biomimetics: its practice and theory. *J R Soc Interface* 2006;3:471–82.
- [21] Vincent JFV, Mann DL. Systematic technology transfer from biology to engineering. *Philos Trans R Soc London Ser A – Math Phys Eng Sci* 2002;360:159–73.
- [22] Fratzl P. Biomimetic materials research – what can we really learn from Nature's structural materials? *J R Soc Interface* 2007;4:637–42.
- [23] Lipowsky R. The physics of bio-systems. From molecules to network. *Biophys Rev Lett* 2006;1:223–230.
- [24] Nachtigall W. Bionik – Grundlagen und Beispiele für Ingenieure und Naturwissenschaftler. Berlin: Springer-Verlag; 1998. p. 350.
- [25] French M. Invention and evolution – design in Nature and engineering. 2nd ed. Cambridge: Cambridge University Press; 1994. p. 367.
- [26] Mann S. Biomineralization – principles and concepts in bioinorganic chemistry. Oxford University Press; 2001. p. 198.
- [27] Ashby MF, Gibson LJ, Wegst U, Olive R. The mechanical-properties of natural materials. 1. Material property charts. *Proc R Soc London Ser A – Math Phys Sci* 1995;450:123–40.

- [28] Gibson LJ, Ashby MF, Karam GN, Wegst U, Shercliff HR. The mechanical-properties of natural materials. 2. Microstructures for mechanical efficiency. Proc R Soc London Ser A – Math Phys Sci 1995;450:141–62.
- [29] Wegst UGK, Ashby MF. The mechanical efficiency of natural materials. Philos Mag 2004;84:2167–81.
- [30] Mattheck C, Bethge K. The structural optimization of trees. Naturwissenschaften 1998;85:1–10.
- [31] Meyers MA, Chen, P-Y, Lin AYM, Yasuaki Seki Y. Biological Materials: structure and mechanical properties. Progr Mater Sci, this issue. doi:10.1016/j.pmatsci.2007.05.002.
- [32] Fengel D, Wegener G. Wood: chemistry, ultrastructure, reactions. Berlin: de Gruyter; 1989.
- [33] Fratzl P. Cellulose and collagen: from fibres to tissues. Curr Opin Colloid Interface Sci 2003;8:32–9.
- [34] Lichtenegger H, Muller M, Paris O, Riekel C, Fratzl P. Imaging of the helical arrangement of cellulose fibrils in wood by synchrotron X-ray microdiffraction. J Appl Crystallogr 1999;32:1127–33.
- [35] Fahlen J, Salmen L. On the lamellar structure of the tracheid cell wall. Plant Biol 2002;4:339–45.
- [36] Fahlen J, Salmen L. Pore and matrix distribution in the fiber wall revealed by atomic force microscopy and image analysis. Biomacromolecules 2005;6:433–8.
- [37] Lichtenegger H, Reiterer A, Tschegg SE, Müller M, Riekel C, Paris O, et al. In: Spatz HC, Speck T, Thieme G, editors. Microfibril angle determined by X-ray scattering and the correlation with the mechanical properties of wood. Plant Biomechanics 2000, Stuttgart, 2000.
- [38] Jakob HF, Fratzl P, Tschegg SE. Size and arrangement of elementary cellulose fibrils in wood cells – a small-angle X-ray-scattering study of *Picea abies*. J Struct Biol 1994;113:13–22.
- [39] Jakob HF, Fengel D, Tschegg SE, Fratzl P. The elementary cellulose fibril in *Picea abies*: comparison of transmission electron microscopy, small-angle X-ray scattering, and wide-angle X-ray scattering results. Macromolecules 1995;28:8782–7.
- [40] Zimmermann T, Thommen V, Reimann P, Hug H. Ultrastructural appearance of embedded and polished wood cell walls as revealed by atomic force microscopy. J Struct Biol 2006;156:363–9.
- [41] Jakob HF, Tschegg SE, Fratzl P. Hydration dependence of the wood-cell wall structure in *Picea abies*. A small-angle X-ray scattering study. Macromolecules 1996;29:8435–40.
- [42] Fratzl P, Jakob HF, Rinnerthaler S, Roschger P, Klaushofer K. Position-resolved small-angle X-ray scattering of complex biological materials. J Appl Crystallogr 1997;30:765–9.
- [43] Bergander A, Salmen L. Variations in transverse fibre wall properties: relations between elastic properties and structure. Holzforschung 2000;54:654–60.
- [44] Bergander A, Salmen L. Cell wall properties and their effects on the mechanical properties of fibers. J Mater Sci 2002;37:151–6.
- [45] Keckes J, Burgert I, Fruhmann K, Muller M, Kolln K, Hamilton M, et al. Cell-wall recovery after irreversible deformation of wood. Nat Mater 2003;2:810–4.
- [46] Weiner S, Wagner HD. The material bone: structure–mechanical function relations. Ann Rev Mater Sci 1998;28:271–98.
- [47] Rho JY, Kuhn-Spearing L, Ziopoulos P. Mechanical properties and the hierarchical structure of bone. Med Eng Phys 1998;20:92–102.
- [48] Fratzl P, Gupta HS, Paschalidis EP, Roschger P. Structure and mechanical quality of the collagen-mineral nano-composite in bone. J Mater Chem 2004;14:2115–23.
- [49] Roschger P, Fratzl P, Eschberger J, Klaushofer K. Validation of quantitative backscattered electron imaging for the measurement of mineral density distribution in human bone biopsies. Bone 1998;23:319–26.
- [50] Roschger P, Gupta HS, Berzanovich A, Ittner G, Dempster DW, Fratzl P, et al. Constant mineralization density distribution in cancellous human bone. Bone 2003;32:316–23.
- [51] Weiner S, Arad T, Sabanay I, Traub W. Rotated plywood structure of primary lamellar bone in the rat: orientations of the collagen fibril arrays. Bone 1997;20:509–14.
- [52] Weiner S, Traub W, Wagner HD. Lamellar bone: structure–function relations. J Struct Biol 1999;126:241–55.
- [53] Ascenzi A, Bonucci E, Generali P, Ripamonti A, Roveri N. Orientation of apatite in single osteon samples as studied by pole figures. Calcified Tissue Int 1979;29:101–5.
- [54] Rho JY, Ziopoulos P, Currey JD, Pharr GM. Variations in the individual thick lamellar properties within osteons by nanoindentation. Bone 1999;25:295–300.
- [55] Martin R, Farjanel J, Eichenberger D, Colige A, Kessler E, Hulmes DJS, et al. Liquid crystalline ordering of procollagen as a determinant of three-dimensional extracellular matrix architecture. J Mol Biol 2000;301:11–7.
- [56] Hulmes DJS. Building collagen molecules, fibrils, and suprafibrillar structures. J Struct Biol 2002;137:2–10.

- [57] Giraud-Guille MM. Twisted plywood architecture of collagen fibrils in human compact-bone osteons. *Calcified Tissue Int* 1988;42:167–80.
- [58] Bigi A, Burghammer M, Falconi R, Koch MHJ, Panzavolta S, Riekel C. Twisted plywood pattern of collagen fibrils in teleost scales: an X-ray diffraction investigation. *J Struct Biol* 2001;136:137–43.
- [59] Jaschouz D, Paris O, Roschger P, Hwang HS, Fratzl P. Pole figure analysis of mineral nanoparticle orientation in individual trabecula of human vertebral bone. *J Appl Crystallogr* 2003;36:494–8.
- [60] Rinnerthaler S, Roschger P, Jakob HF, Nader A, Klaushofer K, Fratzl P. Scanning small angle X-ray scattering analysis of human bone sections. *Calcified Tissue Int* 1999;64:422–9.
- [61] Camacho NP, Rinnerthaler S, Paschalis EP, Mendelsohn R, Boskey AL, Fratzl P. Complementary information on bone ultrastructure from scanning small angle X-ray scattering and Fourier-transform infrared microspectroscopy. *Bone* 1999;25:287–93.
- [62] Roschger P, Grabner BM, Rinnerthaler S, Tesch W, Kneissel M, Berzlanovich A, et al. Structural development of the mineralized tissue in the human L4 vertebral body. *J Struct Biol* 2001;136:126–36.
- [63] Termine JD, Robey PG. Bone matrix proteins and the mineralization process. In: Favus MJ, editor. *Primer on the metabolic bone diseases and disorders of mineral metabolism. An Official Publication of the American Society for Bone and Mineral Research*, Lippincott-Raven Publishers; 1996.
- [64] Hodge AJ, Petruska JA. Aspects of protein structure. In: Ramachandran GN, editor. New York: Academic Press; 1963. p. 289–300.
- [65] Landis WJ, Hodgens KJ, Arena J, Song MJ, McEwen BF. Structural relations between collagen and mineral in bone as determined by high voltage electron microscopic tomography. *Microsc Res Tech* 1996;33:192–202.
- [66] White SW, Hulmes DJS, Miller A, Timmins PA. Collagen-mineral axial relationship in calcified Turkey leg tendon by X-ray and neutron-diffraction. *Nature* 1977;266:421–5.
- [67] Landis WJ. Mineral characterization in calcifying tissues: atomic, molecular and macromolecular perspectives. *Connect Tissue Res* 1996;35:1–8.
- [68] Hassenkam T, Fantner GE, Cutroni JA, Weaver JC, Morse DE, Hansma PK. High-resolution AFM imaging of intact and fractured trabecular bone. *Bone* 2004;35:4–10.
- [69] Sodek J, Ganss B, McKee MD. Osteopontin. *Crit Rev Oral Biol Med* 2000;11:279–303.
- [70] Landis WJ, Hodgens KJ, Song MJ, Arena J, Kiyonaga S, Marko M, et al. Mineralization of collagen may occur on fibril surfaces: evidence from conventional and high-voltage electron microscopy and three-dimensional imaging. *J Struct Biol* 1996;117:24.
- [71] Traub W, Arad T, Weiner S. Origin of mineral crystal-growth in collagen fibrils. *Matrix* 1992;12:251–5.
- [72] Fratzl P, Fratzl-Zelman N, Klaushofer K, Vogl G, Koller K. Nucleation and growth of mineral crystals in bone studied by small-angle X-ray-scattering. *Calcified Tissue Int* 1991;48:407–13.
- [73] Glimcher MJ. Recent studies of the mineral phase in bone and its possible linkage to the organic matrix by protein-bound phosphate bonds. *Philos Trans R Soc London Ser B – Biol Sci* 1984;304:479–508.
- [74] Grynpas M, Bonar LC, Glimcher MJ. X-ray diffraction radial distribution function studies on bone mineral and synthetic calcium phosphates. *J Mater Sci* 1985;19.
- [75] Posner AS. The mineral of bone. *Clinical Orthopaedics and Related Research* 1985;200:87–98.
- [76] Rubin MA, Rubin J, Jasiek W. SEM and TEM study of the hierarchical structure of C57BL/6J and C3H/HeJ mice trabecular bone. *Bone* 2004;35:11–20.
- [77] Fratzl P, Groschner M, Vogl G, Plenk H, Eschberger J, Fratzl-Zelman N, et al. Mineral crystals in calcified tissues – a comparative-study by SAXS. *J Bone Min Res* 1992;7:329–34.
- [78] Weiner S, Traub W. Bone-structure – from angstroms to microns. *FASEB J* 1992;6:879–85.
- [79] Fratzl P, Fratzl-Zelman N, Klaushofer K. Collagen packing and mineralization – an X-ray-scattering investigation of Turkey leg tendon. *Biophys J* 1993;64:260–6.
- [80] Fratzl P. Small-angle scattering in materials science: a short review of applications in alloys, ceramics and composite materials. *J Appl Crystallogr* 2003;36:397–404.
- [81] Paris O, Zizak I, Lichtenegger H, Roschger P, Klaushofer K, Fratzl P. Analysis of the hierarchical structure of biological tissues by scanning X-ray scattering using a micro-beam. *Cell Mol Biol* 2000;46:993–1004.
- [82] Fantner GE, Hassenkam T, Kindt JH, Weaver JC, Birkedal H, Pechenik L, et al. Sacrificial bonds and hidden length dissipate energy as mineralized fibrils separate during bone fracture. *Nat Mater* 2005;4:612–6.
- [83] Landis WJ, Song MJ, Leith A, McEwen L, McEwen BF. Mineral and organic matrix interaction in normally calcifying tendon visualized in 3 dimensions by high-voltage electron-microscopic tomography and graphic image-reconstruction. *J Struct Biol* 1993;110:39–54.

- [84] Lees S, Mook HA. Equatorial diffraction spacing as a function of water-content in fully mineralized cow bone determined by neutron-diffraction. *Calcified Tissue Int* 1986;39:291–2.
- [85] Carty EG, Kadler KE. Collagen fibril biosynthesis in tendon: a review and recent insights. *Comp Biochem Physiol A – Mol Integr Physiol* 2002;133:979–85.
- [86] Kadler KE, Holmes DFT, Chapman JA. Collagen fibril formation. *Biochem J* 1996;316:1–11.
- [87] Veis A. Collagen fibrillar structure in mineralized and nonmineralized tissues. *Curr Opin Solid State Mater Sci* 1997;2:370–8.
- [88] Wess TJ. Collagen fibrillar form and function. In: Parry D, Squire J, editors. *Fibrous proteins: coiled-coils, collagen and elastomers*, vol. 70. Burlington: Elsevier Inc.; 2005. p. 341–74.
- [89] Knott L, Bailey AJ. Collagen cross-links in mineralizing tissues: a review of their chemistry, function, and clinical relevance. *Bone* 1998;22:181–7.
- [90] Prockop DJ, Kivirikko KI. Heritable diseases of collagen. *N Engl J Med* 1984;311:376–96.
- [91] Yamauchi M. Collagen: the major matrix molecule in mineralized tissues. In: Anderson JJB, Garner SC, editors. *Calcium Phosphorus Health Dis.* New York: CRC Press; 1996. p. 127–41.
- [92] Prockop DJ, Kivirikko KI. Collagens: molecular biology, diseases, and potentials for therapy [review]. *Ann Rev Biochem* 1995;64:403–34.
- [93] Levi C, Barton JL, Guillemet C, Le Bras E, Lehude P. A remarkably strong natural glassy rod: the anchoring spicule of the *Monorhaphis* sponge. *J Mater Sci Lett* 1989;8:337–9.
- [94] Hamm CE, Merkel R, Springer O, Jurkojc P, Maier C, Prechtel K, et al. Architecture and material properties of diatom shells provide effective mechanical protection. *Nature* 2003;421:841–3.
- [95] Sarikaya M, Fong H, Sunderland N, Flinn BD, Mayer G, Mescher A, et al. Biomimetic model of a sponge-spicular optical fiber – mechanical properties and structure. *J Mater Res* 2001;16:1420–8.
- [96] Woesz A, Weaver JC, Kazanci M, Dauphin Y, Aizenberg J, Morse DE, et al. Micromechanical properties of biological silica in skeletons of deep-sea sponges. *J Mater Res* 2006;21:2068–78.
- [97] Aizenberg J, Weaver JC, Thanawala MS, Sundar VC, Morse DE, Fratzl P. Skeleton of *Euplectella* sp.: structural hierarchy from the nanoscale to the macroscale. *Science* 2005;309:275–8.
- [98] Aizenberg J, Sundar VC, Yablon AD, Weaver JC, Chen G. Biological glass fibers: correlation between optical and structural properties. *Proc Natl Acad Sci USA* 2004;101:3358–63.
- [99] Sundar VC, Yablon AD, Grazul JL, Ilan M, Aizenberg J. Fibre-optical features of a glass sponge – some superior technological secrets have come to light from a deep-sea organism. *Nature* 2003;424:899–900.
- [100] Saito T, Uchida I, Takeda M. Skeletal growth of the deep-sea hexactinellid sponge *Euplectella oweni*, and host selection by the symbiotic shrimp *Spongicola japonica* (Crustacea:Decapoda:Spongicolidae). *J Zool* 2002;258:521–9.
- [101] Weaver JC, Aizenberg J, Fantner GE, Kisailus D, Woesz A, Allen P, et al. Hierarchical assembly of the siliceous skeletal lattice of the Hexactinellid Sponge *Euplectella aspergillum*. *J Struct Biol* 2007;158:93–106.
- [102] Heaney RP. Is the paradigm shifting? *Bone* 2003;33:457–65.
- [103] Woesz A, Stampfli J, Fratzl P. Cellular solids beyond the apparent density – an experimental assessment of mechanical properties. *Adv Eng Mater* 2004;6:134–8.
- [104] Banhart J. Aluminum foams: on the road to real applications. *Mrs Bull* 2003;28:290–5.
- [105] Green DJ, Colombo R. Cellular ceramics: intriguing structures, novel properties, and innovative applications. *Mrs Bull* 2003;28:296–300.
- [106] Roberts AP, Garboczi EJ. Elastic properties of model random three-dimensional open-cell solids. *J Mech Phys Solids* 2002;50:33–55.
- [107] Huiskes R. If bone is the answer, then what is the question? *J Anat* 2000;197:145–56.
- [108] Cowin SC. The false premise of Wolff's law. *Forma* 1997;12:247–62.
- [109] Thurner PJ, Wyss P, Voide R, Stauber M, Stampanoni M, Sennhauser U, et al. Time-lapsed investigation of three-dimensional failure and damage accumulation in trabecular bone using synchrotron light. *Bone* 2006;39:289–99.
- [110] Homminga J, Van-Rietbergen B, Lochmuller EM, Weinans H, Eckstein F, Huiskes R. The osteoporotic vertebral structure is well adapted to the loads of daily life, but not to infrequent “error” loads. *Bone* 2004;34:510–6.
- [111] Gibson LJ. Biomechanics of cellular solids. *J Biomech* 2005;38:377–99.
- [112] Greenhill G. Determination of the greatest height consistent with stability that a vertical pole or mast can be made, and the greatest height to which a tree of given proportions can grow. *Proc Cambridge Philos Soc* 1881;4:65–73.
- [113] McMahon T. Size and shape in biology. *Science* 1973;179:1201–4.

- [114] Landau LD, Lifshitz EM. Theory of elasticity. 3rd English ed. Butterworth-Heinemann; 1986. p. viii, 187 p.
- [115] Ashby MF. The mechanical-properties of cellular solids. *Metall Trans A – Phys Metall Mater Sci* 1983;14:1755–69.
- [116] Lichtenegger H, Reiterer A, Stanzl-Tschegg SE, Fratzl P. Variation of cellulose microfibril angles in softwoods and hardwoods – a possible strategy of mechanical optimization. *J Struct Biol* 1999;128:257–69.
- [117] Ashby MF. Materials selection in mechanical design. 2nd ed. Oxford: Butterworth-Heinemann; 1999.
- [118] Morgan EF, Yeh OC, Chang WC, Keaveny TW. Nonlinear behavior of trabecular bone at small strains. *J Biomech Eng – Trans ASME* 2001;123:1–9.
- [119] van Rietbergen B, Huiskes R. Elastic constants of cancellous bone. In: Cowin SC, editor. *Bone mechanics handbook*. Boca Raton: CRC Press; 2001.
- [120] van Lenthe GH, Stauber M, Muller R. Specimen-specific beam models for fast and accurate prediction of human trabecular bone mechanical properties. *Bone* 2006;39:1182–9.
- [121] Harrigan TP, Jasty M, Mann RW, Harris WH. Limitations of the continuum assumption in cancellous bone. *J Biomech* 1988;21:269–75.
- [122] Yang GY, Kabel J, Van Rietbergen B, Odgaard A, Huiskes R, Cowin SC. The anisotropic Hooke's law for cancellous bone and wood. *J Elasticity* 1999;53:125–46.
- [123] Morgan EF, Bayraktar HH, Keaveny TM. Trabecular bone modulus–density relationships depend on anatomic site. *J Biomech* 2003;36:897–904.
- [124] Odgaard A. Three-dimensional methods for quantification of cancellous bone architecture. *Bone* 1997;20:315–28.
- [125] Odgaard A. Quantification of cancellous bone architecture. In: Cowin SC, editor. *Bone mechanics handbook*. Boca Raton: CRC Press; 2001.
- [126] Odgaard A, Kabel J, vanRietbergen B, Dalstra M, Huiskes R. Fabric and elastic principal directions of cancellous bone are closely related. *J Biomech* 1997;30:487–95.
- [127] Cowin SC. The relationship between the elasticity tensor and the fabric tensor. *Mech Mater* 1985;4:137–47.
- [128] Zysset PK. A review of morphology–elasticity relationships in human trabecular bone: theories and experiments. *J Biomech* 2003;36:1469–85.
- [129] Kinney JH, Ladd AJC. The relationship between three-dimensional connectivity and the elastic properties of trabecular bone. *J Bone Min Res* 1998;13:839–45.
- [130] Kabel J, Odgaard A, van Rietbergen B, Huiskes R. Connectivity and the elastic properties of cancellous bone. *Bone* 1999;24:115–20.
- [131] Deshpande VS, Ashby MF, Fleck NA. Foam topology bending versus stretching dominated architectures. *Acta Mater* 2001;49:1035–40.
- [132] Fyhrie DP, Schaffler MB. Failure mechanisms in human vertebral cancellous bone. *Bone* 1994;15:105–9.
- [133] Keaveny TM. Strength of trabecular bone. In: Cowin SC, editor. *Bone mechanics handbook*. Boca Raton: CRC Press; 2001.
- [134] Mosekilde L, Mosekilde L, Danielsen CC. Biomechanical competence of vertebral trabecular bone in relation to ash density and age in normal individuals. *Bone* 1987;8:79–85.
- [135] Hernandez CJ, Keaveny TM. A biomechanical perspective on bone quality. *Bone* 2006;39:1173–81.
- [136] Nazarian A, Muller R. Time-lapsed microstructural imaging of bone failure behavior. *J Biomech* 2004;37:55–65.
- [137] Kopperdahl DL, Keaveny TM. Yield strain behavior of trabecular bone. *J Biomech* 1998;31:601–8.
- [138] Keaveny TM, Morgan EF, Niebur GL, Yeh OC. Biomechanics of trabecular bone. *Ann Rev Biomed Eng* 2001;3:307–33.
- [139] Bayraktar HH, Keaveny TM. Mechanisms of uniformity of yield strains for trabecular bone. *J Biomech* 2004;37:1671–8.
- [140] Silva MJ, Gibson LJ. Modeling the mechanical behavior of vertebral trabecular bone: effects of age-related changes in microstructure. *Bone* 1997;21:191–9.
- [141] Vajjhala S, Kraynik AM, Gibson LJ. A cellular solid model for modulus reduction due to resorption of trabeculae in bone. *J Biomech Eng – Trans ASME* 2000;122:511–5.
- [142] Guo XE, Kim CH. Mechanical consequence of trabecular bone loss and its treatment: a three-dimensional model simulation. *Bone* 2002;30:404–11.
- [143] Davy DT, Jepsen KJ. Bone damage mechanics. In: Cowin SC, editor. *Bone mechanics handbook*. Boca Raton: CRC Press; 2001.
- [144] Zysset PK, Curnier A. A 3D damage model for trabecular bone based on fabric tensors. *J Biomech* 1996;29:1549–58.

- [145] Wachtel EF, Keaveny TM. Dependence of trabecular damage on mechanical strain. *J Orthopaed Res* 1997;15:781–7.
- [146] Sahar ND, Hong SI, Kohn DH. Micro- and nano-structural analyses of damage in bone. *Micron* 2005;36:617–29.
- [147] Lee TC, Mohsin S, Taylor D, Parkesh R, Gunnlaugsson T, O'Brien FJ, et al. Detecting microdamage in bone. *J Anat* 2003;203:161–72.
- [148] Haddock SM, Yeh OC, Mummaneni PV, Rosenberg WS, Keaveny TM. Similarity in the fatigue behavior of trabecular bone across site and species. *J Biomech* 2004;37:181–7.
- [149] Haddock SM, Yeh OC, Mummaneni PV, Rosenberg WS, Keaveny TM. Similarity in the fatigue behavior of trabecular bone across site and species (vol. 37, p. 181, 2004). *J Biomech* 2006;39:593.
- [150] Rapillard L, Charlebois M, Zysset PK. Compressive fatigue behavior of human vertebral trabecular bone. *J Biomech* 2006;39:2133–9.
- [151] Vollrath F, Knight DP. Liquid crystalline spinning of spider silk. *Nature* 2001;410:541–8.
- [152] Gosline JM, Demont ME, Denny MW. The structure and properties of spider silk. *Endeavour* 1986;10:37–43.
- [153] Landis WJ. A study of calcification in the leg tendons from the domestic Turkey. *J Ultrastruct Mol Struct Res* 1986;94:217–38.
- [154] Landis WJ, Silver FH. The structure and function of normally mineralizing avian tendons. *Comp Biochem Physiol A – Mol Integr Physiol* 2002;133:1135–57.
- [155] Gupta HS, Roschger P, Zizak I, Fratzl-Zelman N, Nader A, Klaushofer K, et al. Mineralized microstructure of calcified avian tendons: a scanning small angle X-ray scattering study. *Calcified Tissue Int* 2003;72:567–76.
- [156] Gupta HS, Messmer P, Roschger P, Bernstorff S, Klaushofer K, Fratzl P. Synchrotron diffraction study of deformation mechanisms in mineralized tendon. *Phys Rev Lett* 2004;93:158101.
- [157] Hulmes DJS, Wess TJ, Prockop DJ, Fratzl P. Radial packing, order, and disorder in collagen fibrils. *Biophys J* 1995;68:1661–70.
- [158] Orgel J, Miller A, Irving TC, Fischetti RF, Hammersley AP, Wess TJ. The in situ supermolecular structure of type I collagen. *Structure* 2001;9:1061–9.
- [159] Ottani V, Raspanti M, Ruggeri A. Collagen structure and functional implications. *Micron* 2001;32: 251–60.
- [160] Baer E, Cassidy JJ, Hiltner A. Hierarchical structure of collagen composite systems – lessons from biology. *Pure Appl Chem* 1991;63:961–73.
- [161] Baer E, Hiltner A, Jarus D. Relationship of hierarchical structure to mechanical properties. *Macromol Symp* 1999;147:37–61.
- [162] Diamant J, Arridge RGC, Baer E, Litt M, Keller A. Collagen – ultrastructure and its relation to mechanical properties as a function of aging. *Proc R Soc London Ser B – Biol Sci* 1972;180:293.
- [163] Misof K, Rapp G, Fratzl P. A new molecular model for collagen elasticity based on synchrotron X-ray scattering evidence. *Biophys J* 1997;72:1376–81.
- [164] Folkhard W, Geercken W, Knorzer E, Mosler E, Nemetschekgansler H, Nemetschek T, et al. Structural dynamic of native tendon collagen. *J Mol Biol* 1987;193:405–7.
- [165] Folkhard W, Mosler E, Geercken W, Knorzer E, Nemetschekgansler H, Nemetschek T, et al. Quantitative-analysis of the molecular sliding mechanism in native tendon collagen – time-resolved dynamic studies using synchrotron radiation. *Int J Biol Macromol* 1987;9:169–75.
- [166] Fratzl P, Misof K, Zizak I, Rapp G, Amenitsch H, Bernstorff S. Fibrillar structure and mechanical properties of collagen. *J Struct Biol* 1998;122:119–22.
- [167] Mosler E, Folkhard W, Knorzer E, Nemetschekgansler H, Nemetschek T, Koch MHJ. Stress-induced molecular rearrangement in tendon collagen. *J Mol Biol* 1985;182:589–96.
- [168] Sasaki N, Odajima S. Elongation mechanism of collagen fibrils and force-strain relations of tendon at each level of structural hierarchy. *J Biomech* 1996;29:1131–6.
- [169] Sasaki N, Odajima S. Stress-strain curve and Young's modulus of a collagen molecule as determined by the X-ray diffraction technique. *J Biomech* 1996;29:655–8.
- [170] Sasaki N, Shukunami N, Matsushima N, Izumi Y. Time-resolved X-ray diffraction from tendon collagen during creep using synchrotron radiation. *J Biomech* 1999;32:285–92.
- [171] Puxkandl R, Zizak I, Paris O, Keckes J, Tesch W, Bernstorff S, et al. Viscoelastic properties of collagen: synchrotron radiation investigations and structural model. *Philos Trans R Soc London Ser B – Biol Sci* 2002;357:191–7.

- [172] Cribb AM, Scott JE. Tendon response to tensile-stress – an ultrastructural investigation of collagen–proteoglycan interactions in stressed tendon. *J Anat* 1995;187:423–8.
- [173] Light ND, Bailey AJ. Covalent cross-links in collagen. *Methods Enzymol* 1982;82A:360–72.
- [174] Bailey AJ, Paul RG, Knott L. Mechanisms of maturation and ageing of collagen. *Mech Ageing Dev* 1998;106:1–56.
- [175] Davison PF. The contribution of labile crosslinks to the tensile behavior of tendons. *Connect Tissue Res* 1989;18:293–305.
- [176] Eyre DR, Paz MA, Gallop PM. Cross-linking in collagen and elastin. *Ann Rev Biochem* 1984;53:717–48.
- [177] Lees S, Eyre DR, Barnard SM. BAPN dose dependence of mature crosslinking in bone matrix collagen of rabbit compact bone: corresponding variation of sonic velocity and equatorial diffraction spacing. *Connect Tissue Res* 1990;24:95–105.
- [178] Kastelic J, Galeski A, Baer E. Multicomposite structure of tendon. *Connect Tissue Res* 1978;6:11–23.
- [179] Buehler MJ. Nature designs tough collagen: explaining the nanostructure of collagen fibrils. *Proc Natl Acad Sci USA* 2006;103:12285–90.
- [180] Bozec L, Horton M. Topography and mechanical properties of single molecules of type I collagen using atomic force microscopy. *Biophys J* 2005;88:4223–31.
- [181] Bozec L, van der Heijden G, Horton M. Collagen fibrils: nanoscale ropes. *Biophys J* 2007;92:70–5.
- [182] Sun YL, Luo ZP, Fertala A, An KN. Direct quantification of the flexibility of type I collagen monomer. *Biochem Biophys Res Commun* 2002;295:382–6.
- [183] Bustamante C, Marko JF, Siggia ED, Smith S. Entropic elasticity of lambda-phage DNA. *Science* 1994;265:1599–600.
- [184] Buehler MJ. Atomistic and continuum modeling of mechanical properties of collagen: elasticity, fracture, and self-assembly. *J Mater Res* 2006;21:1947–61.
- [185] Fratzl P, Gupta HS. Nanoscale mechanisms of bone deformation and fracture. In: Bäuerlein E, editor. *Handbook of biominerization*, vol. 1. Weinheim: Wiley-VCH Verlag GmbH; 2007. p. 397–414.
- [186] Gebhardt W. Regarding the functionally important assembly techniques of the small scale and large scale building blocks of the vertebral bone II: special part: the building of the Haversian lamellar system and its functional meaning. *Arch Entwickl Mech Org* 1906;20:187–322.
- [187] Boyde A, Bianco P, Barbos MP, Ascenzi A. Collagen orientation in compact-bone. 1. A new method for the determination of the proportion of collagen parallel to the plane of compact-bone sections. *Metab Bone Dis Relat Res* 1984;5:299–307.
- [188] Barbos MP, Bianco P, Ascenzi A, Boyde A. Collagen orientation in compact-bone. 2. Distribution of lamellae in the whole of the human femoral-shaft with reference to its mechanical-properties. *Metab Bone Dis Relat Res* 1984;5:309–15.
- [189] Ascenzi A, Bonucci E, Bocciare Ds. An electron microscope study of osteon calcification. *J Ultrastruct Res* 1965;12:287.
- [190] Marotti G, Muglia MA, Palumbo C. Structure and function of lamellar bone. *Clin Rheumatol* 1994;13:63–8.
- [191] Wagermaier W, Gupta HS, Gourrier A, Burghammer M, Roschger P, Fratzl P. Spiral twisting of fiber orientation inside bone lamellae. *Biointerphases* 2006;1:1–5.
- [192] Wagermaier W, Gupta HS, Gourrier A, Paris O, Roschger P, Burghammer M, et al. Scanning texture analysis of lamellar bone using microbeam synchrotron X-ray radiation. *J Appl Crystallogr* 2007;40:115–20.
- [193] Neville AC. Biology of fibrous composites: development beyond the cell membrane. New York, NY: Cambridge University Press; 1993.
- [194] Ziopoulos P. On microcracks, microcracking, in vivo, in vitro, in situ and other issues. *J Biomech* 1999;32:209–11.
- [195] Gupta HS, Stachewicz U, Wagermaier W, Roschger P, Wagner HD, Fratzl P. Mechanical modulation at the lamellar level in osteonal bone. *J Mater Res* 2006;21:1913–21.
- [196] Qiu SJ, Rao DS, Fyhrie DP, Palnitkar S, Parfitt AM. The morphological association between microcracks and osteocyte lacunae in human cortical bone. *Bone* 2005;37:10–5.
- [197] Suresh S, Sugimura Y, Ogawa T. Fatigue cracking in materials with brittle surface-coatings. *Scripta Metall Mater* 1993;29:237–42.
- [198] Simha NK, Fischer FD, Kolednik O, Chen CR. Inhomogeneity effects on the crack driving force in elastic and elastic-plastic materials. *J Mech Phys Solids* 2003;51:209–40.

- [199] Kolednik O. The yield stress gradient effect in inhomogeneous materials. *Int J Solids Struct* 2000;37:781–808.
- [200] Reiterer A, Lichtenegger H, Fratzl P, Stanzl-Tschegg SE. Deformation and energy absorption of wood cell walls with different nanostructure under tensile loading. *J Mater Sci* 2001;36:4681–6.
- [201] Reiterer A, Lichtenegger H, Tschegg S, Fratzl P. Experimental evidence for a mechanical function of the cellulose microfibril angle in wood cell walls. *Philos Mag A – Phys Condens Matter Struct Defects Mech Prop* 1999;79:2173–84.
- [202] Wimmer R, Downes GM, Evans R. Temporal variation of microfibril angle in *Eucalyptus nitens* grown in different irrigation regimes (vol. 22, p. 449, 2002). *Tree Physiol* 2002;22:817.
- [203] Lindstrom H, Evans JW, Verrill SP. Influence of cambial age and growth conditions on microfibril angle in young Norway spruce (*Picea abies* [L.] Karst.). *Holzforschung* 1998;52:573–81.
- [204] Evans R, Stringer S, Kibblewhite RP. Variation of microfibril angle, density and fibre orientation in twenty-nine *Eucalyptus nitens* trees. *Appita J* 2000;53:450–7.
- [205] Kibblewhite RP, Evans R, Riddell MJC, Shelbourne CJA. Changes in density and wood-fibre properties with height position in 15/16-year-old *Eucalyptus nitens* and *E-fastigata*. *Appita J* 2004;57:240–7.
- [206] Kibblewhite RP, Evans R, Grace JC, Riddell MJC. Fibre length, microfibril angle and wood colour variation and interrelationships for two radiata pine trees with mild and severe compression wood. *Appita J* 2005;58:316–22.
- [207] Bonham VA, Barnett JR. Fibre length and microfibril angle in silver birch (*Betula pendula* Roth). *Holzforschung* 2001;55:159–62.
- [208] Mosbrugger V. The tree habit in land plants: a functional comparison of trunk constructions with a brief introduction into the biomechanics of trees. Berlin, New York: Springer-Verlag; 1990. p. 161.
- [209] Astley OM, Donald AM. A small-angle X-ray scattering study of the effect of hydration on the microstructure of flax fibers. *Biomacromolecules* 2001;2:672–80.
- [210] Yamamoto H, Kojima Y. Properties of cell wall constituents in relation to longitudinal elasticity of wood – Part 1. Formulation of the longitudinal elasticity of an isolated wood fiber. *Wood Sci Technol* 2002;36:55–74.
- [211] Yamamoto H, Kojima Y, Okuyama T, Abasolo WP, Gril J. Origin of the biomechanical properties of wood related to the fine structure of the multi-layered cell wall. *J Biomech Eng – Trans ASME* 2002;124:432–40.
- [212] Yamamoto H, Yoshida M, Okuyama T. Growth stress controls negative gravitropism in woody plant stems. *Planta* 2002;216:280–92.
- [213] Brown RM. Cellulose structure and biosynthesis. *Pure Appl Chem* 1999;71:767–75.
- [214] Ferl R, Wheeler R, Levine HG, Paul AL. Plants in space. *Curr Opin Plant Biol* 2002;5:258–63.
- [215] Brett CT. Cellulose microfibrils in plants: biosynthesis, deposition, and integration into the cell wall. In: International review of cytology – a survey of cell biology, vol. 199, 2000; vol. 199, p. 161–99.
- [216] Kimura S, Kondo T. Recent progress in cellulose biosynthesis. *J Plant Res* 2002;115:297–302.
- [217] Nishiyama Y, Langan P, Chanzy H. Crystal structure and hydrogen-bonding system in cellulose I beta from synchrotron X-ray and neutron fiber diffraction. *J Am Chem Soc* 2002;124:9074–82.
- [218] Baker AA, Helbert W, Sugiyama J, Miles MJ. New insight into cellulose structure by atomic force microscopy shows the I-alpha crystal phase at near-atomic resolution. *Biophys J* 2000;79:1139–45.
- [219] Kondo T, Togawa E, Brown RM. Nematic ordered cellulose: a concept of glucan chain association. *Biomacromolecules* 2001;2:1324–30.
- [220] Somerville C, Bauer S, Brininstool G, Facette M, Hamann T, Milne J, et al. Toward a systems approach to understanding plant-cell walls. *Science* 2004;306:2206–11.
- [221] Baskin TI. On the alignment of cellulose microfibrils by cortical microtubules: a review and a model. *Protoplasma* 2001;215:150–71.
- [222] Funada R, Miura H, Shibagaki M, Furusawa O, Miura T, Fukatsu E, et al. Involvement of localized cortical microtubules in the formation of a modified structure of wood. *J Plant Res* 2001;114:491–7.
- [223] Paredez AR, Somerville CR, Ehrhardt DW. Visualization of cellulose synthase demonstrates functional association with microtubules. *Science* 2006;312:1491–5.
- [224] Emons AMC, Mulder BM. How the deposition of cellulose microfibrils builds cell wall architecture. *Trends Plant Sci* 2000;5:35–40.
- [225] Gassan J, Chate A, Bledzki AK. Calculation of elastic properties of natural fibers. *J Mater Sci* 2001;36:3715–20.

- [226] Spatz HC, Köhler L, Niklas KJ. Mechanical behaviour of plant tissues: composite materials or structures? *J Exp Biol* 1999;202:3269–72.
- [227] Köhler L, Spatz HC. Micromechanics of plant tissues beyond the linear-elastic range. *Planta* 2002;215:33–40.
- [228] Burgert I, Keckes J, Fruhmann K, Fratzl P, Tschegg SE. A comparison of two techniques for wood fibre isolation evaluation by tensile tests on single fibres with different microfibril angle. *Plant Biol* 2002;4:9–12.
- [229] Fratzl P. Hierarchical structure and mechanical adaptation of biological materials. In: Reis RL, Weiner S, editors. Learning from Nature – how to design new implantable biomaterials. NATO science series – II, vol. 171. Kluwer Academic Publishers.; 2004. p. 15–34.
- [230] Fratzl P, Burgert I, Keckes J. Mechanical model for the deformation of the wood cell wall. *Z Metallkd* 2004;95:579–84.
- [231] Fratzl P, Burgert I, Gupta HS. On the role of interface polymers for the mechanics of natural polymeric composites. *Phys Chem Chem Phys* 2004;6:5575–9.
- [232] Currey JD. The design of mineralised hard tissues for their mechanical functions. *J Exp Biol* 1999;202:3285–94.
- [233] Currey JD. How well are bones designed to resist fracture? *J Bone Min Res* 2003;18:591–8.
- [234] Peterlik H, Roschger P, Klaushofer K, Fratzl P. From brittle to ductile fracture of bone. *Nat Mater* 2006;5:52–5.
- [235] Ziopoulos P, Currey JD. The extent of microcracking and the morphology of microcracks in damaged bone. *J Mater Sci* 1994;29:978–86.
- [236] Vashishth D, Tanner KE, Bonfield W. Experimental validation of a microcracking-based toughening mechanism for cortical bone. *J Biomech* 2003;36:121–4.
- [237] Liu DM, Weiner S, Wagner HD. Anisotropic mechanical properties of lamellar bone using miniature cantilever bending specimens. *J Biomech* 1999;32:647–54.
- [238] Nalla RK, Kruzic JJ, Ritchie RO. On the origin of the toughness of mineralized tissue: microcracking or crack bridging? *Bone* 2004;34:790–8.
- [239] Nalla RK, Kinney JH, Ritchie RO. Mechanistic fracture criteria for the failure of human cortical bone. *Nat Mater* 2003;2:164–8.
- [240] Nalla RK, Kruzic JJ, Kinney JH, Ritchie RO. Mechanistic aspects of fracture and *R*-curve behavior in human cortical bone. *Biomaterials* 2005;26:217–31.
- [241] Landis WJ. The strength of a calcified tissue depends in part on the molecular-structure and organization of its constituent mineral crystals in their organic matrix. *Bone* 1995;16:533–44.
- [242] Ziopoulos P, Currey JD. Changes in the stiffness, strength, and toughness of human cortical bone with age. *Bone* 1998;22:57–66.
- [243] Ziopoulos P, Currey JD, Hamer AJ. The role of collagen in the declining mechanical properties of aging human cortical bone. *J Biomed Mater Res* 1999;45:108–16.
- [244] Ziopoulos P. Ageing human bone: factors affecting its biomechanical properties and the role of collagen. *J Biomater Appl* 2001;15:187–229.
- [245] Wang XD, Bank RA, TeKoppele JM, Agrawal CM. The role of collagen in determining bone mechanical properties. *J Orthopaed Res* 2001;19:1021–6.
- [246] Wang X, Shen X, Li X, Agrawal CM. Age-related changes in the collagen network and toughness of bone. *Bone* 2002;31:1–7.
- [247] Landis WJ, Librizzi JJ, Dunn MG, Silver FH. A study of the relationship between mineral-content and mechanical-properties of Turkey gastrocnemius tendon. *J Bone Min Res* 1995;10:859–67.
- [248] Gupta HS, Seto J, Wagermaier W, Zaslansky P, Boesecke P, Fratzl P. Cooperative deformation of mineral and collagen in bone at the nanoscale. *Proc Natl Acad Sci USA* 2006;103:17741–6.
- [249] Braidotti P, Bemporad E, D'Alessio T, Sciuto SA, Stagni L. Tensile experiments and SEM fractography on bovine subchondral bone. *J Biomech* 2000;33:1153–7.
- [250] Craig AS, Birtles MJ, Conway JF, Parry DAD. An estimate of the mean length of collagen fibrils in rat tail-tendon as a function of age. *Connect Tissue Res* 1989;19:51–62.
- [251] Gupta HS, Wagermaier W, Zickler GA, Aroush DRB, Funari SS, Roschger P, et al. Nanoscale deformation mechanisms in bone. *Nano Lett* 2005;5:2108–11.
- [252] Thompson JB, Kindt JH, Drake B, Hansma HG, Morse DE, Hansma PK. Bone indentation recovery time correlates with bond reforming time. *Nature* 2001;414:773–6.
- [253] Bonar LC, Lees S, Mook HA. Neutron-diffraction studies of collagen in fully mineralized bone. *J Mol Biol* 1985;181:265–70.

- [254] Tai K, Ulm FJ, Ortiz C. Nanogranular origins of the strength of bone. *Nano Lett* 2006;6:2520–5.
- [255] Gupta HS, Fratzl P, Kerschnitzki M, Benecke G, Wagermaier W, Kirchner HOK. Evidence for an elementary process in bone plasticity with an activation enthalpy of 1 eV. *J R Soc Interface* 2007;4:277–82.
- [256] Fantner GE, Oroudjev E, Schitter G, Golde LS, Thurner P, Finch MM, et al. Sacrificial bonds and hidden length: unraveling molecular mesostructures in tough materials. *Biophys J* 2006;90:1411–8.
- [257] Heiss A, DuChesne A, Denecke B, Grotzinger J, Yamamoto K, Renne T, et al. Structural basis of calcification inhibition by alpha(2)-HS glycoprotein/fetuin-A – formation of colloidal calciprotein particles. *J Biol Chem* 2003;278:13333–41.
- [258] Scott JE, Parry DAD. Control of collagen fibril diameters in tissues. *Int J Biol Macromol* 1992;14:292–3.
- [259] Leporatti S, Gao C, Voigt A, Donath E, Mohwald H. Shrinking of ultrathin polyelectrolyte multilayer capsules upon annealing: a confocal laser scanning microscopy and scanning force microscopy study. *Euro Phys J E* 2001;5:13–20.
- [260] Burr DB, Milgrom C, Fyhrie D, Forwood M, Nyska M, Finestone A, et al. In vivo measurement of human tibial strains during vigorous activity. *Bone* 1996;18:405–10.
- [261] Smith BL, Schaffer TE, Viani M, Thompson JB, Frederick NA, Kindt J, et al. Molecular mechanistic origin of the toughness of natural adhesives, fibres and composites. *Nature* 1999;399:761–3.
- [262] Gutsmann T, Hassenkam T, Cutroni JA, Hansma PK. Sacrificial bonds in polymer brushes from rat tail tendon functioning as nanoscale velcro. *Biophys J* 2005;89:536–42.
- [263] Fantner G, Hassenkam T, Kindt JH, Weaver JC, Birkedal H, Pechenik L, et al. Sacrificial bonds and hidden length dissipate energy as mineralized fibrils separate during bone fracture. *Nat Mater* 2005;4:612–6.
- [264] Jager I, Fratzl P. Mineralized collagen fibrils: a mechanical model with a staggered arrangement of mineral particles. *Biophys J* 2000;79:1737–46.
- [265] Gao HJ, Ji BH, Jager IL, Arzt E, Fratzl P. Materials become insensitive to flaws at nanoscale: lessons from nature. *Proc Natl Acad Sci USA* 2003;100:5597–600.
- [266] Gupta HS, Schratter S, Tesch W, Roschger P, Berzlanovich A, Schoeberl T, et al. Two different correlations between nanoindentation modulus and mineral content in the bone-cartilage interface. *J Struct Biol* 2005;149:138–48.
- [267] Gao HJ. Application of fracture mechanics concepts to hierarchical biomechanics of bone and bone-like materials. *Int J Fract* 2006;138:101–37.
- [268] Mosekilde L, Ebbesen EN, Tornvig L, Thomsen JS. Trabecular bone structure and strength – remodelling and repair. *J Musculoskel Neuron Interact* 2000;1:25–30.
- [269] Chalmers J, Ray RD. The growth of transplanted foetal bones in different immunological environments. *J Bone Joint Surg Br Vol* 1962;44:149–64.
- [270] Goodship AE, Cunningham JL. Pathophysiology of functional adaptation of bone in remodeling and repair in vivo. In: Cowin SC, editor. *Bone mechanics handbook*. Boca Raton: CRC Press; 2001.
- [271] Farber J, Lichtenegger HC, Reiterer A, Stanzl-Tschegg S, Fratzl P. Cellulose microfibril angles in a spruce branch and mechanical implications. *J Mater Sci* 2001;36:5087–92.
- [272] Huiskes R, Ruimerman R, van Lenthe GH, Janssen JD. Effects of mechanical forces on maintenance and adaptation of form in trabecular bone. *Nature* 2000;405:704–6.
- [273] Weinans H, Odgaard A. Bone structure & remodeling: an introduction. In: Odgaard A, Weinans H, editors. *Bone structure and remodeling*. Singapore: World Scientific; 1995.
- [274] Jee WSS. Integrated bone tissue physiology: anatomy and physiology. In: Cowin SC, editor. *Bone mechanics handbook*. Boca Raton: CRC Press; 2001.
- [275] Ruffoni D, Fratzl P, Roschger P, Klaushofer K, Weinkamer R. The bone mineralization density distribution as a fingerprint of the mineralization process. *Bone* 2007;40:1308–19.
- [276] Parfitt AM. Misconceptions (2): turnover is always higher in cancellous than in cortical bone. *Bone* 2002;30:807–9.
- [277] Frost HM. Bone mass and the mechanostat – a proposal. *Anat Rec* 1987;219:1–9.
- [278] Frost HM. Bone's mechanostat: a 2003 update. *Anat Rec Part A – Disc Mol Cell Evolut Biol* 2003;275A:1081–101.
- [279] Robling AG, Castillo AB, Turner CH. Biomechanical and molecular regulation of bone remodeling. *Ann Rev Biomed Eng* 2006;8:455–98.
- [280] Pearson OM, Lieberman DE. The aging of Wolff's "law": ontogeny and responses to mechanical loading cortical bone. *Am J Phys Anthropol* 2004;63–99.
- [281] Bertram JEA, Swartz SM. The law of bone transformation – a case of crying Wolff. *Biol Rev Cambridge Philos Soc* 1991;66:245–73.

- [282] Johnson KA, Muir P, Nicoll RG, Roush JK. Asymmetric adaptive modeling of central tarsal bones in racing greyhounds. *Bone* 2000;27:257–63.
- [283] Nikander R, Sievanen H, Heinonen A, Kannus P. Femoral neck structure in adult female athletes subjected to different loading modalities. *J Bone Min Res* 2005;20:520–8.
- [284] Heinonen A, Sievanen H, Kyrolainen H, Perttunen J, Kannus P. Mineral mass, size, and estimated mechanical strength of triple jumpers' lower limb. *Bone* 2001;29:279–85.
- [285] Goodship AE, Lanyon LE, Mcfie H. Functional adaptation of bone to increased stress – experimental study. *J Bone Joint Surg Am Vol* 1979;61:1539–46.
- [286] Rubin CT, Lanyon LE. Regulation of bone-formation by applied dynamic loads. *J Bone Joint Surg Am Vol* 1984;66A:397–402.
- [287] Lanyon LE, Rubin CT. Static vs dynamic loads as an influence on bone remodeling. *J Biomech* 1984;17:897–905.
- [288] Mosley JR, Lanyon LE. Strain rate as a controlling influence on adaptive modeling in response to dynamic loading of the ulna in growing male rats. *Bone* 1998;23:313–8.
- [289] Rubin C, Turner AS, Bain S, Mallinckrodt C, McLeod K. Anabolism – low mechanical signals strengthen long bones. *Nature* 2001;412:603–4.
- [290] Turner CH, Takano Y, Owan I. Aging changes mechanical loading thresholds for bone-formation in rats. *J Bone Min Res* 1995;10:1544–9.
- [291] De Souza RL, Matsuura M, Eckstein F, Rawlinson SCF, Lanyon LE, Pitsillides AA. Non-invasive axial loading of mouse tibiae increases cortical bone formation and modifies trabecular organization: a new model to study cortical and cancellous compartments in a single loaded element. *Bone* 2005;37:810–8.
- [292] Vico L, Collet P, Guignandon A, Lafage-Proust MH, Thomas T, Rehailia M, et al. Effects of long-term microgravity exposure on cancellous and cortical weight-bearing bones of cosmonauts. *Lancet* 2000;355:1607–11.
- [293] Rittweger J, Frost HM, Schiessl H, Ohshima H, Alkner B, Tesch P, et al. Muscle atrophy and bone loss after 90 days' bed rest and the effects of flywheel resistive exercise and pamidronate: results from the LTBR study. *Bone* 2005;36:1019–29.
- [294] Ehrlich PJ, Lanyon LE. Mechanical strain and bone cell function: a review. *Osteoporosis Int* 2002;13:688–700.
- [295] Burger EH. Experiments on cell mechanosensitivity: bone cells as mechanical engineers. In: Cowin SC, editor. *Bone mechanics handbook*. Boca Raton: CRC Press; 2001.
- [296] Burger EH, Klein-Nulend J. Mechanotransduction in bone – role of the lacuno-canalicular network. *FASEB J* 1999;13:S101–12.
- [297] Klein-Nulend J, Vanderplas A, Semeins CM, Ajubi NE, Frangos JA, Nijweide PJ, et al. Sensitivity of osteocytes to biomechanical stress in-vitro. *FASEB J* 1995;9:441–5.
- [298] Jacobs CR, Yellowley CE, Davis BR, Zhou Z, Cimbala JM, Donahue HJ. Differential effect of steady versus oscillating flow on bone cells. *J Biomech* 1998;31:969–76.
- [299] Hughes-Fulford M. Signal transduction and mechanical stress. *Science's STKE* 2004;249:re12.
- [300] Burr DB. Targeted and nontargeted remodeling. *Bone* 2002;30:2–4.
- [301] Verborgt O, Gibson GJ, Schaffler MB. Loss of osteocyte integrity in association with microdamage and bone remodeling after fatigue in vivo. *J Bone Min Res* 2000;15:60–7.
- [302] Cowin SC. Bone stress-adaptation models. *J Biomech Eng – Trans ASME* 1993;115:528–33.
- [303] Huiskes R, Weinans H, Vanrietbergen B. The relationship between stress shielding and bone-resorption around total hip stems and the effects of flexible materials. *Clin Orthopaed Relat Res* 1992;124–34.
- [304] Pettermann HE, Reiter TJ, Rammerstorfer FG. Computational simulation of internal bone remodeling. *Arch Comput Methods Eng* 1997;4:295–323.
- [305] Huiskes R. The law of adaptive bone remodeling: a case for crying Newton? In: Odgaard A, Weinans H, editors. *Bone structure and remodeling*. Singapore: World Scientific; 1995.
- [306] Hegedus DH, Cowin SC. Bone remodeling-II – small strain adaptive elasticity. *J Elasticity* 1976;6: 337–52.
- [307] Hart RT. Bone modeling and remodeling: theories and computation. In: Cowin SC, editor. *Bone mechanics handbook*. Boca Raton: CRC Press; 2001.
- [308] Hernandez CJ, Beaupre GS, Carter DR. A model of mechanobiologic and metabolic influences on bone adaptation. *J Rehab Res Dev* 2000;37:235–44.
- [309] Weinkamer R, Hartmann MA, Brechet Y, Fratzl P. Stochastic lattice model for bone remodeling and aging. *Phys Rev Lett* 2004;93:228102.

- [310] Ruimerman R, Hilbers P, van Rietbergen B, Huiskes R. A theoretical framework for strain-related trabecular bone maintenance and adaptation. *J Biomech* 2005;38:931–41.
- [311] Carter DR, Orr TE, Fyhrie DP. Relationships between loading history and femoral cancellous bone architecture. *J Biomech* 1989;22:231–44.
- [312] Currey JD. The validation of algorithms used to explain adaptive bone remodeling in bone. In: Odgaard A, Weinans H, editors. *Bone structure and remodeling*. Singapore: World Scientific; 1995.
- [313] Ruimerman R, van Rietbergen B, Hilbers P, Huiskes R. The effects of trabecular-bone loading variables on the surface signaling potential for bone remodeling and adaptation. *Ann Biomed Eng* 2005;33:71–8.
- [314] Prendergast PJ, Taylor D. Prediction of bone adaptation using damage accumulation. *J Biomech* 1994;27:1067–76.
- [315] Mullender MG, Huiskes R. Proposal for the regulatory mechanism of Wolff's law. *J Orthopaed Res* 1995;13:503–12.
- [316] Tsubota K, Adachi T. Spatial and temporal regulation of cancellous bone structure: characterization of a rate equation of trabecular surface remodeling. *Med Eng Phys* 2005;27:305–11.
- [317] Tanck E, Ruimerman R, Huiskes R. Trabecular architecture can remain intact for both disuse and overload enhanced resorption characteristics. *J Biomech* 2006;39:2631–7.
- [318] Hartmann MA. Lattice models in materials science. PhD thesis. Humboldt University, Berlin, 2006.
- [319] Alvarado AS. Regeneration in the metazoans: why does it happen? *Bioessays* 2000;22:578–90.
- [320] Gerstenfeld LC, Cullinane DM, Barnes GL, Graves DT, Einhorn TA. Fracture healing as a post-natal developmental process: molecular, spatial, and temporal aspects of its regulation. *J Cell Biochem* 2003;88:873–84.
- [321] Einhorn TA. The cell and molecular biology of fracture healing. *Clin Orthopaed Relat Res* 1998;S7–21.
- [322] Prendergast PJ, Van der Meulen MCH. Mechanics of bone regeneration. In: Cowin SC, editor. *Bone mechanics handbook*. Boca Raton: CRC Press; 2001.
- [323] Carter DR, Beaupré GS. Skeletal function and form, mechanobiology of skeletal development, aging, and regeneration. Cambridge: Cambridge University Press; 2001.
- [324] McKibbin B. Biology of fracture healing in long bones. *J Bone Joint Surg Br Vol* 1978;60:150–62.
- [325] Li R, Ahmad T, Spetea M, Ahmed M, Kreicbergs A. Bone reinnervation after fracture: a study in the rat. *J Bone Min Res* 2001;16:1505–10.
- [326] Claes L, Augat P, Suger G, Wilke HJ. Influence of size and stability of the osteotomy gap on the success of fracture healing. *J Orthopaed Res* 1997;15:577–84.
- [327] Goodship AE, Watkins PE, Rigby HS, Kenwright J. The role of fixator frame stiffness in the control of fracture-healing – an experimental-study. *J Biomech* 1993;26:1027–35.
- [328] Claes LE, Heigle CA, Neidlinger-Wilke C, Kaspar D, Seidl W, Margevicius KJ, et al. Effects of mechanical factors on the fracture healing process. *Clin Orthopaed Relat Res* 1998;S132–47.
- [329] Epari DR, Schell H, Bail HJ, Duda GN. Instability prolongs the chondral phase during bone healing in sheep. *Bone* 2006;38:864–70.
- [330] Seebeck P, Thompson MS, Parwani A, Taylor WR, Schell H, Duda GN. Gait evaluation: a tool to monitor bone healing? *Clin Biomech* 2005;20:883–91.
- [331] Kassi JP, Hoffmann JE, Heller M, Raschke M, Duda GN. Assessment of the stability of fracture fixation systems: mechanical device to investigate the 3-D stiffness in vitro. *Biomed Tech* 2001;46:247–52.
- [332] Goodship AE, Cunningham JL, Kenwright J. Strain rate and timing of stimulation in mechanical modulation of fracture healing. *Clin Orthopaed Relat Res* 1998;S105–15.
- [333] Roux W. *Gesammelte Abhandlungen über Entwicklungsmechanik der Organismen*. Leipzig: Wilhelm Engelmann's Verlag; 1895. p. 436.
- [334] Perren SM, Cordey J. The concept of interfragmentary strain. In: Uthhoff HK, editor. *Current concepts of internal fixation of fractures*. Berlin: Springer; 1980. p. 63–77.
- [335] Pauwels F. Grundriss einer Biomechanik der Frakturheilung. In: *Verhandlungen der Deutschen Orthopädischen Gesellschaft*. Stuttgart: Ferdinand Enke Verlag; 1941. p. 62–108. Translated in: *Biomechanics of fracture healing*, in: *Biomechanics of the locomotor apparatus*, Springer-Verlag, Berlin, 1980.
- [336] Weinans H, Prendergast PJ. Tissue adaptation as a dynamical process far from equilibrium. *Bone* 1996;19:143–9.
- [337] Carter DR, Blenman PR, Beaupré GS. Correlations between mechanical-stress history and tissue differentiation in initial fracture-healing. *J Orthopaed Res* 1988;6:736–48.
- [338] Giori NJ, Beaupré GS, Carter DR. Cellular-shape and pressure may mediate mechanical control of tissue composition in tendons. *J Orthopaed Res* 1993;11:581–91.

- [339] Claes LE, Heigle CA. Magnitudes of local stress and strain along bony surfaces predict the course and type of fracture healing. *J Biomech* 1999;32:255–66.
- [340] Cowin SC. Bone poroelasticity. *J Biomech* 1999;32:217–38.
- [341] Prendergast PJ, Huiskes R, Soballe K. Biophysical stimuli on cells during tissue differentiation at implant interfaces. *J Biomech* 1997;30:539–48.
- [342] Lacroix D, Prendergast PJ. A mechano-regulation model for tissue differentiation during fracture healing: analysis of gap size and loading. *J Biomech* 2002;35:1163–71.
- [343] Lacroix D, Prendergast PJ, Li G, Marsh D. Biomechanical model to simulate tissue differentiation and bone regeneration: application to fracture healing. *Med Biol Eng Comput* 2002;40:14–21.
- [344] Isaksson H, Wilson W, van Donkelaar CC, Huiskes R, Ito K. Comparison of biophysical stimuli for mechano-regulation of tissue differentiation during fracture healing. *J Biomech* 2006;39:1507–16.
- [345] Isaksson H, Van Donkelaar CC, Huiskes R, Ito K. Corroboration of mechanoregulatory algorithms for tissue differentiation during fracture healing: comparison with *in vivo* results. *J Orthopaed Res* 2006;24:898–907.
- [346] Canalis E, Economides AN, Gazzero E. Bone morphogenetic proteins, their antagonists, and the skeleton. *Endocrine Rev* 2003;24:218–35.
- [347] Groeneweld EHJ, Burger EH. Bone morphogenetic proteins in human bone regeneration. *Euro J Endocrinol* 2000;142:9–21.
- [348] Bailon-Plaza A, van der Meulen MCH. A mathematical framework to study the effects of growth factor influences on fracture healing. *J Theor Biol* 2001;212:191–209.
- [349] Bailon-Plaza A, van der Meulen MCH. Beneficial effects of moderate, early loading and adverse effects of delayed or excessive loading on bone healing. *J Biomech* 2003;36:1069–77.
- [350] Iqbal J, Zaidi M. Molecular regulation of mechanotransduction. *Biochem Biophys Res Commun* 2005;328:751–5.
- [351] De Jong H. Modeling and simulation of genetic regulatory systems: a literature review. *J Comput Biol* 2002;9:67–103.
- [352] Vogel S. Cats' paws and catapults: mechanical worlds of Nature and people. W.W. Norton & Company; 2000. p. 384.